2018

UNDERSTANDING THE THERMODYNAMICS AND ORAL ABSORPTION POTENTIAL OF PHARMACEUTICAL AMORPHOUS SOLID DISPERSIONS

Nico Setiawan
University of Kentucky, nseti2@gmail.com
Author ORCID Identifier:
https://orcid.org/0000-0002-4945-8851
Digital Object Identifier: https://doi.org/10.13023/ETD.2018.175

STUDENT AGREEMENT:

I represent that my thesis or dissertation and abstract are my original work. Proper attribution has been given to all outside sources. I understand that I am solely responsible for obtaining any needed copyright permissions. I have obtained needed written permission statement(s) from the owner(s) of each third-party copyrighted matter to be included in my work, allowing electronic distribution (if such use is not permitted by the fair use doctrine) which will be submitted to UKnowledge as Additional File.

I hereby grant to The University of Kentucky and its agents the irrevocable, non-exclusive, and royalty-free license to archive and make accessible my work in whole or in part in all forms of media, now or hereafter known. I agree that the document mentioned above may be made available immediately for worldwide access unless an embargo applies.

I retain all other ownership rights to the copyright of my work. I also retain the right to use in future works (such as articles or books) all or part of my work. I understand that I am free to register the copyright to my work.

REVIEW, APPROVAL AND ACCEPTANCE

The document mentioned above has been reviewed and accepted by the student's advisor, on behalf of the advisory committee, and by the Director of Graduate Studies (DGS), on behalf of the program; we verify that this is the final, approved version of the student's thesis including all changes required by the advisory committee. The undersigned agree to abide by the statements above.

Nico Setiawan, Student

Dr. Patrick J. Marsac, Major Professor

Dr. David J. Feola, Director of Graduate Studies

UNDERSTANDING THE THERMODYNAMICS AND ORAL ABSORPTION POTENTIAL OF PHARMACEUTICAL AMORPHOUS SOLID DISPERSIONS

DISSERTATION

A dissertation submitted in partial fulfillment of the requirements for the degree of

Doctor of Philosophy in the College of Pharmacy at the University of Kentucky

By

Nico Setiawan

Lexington, Kentucky

Director: Dr. Patrick J. Marsac, Associate Professor of Pharmaceutical Sciences,

Lexington, Kentucky

2018

ABSTRACT OF DISSERTATION

UNDERSTANDING THE THERMODYNAMICS AND ORAL ABSORPTION POTENTIAL OF PHARMACEUTICAL AMORPHOUS SOLID DISPERSIONS

Supersaturating drug delivery systems, such as amorphous solid dispersions (ASDs), have been used extensively to elevate the apparent solubility and oral bioavailability of poorly water-soluble drugs. However, despite the numerous examples of success in increasing solubility and oral bioavailability using ASDs, physical stability challenges remain as formulators seek to employ high drug loading for cost reduction and improved patient compliance. Therefore, stability in both the solid and solution state must be considered for ASDs to be successful. In the solid state, the drug must remain amorphous in the solid matrix throughout the shelf life of the product. Although excipients, such as polymers, have been known to stabilize the amorphous drug in the solid state, stresses encountered during manufacturing and fluctuations in storage conditions may have a detrimental impact on the physical stability of ASDs. Numerous studies have been performed on the impact of each process on ASD stability, yet the relative quantitative impact of each process with respect to the overall energetics landscape is not well understood.

Further, ASDs must dissolve after administration and maintain the intended supersaturation in the gastrointestinal (GI) tract during the GI transit time to achieve maximum oral absorption. In solution, the energetics advantage of the amorphous over the crystalline material is a “double-edged sword,” in that it produces not only a high absorption driving force but also an undesirable high crystallization potential. An approach to quantitatively measure the thermodynamic activity of amorphous materials is, thus, desirable. However, it is difficult to measure thermodynamic activity

quantitatively, especially due to the speciation process induced by formulation excipients and endogenous materials. Hence, it is often difficult to assess the true enhancement in the absorption for a given ASD and to measure its crystallization tendency in solution. Overall, this dissertation aims to address the following:

1. The relative thermodynamics magnitude of various processes with respect to the crystallization energy associated with amorphous drugs
2. The development of a practical tool to measure the thermodynamic activity of amorphous materials over its crystalline counterpart in solution to assess the enhancement in absorption in the presence of excipients
3. The impact of measured thermodynamic activity on drug crystallization energetics in the presence of excipients

KEYWORDS: supersaturation, crystallization, amorphous, poorly water-soluble drugs, excipients, absorption

Nico Setiawan
Author's signature

April 27, 2018
Date

UNDERSTANDING THE THERMODYNAMICS AND ORAL ABSORPTION POTENTIAL OF PHARMACEUTICAL AMORPHOUS SOLID DISPERSIONS

By

Nico Setiawan

Patrick J. Marsac, Ph.D.

Director of Dissertation

David J. Feola, Ph.D.

Director of Graduate Studies

April 27, 2018

Date

To my beloved parents

ACKNOWLEDGEMENTS

I would like to express my sincere gratitude to all who have helped and supported me throughout my graduate work. This dissertation would not have been possible without all of you.

First, I would like to thank my committee. Each of you has uniquely contributed invaluable guidance and support throughout my graduate study. I would like to offer special thanks to Dr. Paul Bummer, who, although no longer with us, continues to inspire by his example and dedication to the students he served over the course of his career. To my advisor, Dr. Patrick Marsac, thank you for challenging me to continuously think outside the box and to “tie up” the observations to the fundamentals. I am blessed by your kindness, patience, and friendship throughout my graduate study. To Dr. Eric Munson, thank you for serving as my co-advisor after the passing of Dr. Paul Bummer. Your guidance and support to this dissertation is truly appreciated. To Dr. Brad Anderson, thank you for challenging my thought process and helping me to be a better scientist and communicator. Your advice and support have been invaluable throughout my graduate study. To Dr. Barbara Knutson, thank you for contributing valuable advice and sharing your laboratory equipment.

I would also like to thank all of the people in Marsac and Munson groups that I had the privilege to work with: Dr. Sadegh Poozesh, Dr. Jonas Alin, Matt Defrese, Freddy Arce, Dr. Matt Nethercott, Dr. Sean Delaney, Dr. Xiaoda Yuan, Kanika Sarpal, Ashley Lay, Julie Calahan, and Travis Jarrells. I would like to thank Poozesh for helping

me to be a better writer and for our friendship. I would like to thank Jonas for your support on this dissertation. In addition, I would like to thank Matt Defrese for the advice on job hunting and his challenging questions. Many thanks to Freddy who helped me to execute SEM experiments. I would like to thank Matt Nethercott for your help with NMR and writing, and all memorable friendship. Thanks to Sean who helped me with NMR experiments and daily lab work; I truly cherished our friendship.

In addition to the Marsac and Munson groups, I would like to thank the following people whose friendship and support have made my graduate work journey enjoyable: Dr. Xiaojian Li, Dr. Derek Reichel, Dr. Nilay Thakkar, Emily Denehy, and Na-Ra Lee. I would also like to thank several excellent undergraduate students whom I had the privilege to mentor: Emily Daley, Heather Campbell, Sean Gillette, Jack Oliver, and Endras Fadhilah.

On a personal note, I would like to thank my family and friends for their love and support. To my mom and dad, thank you for your unconditional love and sacrifice. I certainly would not have made it this far if it were not for you. Above all, I acknowledge my Creator, who has given me the platform and wisdom to carry on my life purpose in improving the health and wellness of human beings.

TABLE OF CONTENTS

LIST OF TABLES

LIST OF FIGURES

Chapter 1 - Introduction

1.1 Background

With the goal of producing more efficacious new chemical entities (NCE), the use of high throughput screening in the drug discovery space has resulted in a massive increase of hydrophobic compounds. As high as 90% of NCEs have been identified as being poorly water-soluble, which is inextricably linked to the resulting poor oral bioavailability of these compounds [1]. Supersaturating drug delivery systems (SDDS) are formulation approaches that have been developed to overcome these solubility issues and enhance oral bioavailability [2]. Amorphous solid dispersions (ASDs) are an example of SDDS, and their success in increasing oral bioavailability have been well documented in the literature [3]. The success of ASD relies upon its solid-state stability throughout the processing and storage period as well as its supersaturation stability in solution after its administration into gastrointestinal (GI) environment. Despite extensive research on ASD solid-state stability, its assessment is a strong function of the sensitivity of the analytical tools employed. However, the selection of analytical tools in the pharmaceutical area tends to be limited compared to the availability at large. Similarly, while supersaturation stability in solution have been widely studied, successful construction of in vitro-in vivo correlations (IVIVC) in this space is still minimal. The lack of IVIVC is perhaps mostly attributable to the insufficient understanding of the mechanisms by which ASD enhance bioperformance in vivo. As such, this review examines the analytical tools available for detection of ASDs solid-state failure modes detection and explores the mechanisms by which ASDs enhance bioperformance. The knowledge gained from this review is

expected to aid formulators in making a scientific-based decision throughout the development of ASDs.

1.2 Potential solid-state failure modes in ASD and their detection methods

An amorphous solid is defined by the absence of a long-range order of intermolecular arrangement, an otherwise characteristic property of its stable crystalline counterpart. From the solubility theory, dissolution of a solute into a solvent involves the energy penalties from the breaking of solute-solute interactions in the solid-state while creating a void in the solvent and the subsequent energy gained from placing the solute molecule into the solvent void. Since amorphous materials lack long-range order in the solid state, the energy penalty associated with the breaking of solute-solute interaction is significantly reduced, thus the amorphous solids are said to have a higher free energy state relative to the crystalline solid. As a result, the higher free energy of the amorphous solids confers a greater solubility and dissolution rate compared to the crystalline form. However, this advantage comes with inherent stability liabilities. In other words, because of its high free energy, amorphous solids will tend to "seek out" a more stable thermodynamic state [4].

In order to stabilize the amorphous drug, excipients (often polymers) are added to create a solid *dispersion* of drug and polymer. The goal is to create a uniform miscible dispersion where each drug molecule is "dissolved" in the polymer matrix, which is also known as solid solution. Physical stability of ASDs is governed by thermodynamics, kinetics, and drug-excipient interactions [5]. Further, ASD thermodynamic properties are governed by the drug heat of fusion, degree of supercooling, and configurational entropy,

whereas the kinetic contributions to ASD physical stability are associated with translational, vibrational, and rotational modes of motion. The stabilization conferred by the added excipients results in a reduction of the dispersed drug activity due to the diluent effect and/or favorable drug-excipient intermolecular interactions, which in turn impacts the thermodynamic and kinetic properties of amorphous drug in ASDs. The greatest challenge with ASD is perhaps its heterogeneous nature that is heavily dependent on its "thermal history" (i.e. what is the state of the glass produced?). For example, it has been reported that the method by which ASDs are produced, via a melt or solvent evaporation, could significantly impact its physical stability [6]. Consider producing an amorphous material via rapid cooling of the melt, different rates of cooling would produce different states of glass, i.e. glasses with two different Tg's as shown in Figure 1.1. The difference in the glassy states is critical since the glass with the higher Tg exhibits a higher energetics. Similarly, solvent evaporation process would generate different characteristics of glass depending on the rate of solvent removal as well as the amount of residual solvent. Although analytical tools are available to measure the different Tg's and equations have been developed to understand the properties of the different glassy states at the operating temperature, the dependence of the glassy state on the processing must be recognized. In addition, glassy materials may relax over time, thus the properties of the glass may be different compared to freshly prepared glass.

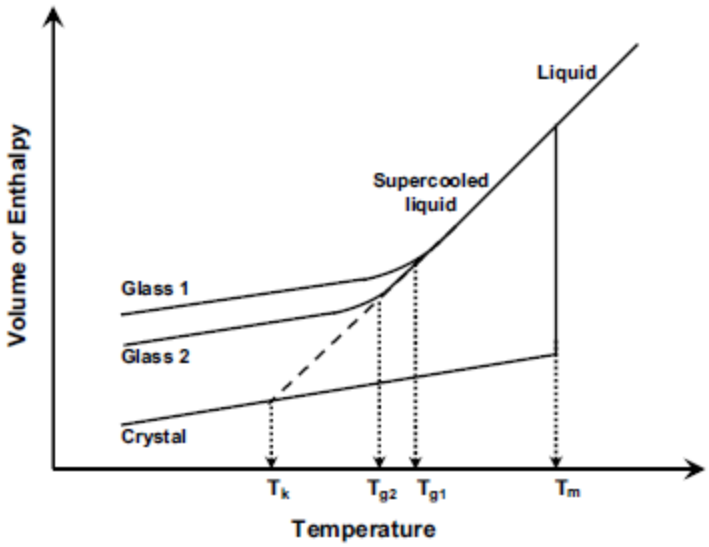

Figure 1.1 Specific volume/enthalpy diagram versus temperature for crystalline and two glassy materials of the same hypothetical compound.

Furthermore, ASDs undergo further manufacturing processes and exposure to storage conditions before distribution to consumers, as shown in the schematic in Figure 1.2. Mechanical stresses, such as milling, compaction, or compression during manufacturing may create imperfections, such as cracks and defects with enhanced surface energy, which may induce phase changes in ASD solid matrix. Similarly, moisture exposure during storage may change the strength of interaction or activity of drug in polymer. Therefore, it is often difficult to make accurate predictions of ASD stability since the starting glassy state might be different for different thermal histories experienced. Nevertheless, understanding the potential failure modes associated with ASDs such as amorphous-amorphous phase separation and crystallization, which may be caused by the aforementioned processes, and the awareness of the analytical tools

available for detection of these failure modes are critical to the successful development of ASD.

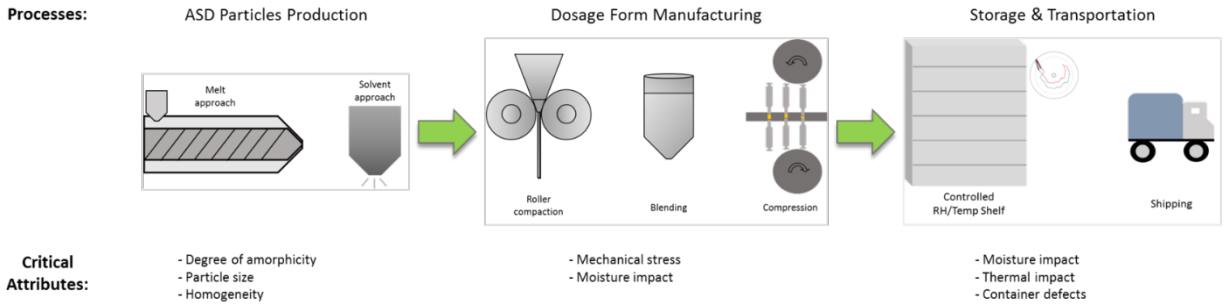

Figure 1.2 Schematic of various processes that ASDs may be exposed to and the critical attributes associated with each process that may contribute to the solid-state failure modes.

1.2.1 Amorphous-amorphous phase separation (AAPS) risk

One avenue by which ASDs are de-mixed is through AAPS, a condition where amorphous phases of drug-rich and polymer-rich regions coexist. AAPS is believed to be a precursor to crystallization [7]. The impact of storage conditions, such as relative humidity (RH) and temperature, on AAPS of ASDs has been evaluated in the literature. For example, Marsac et al. observed a reversible temperature-induced de-mixing of felodipine and polyvinyl pyrrolidone (PVP), whereas an irreversible de-mixing was observed with changing RH [7]. Rumondor et al. investigated several poorly soluble drugs with PVP and concluded that miscibility could be maintained with low ASD hygroscopicity, less hydrophobic drug as determined by the drug's log P, and strong

drug-polymer interaction as determined by ΔpKa of hydrogen bonding acceptor and donor [8]. Interestingly, the authors observed that for some systems that underwent moisture-induced AAPS, the drug did not crystallize even at a higher RH. Lakshman et al. also observed a similar phenomenon where crystallization did not occur despite observation of AAPS under accelerated conditions [9]. Perhaps this phenomenon may be explained by the slow re-organization step of drug molecules to form a critical nucleus for subsequent crystallization processes [7], thus it is intuitive that drug crystallization tendency [10] be evaluated early so as to gauge the rate determining step (bulk diffusion vs. re-orientation step) for crystallization. On the other hand, process-induced AAPS from manufacturing steps has not been extensively evaluated, albeit it is intuitive that the variety of forces associated with typical processing have potential to induce phase transformations [11]. Poozesh et al. recently utilized focused ion beam scanning electron microscopy (FIB-SEM) to investigate particles produced from the same spray drying batch and observed a large size distribution with the larger particles displaying drug-rich and polymer-rich regions phase separation [12]. In addition, Ayenew et al. observed AAPS of a naproxen-PVP system after compression [13]. While some evidence indicates that AAPS may not necessarily lead to deleterious crystallization, more research needs to be conducted to assess how AAPS influences critical bioperformance characteristics, such as dissolution, supersaturation, and absorption, which will be discussed in the latter part of this review.

1.2.2 Crystallization risk

Crystallization from the amorphous phase is characterized by nucleation and growth steps. Traditionally, the kinetics of crystallization is described by classical nucleation theory. However, due to its many limitations, such as the lack of homogeneous nucleation, changing degree of supercooling, or difficulty to evaluate specific variables experimentally, other models that simultaneously account for both nucleation and growth are often utilized instead. Bhugra et al. has thoroughly summarized this topic [5] and it will not be discussed further here. Although mathematical descriptions of crystallization have been developed, the typical processing and storage conditions that ASDs are exposed to may induce solid-state changes, which complicate the application of these theories. Preparation methods (melt quench, ball mill, spray dry) have been reported to produce ASDs with very diverse physical stability, although the same Tg was observed across all the methods used [14]. Leane et al. observed a difference of at least a 4-fold rate of crystallization at the same storage conditions when comparing a direct compression product to a product produced by a compression preceded by a compaction step, suggesting that process-induced phase transformation occurred [15]. It is also well known that crystallization occurs several orders of magnitude faster on the surface than that in the bulk [16], suggesting that particle size reduction in the manufacturing process may lead to detrimental crystallization due to the higher surface area to volume ratio. Other authors have also reported the impact of moisture during storage, albeit the rate of crystallization is also a function of the physicochemical properties of the ASD itself [17, 18]. Regardless of the process by which crystallization may be induced in an ASD, crystallization negates the intended amorphous advantage. Therefore, an approach that

allows for analyses of ASD physical stability is necessary to evaluate and avoid the downstream risk of crystallization.

1.2.3 Analytical tools for ASD failure modes detection

As mentioned above, understanding the available analytical tools for ASD physical stability assessment is critical in the development of ASDs. While numerous methods have been utilized in different studies, there has been no unified knowledge on the sensitivity of these methods. Herein, a summary of available analytical methods along with each of the time and length sensitivity is presented in Table 1.1. It also needs to be pointed out that no single analytical technique can capture all information necessary for ASD physical stability consideration. In other words, orthogonal approach should be utilized to obtain a comprehensive physical stability information. This section is divided into three groups of analytical tools: calorimetry, spectroscopy, and microscopy.

Calorimetric techniques, such as differential scanning calorimetry (DSC) and solution calorimetry (SC), measures the energetics associated with each phase change that occurs as a function of temperature, e.g. melting or glass transition. Although calorimetry has been utilized extensively in the pharmaceutical arena as it readily provides the thermodynamic properties of a single component, it is difficult to evaluate multicomponent mixtures since the measured calorimetric signal is the sum total of all thermal responses. For instance, DSC has been used extensively to demonstrate ASD miscibility by a measure of Tg, whereby a multicomponent system is assumed to be miscible if a single Tg is observed or immiscible if two or more distinct Tg’s are present. To test this hypothesis/assumption, Qian et al. conducted a study on the miscibility of a

poorly soluble compound, BMS-A, and PVP-VA polymer produced via two different screw rotation speed of a hot-melt extrusion process [19]. The authors observed that although a single Tg was observed for both ASD batches, the confocal Raman microscopy data showed that there is a difference in the homogeneity between the two batches in that the higher screw speed conferred a much more homogeneous dispersion than the other batch, which eventually affected its long-term physical stability. The authors then concluded that the single Tg "rule" may not be sufficient in guaranteeing ASD miscibility/homogeneity and suggested that an orthogonal approach be used to confirm ASD homogeneity. Another potential challenge with DSC is that although a single Tg may be observed, the Tg event could be very broad due to the large distribution or heterogeneity in the solid matrix [20]. For instance, Kim et al. observed a very broad Tg that spanned approximately 65-80°C associated with synthesized gradient copolymers, whereas two distinct Tg's were observed for block copolymers [21]. Gradient copolymers differ from block copolymers in that gradient copolymers vary sinusoidally in composition instead of constant composition in each "block." Although this particular study did not specifically aim at understanding ASD physical stability, the observed broad Tg implied that there are "pockets" of heterogeneity in the system analyzed, resemblance of the AAPS phenomenon that may be observed in ASDs. Furthermore, heat-induced phase transitions associated with the heat cycle performed using DSC may occur. For example, Marsac et al. showed a re-mixing of the drug and polymer as the sample is heated [7]. Interestingly, on the other hand, heat-induced crystallization has also been reported for itraconazole solid dispersions [22]. Solution calorimetry (SC) is another calorimetry technique that measures the thermodynamic

changes of a sample via a complete dissolution of the sample at a constant temperature. The first application of SC in the pharmaceutical arena that the authors are aware of was published approximately 40 years ago, where Pikal et al. utilized SC to determine the degree of crystallinity of β-lactam antibiotics [23]. To date, there have not been many published work on the use of SC, especially related to ASDs. Kayaert et al. used SC to measure the strength of interaction between two drug molecules and HPMC to elucidate the mechanism by which processing affects amorphization of nanocrystals [24]. Recently, Marsac et al. and Alin et al. employed SC to measure the interaction strength or mixing enthalpy between drug and polymer in ASDs [25, 26]. In SC, the heat of mixing is the difference between the heat of solution of the individual component and the weighted average of the components' heat of solution in ASDs. The advantage of determining the mixing enthalpy by SC is that it captures the total intermolecular interaction including the strong hydrogen bonding interaction, which may not be accurately captured in solubility parameter calculation since only positive deviation is accounted for in this approach. Using Flory-Huggins calculation, the authors constructed a mixing free energy diagram from the measured mixing enthalpy as a function of composition, which allowed for drug solubility in polymer to be determined.

Table 1.1 List of analytical tools with their associated time scale and length scale or limit of detection (LOD) capability.

Type	Instrument	Time scale (s)	Length Scale/LOD
Calorimetry	DSC	>100 [27]	20-30 nm [28]; 5 wt% [29]
	SC		1 wt% [30]
Spectroscopy	PXRD/PDF		0.2-5 wt% [31]
	IR		1-2 wt% [29]
	Raman		0.05 wt% [27]
	BCARS		300 nm [32]
	ssNMR	10^{-11}-10^{3} [33]	0.5-50 nm [34]; 0.3-1 wt% [35]
	DEA	10^{-11}-10^{4} [33, 36]	3-50 nm [37]
	TSC	25-3,000 [27]; 10^{3}-10^{4} [36]	1 wt% [30]
	XPS		20 µm (lateral); 10 nm (depth) [34]; 1 wt% [30]
	EDS		200 nm (lateral); 0.5-3 µm (depth); 0.1 wt% [38]
	EELS		1 nm (lateral) [39]
	ToF-SIMS		50 nm (lateral); 1 nm (depth) [40]
	AES		7 nm (lateral); 0.02-20 nm (depth) [41]
	SAXS		3-25 nm [33]
	TPS		1-5 wt% [29]
	DMA		2 wt% [42]
	SHG/Multi-photon fluorescence		90 nm [43]
Microscopy/ Imaging	(FIB) SEM		2 nm [39]
	TEM		0.2 nm [44]
	AFM		0.2 nm [45]
	X-ray CT		1-4 µm [46]

DSC: differential scanning calorimetry, SC: solution calorimetry, PXRD: powder X-ray diffractometer, PDF: pair distribution function, IR: infrared, BCARS: broadband coherent

anti-Stokes Raman scattering, ssNMR: solid-state nuclear magnetic resonance, DEA: dielectric analysis, TSC: thermally stimulated current, XPS: X-ray photoelectron spectroscopy, EDS: energy dispersive X-ray spectroscopy, EELS: electron energy loss spectroscopy, ToF-SIMS: time-of-flight secondary ion mass spectrometry, AES: Auger electron spectroscopy, SAXS: small angle X-ray scattering, TPS: Terahertz pulsed spectroscopy, DMA: dynamic mechanical analysis, FIB-SEM: focused ion beam scanning electron microscopy, TEM: transmission electron microscopy, AFM: atomic force microscopy, XR-CT: X-ray computed tomography, SHG: second harmonic generation.

Spectroscopy involves any technique that captures the interaction between an electromagnetic radiation and an analyte. The majority of spectroscopy tools are nondestructive in nature, thus they lend themselves to characterize ASDs. PXRD, which is also known as wide angle X-ray scattering (WAXS), is an excellent technique to detect structural differences of the analytes as each analyte presents a unique diffractogram fingerprint. Constructive interference (Bragg intensity) can be observed due to the interaction between the X-ray incident beams with the long-range structure of crystalline analytes. This is contrary to the interaction with amorphous materials, which confers an amorphous halo or diffuse scattering instead. Quantifications as low as 5% (or less) of crystalline materials in an amorphous sample have been widely exemplified in the literature [20, 31, 47-49]. In addition, pair distribution function (PDF) can be applied to the resulting diffractogram of the ASD to evaluate its miscibility. PDF is a statistical method analogous to the Rietveld method [50], which is used to deconvolute component

composition from a diffractogram of crystalline mixtures while PDF is used to quantify individual component in an amorphous mixture [51]. A binary ASD is considered miscible if the PDF of the binary is unique from the weighted average of the PDFs of the individual components [49, 52]. Small angle X-ray scattering (SAXS) is another technique that utilizes X-ray beam and may be used to quantify differences in nanoscale density. The difference between SAXS and WAXS lies on the scattering angle where SAXS operates between 0.1-10° whereas WAXS between 10-90° 2θ angle. SAXS has been previously shown to elucidate nanoscale structures of pharmaceuticals [53]. Synchrotron, which uses a radially accelerated X-ray beam, may be used to generate yet a higher X-ray flux and an increased intensity compared to a regular WAXS or SAXS [54].

Vibrational spectroscopy includes Raman and infrared (IR) spectroscopies. These techniques are capable to access vibrational transitions because the energy produced by these techniques corresponds to the vibration frequency, i.e. 10^{13}-10^{14} Hz frequency. The ability of these techniques to detect crystallization and AAPS in an amorphous matrix has been previously reported [7, 8, 55-60]. Further, these techniques have been used to describe the impact of specific intermolecular interactions, e.g. hydrogen bond, on the mobility and stability of amorphous materials [61, 62]. The advantage of Raman over IR is that Raman operates with a stronger electromagnetic field and does not have significant water absorption. This is beneficial, as amorphous materials tend to be hygroscopic, thus the analysis by Raman does not require a correction for water that may be present in the samples. In addition, Coleman and Painter have utilized IR results to correct for hydrogen bonding interaction, which cannot be accounted for when using solubility parameter calculation, in the Flory-Huggins free energy of mixing calculation [63-65]. Broadband

coherent anti-Stokes Raman scattering (BCARS) is a nonlinear approach that has demonstrated significant enhancement in spatial resolution and speed compared to traditional Raman as a result of the use of multiple photons source [32]. Other nonlinear spectroscopy techniques, such as second harmonic generation (SHG) and multi-photon fluorescence, have also been explored recently in the pharmaceutical arena. Several authors have shown the utility of these nonlinear spectroscopy tools in detecting crystals in amorphous matrices [43, 66-68]. Terahertz pulsed spectroscopy (TPS) is a technique that operates in the far-IR region of the electromagnetic spectrum. The spectra produced by TPS relate to the intermolecular vibrations within the lattice structure instead of the intramolecular vibrations that are probed by FT-IR. Because amorphous materials lack the structural long-range order, they do not exhibit any spectral features, which makes TPS a sensitive tool to detect crystallization in amorphous solid matrix [69].

Solid-state nuclear magnetic resonance (ssNMR) involves the excitation of NMR-active molecules with non-zero spins nuclei using a high-powered radio frequency pulse in a static magnetic field [70]. Relaxation of the excited nuclei to the static magnetic field produces a free induction decay (FID), which can be transformed into the observed spectra using Fourier transform. ssNMR has been used to study the crystallization rate of several drug molecules via correlation with molecular mobility as measured by ^{1}H NMR relaxation times [71, 72]. Yuan et al. observed distinct level of miscibility at select compositions of nifedipine-PVP dispersion using T_1 and $T_{1\rho}$ relaxation time experiments [28]. It was found that compositions below 90% drug loading were miscible from the T_1 experiments but only miscible below 75% drug loading from $T_{1\rho}$ experiments. The authors concluded that the much smaller domain size of 2-5 nm captured by $T_{1\rho}$

experiments provided a better nanoscopic view of the ASD compared to the 20-50 nm domain size obtained by T_1 experiments, indicating that sensitivity of analytical tools or methods used dictates the information on ASD physical stability. Further, 2D correlation techniques can be utilized to determine the intermolecular interactions between different components in ASD necessary to form the "glass solution" [73]. For fluorine containing drug molecules, ^{19}F NMR analysis provides higher sensitivity, which allows for a lower LOD and shorter acquisition time [74]. Dynamic mechanical analysis (DMA) exposes an analyte to mechanical stress at various frequencies and measures the resulting strain. DMA can be used to measure Tg of an amorphous system because there is a change in the storage and loss modulus around this transition point [75]. Several authors have also used this technique to study phase separation [75-78] as well as secondary relaxation processes in glasses [79]. Furthermore, Ediger et al. observed that relaxation times associated with thermodynamic variables, such as enthalpy or volume, correspond very well with those of mechanical variables, such as molecular rotation or viscosity, as shown in Figure 1.3 [33]. Dielectric analysis (DEA) operates analogously to that of DMA, except that the mechanical perturbation is replaced with an electrical perturbation. Numerous authors have shown the utility of DEA in detecting crystallization [80-88] and AAPS [89] in amorphous matrices. In addition, since it provides access to both local and secondary relaxations, DEA is found to be a very appealing approach to measure molecular motions in amorphous materials [33]. Thermally stimulated current (TSC) is another technique that uses electrical perturbation on the analyte. A TSC spectrum can be acquired by initially polarizing the sample with a static electrical field at a polarization temperature until the sample reaches equilibrium. The sample is then cooled down such

that the dielectric relaxation proceeds extremely slowly and the depolarization current due to the return to equilibrium temperature is recorded. The resulting TSC spectrum is complex but information from the distribution of relaxation times can be extracted through some fitting parameters. In addition, TSC can help us understand the local-order distribution in heterogeneous amorphous materials [90]. To date, TSC has been primarily utilized only in the polymer science field, but with its powerful capabilities, TSC could be an appealing tool in the pharmaceutical arena.

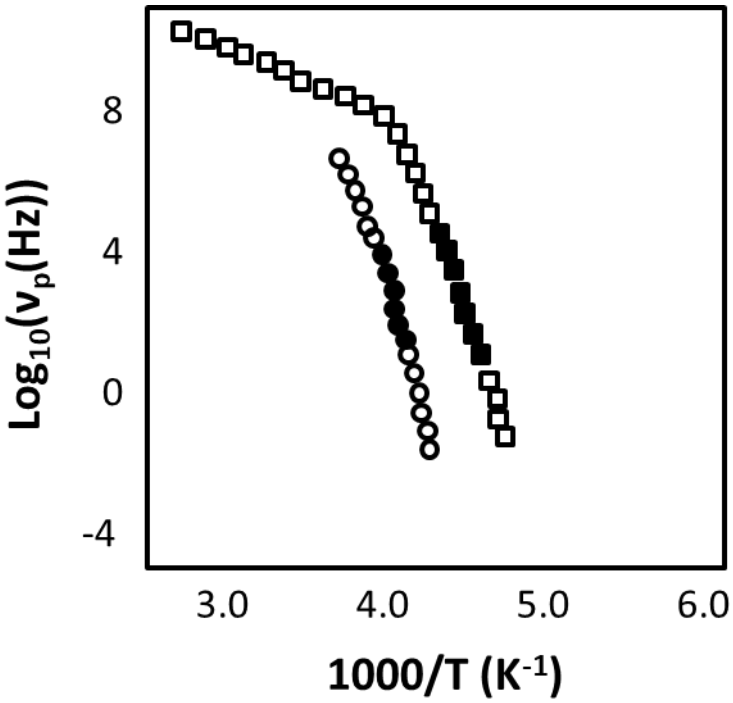

Figure 1.3 Cartoon showing the log of the peak frequency ν_p as a function of inverse temperature for four samples: salol (□) and o-terphenyl mixed with 33% o-phenylphenol (○). The open symbols show dielectric relaxation data, and the corresponding solid

symbols show results from specific heat spectroscopy. Excellent agreement is observed between these two techniques. Adapted from Ediger et al. [33].

Surface analysis is also important for characterization of amorphous materials since surface properties may have an amplified effect on multiple measures of performance. In other words, particles located on the surface are the first ones exposed to potential interactions, such as mechanical stresses introduced during manufacturing processes and/or sorbed water from humid storage conditions. Sorbed water has been demonstrated to induce crystallization of amorphous materials [91-93]. Wu et al. have also shown faster crystallization kinetics at the surface, with rates of surface crystallization up to 150 times greater than the bulk crystallization rate [16]. In addition, localization of hydrophilic polymer on the surface will likely improve wettability required for dissolution process. X-ray photoelectron spectroscopy (XPS), where ionized atoms at the surface by the incident photons produces an ejected electron with a reduced energy, can be used to determine surface chemical composition. Dahlberg et al. have shown the utility of this technique and found that the rate of solvent removal and the solvent system by which ASDs are prepared could impact the surface heterogeneity, which in turn caused a different dissolution behavior across ASD tested [94]. Although the study by Dahlberg et al. demonstrated the great utility of XPS, applications in the pharmaceutical arena is still limited. With the abundance of studies showing surface associated failure mode, it is expected that the use of XPS or other surface characterization techniques will continue to rise.

Atomic force microscopy (AFM) is a high-resolution microscopy technique. As with any microscopy technique, AFM can directly observe phenomena occurring in the sample, such as crystallization and AAPS [7, 95-99]. However, if a crystal is observed, AFM does not have the discriminating power to determine the crystal polymorph. As such, AFM is often coupled with other technique, such as IR (AFM-IR). In addition, AFM-IR combination allows for detection of vibrational information at the nanoscale level, as opposed to the micrometer scale for conventional IR spectroscopy [100]. Focused ion beam scanning electron microscopy (FIB-SEM) is another microscopy technique that has recently been utilized to detect AAPS in a spray-dried felodipine-PVP dispersion [12]. The FIB provides the "cutting tool" to produce a thin slice on the spray-dried particles, which is then followed by imaging via SEM at each cross section of the particles. Based on the SEM images of multiple sizes of particles, it was observed that porous particles were produced with particles >10 μm and AAPS was observed with particles >20 μm as contrast in the SEM images was present. The presence of AAPS was confirmed by electron dispersive X-ray spectrometer installed within the SEM that shows heterogeneity of chlorine content, which represents felodipine concentration in the particles.

Other techniques include dynamic vapor sorption (DVS), inverse gas chromatography (IGC), and density measurement. DVS may provide information on amorphous content as amorphous materials tend to be hygroscopic [101]. Several studies have shown the utility of IGC to monitor the rapid surface crystallization event [14, 102]. Density measurement can be performed to quantify amorphous materials because these

materials exhibit a significantly lower density than crystalline materials. Pycnometry, either gas or liquid, is typically used for density measurement [20, 47].

In summary, although by no means has this section captured all the available analytical tools, several commonly employed techniques and others that may perhaps be used more extensively in other fields than in the pharmaceutical arena are presented here. In addition, it needs to be stressed that no single technique can provide a holistic information of the glassy state, thus the use of an orthogonal approach is encouraged. As such, discretion should be employed by addressing the following questions:

- *What information (e.g. miscibility, crystallization rate, phase transition, etc.) is needed?*
- *What detection/analytical tools are available? What information can these available tools provide? What are the limitations of the available techniques?*
- *How much time is available for measurement?*

1.3 Bioperformance of ASD

When a solid dosage form are administered orally, the drug must undergo dissolution in the GI fluids and achieve a concentration sufficient for its absorption through the intestinal membrane. However, a combination of poor aqueous solubility and a high efficacious dose of the compounds in drug development pipelines lead to a high dose to volume ratio, i.e. a high dose number [103]. Herein, volume is defined as the theoretical liquid volume of 250 mL taken with administration of oral dosage form. The high dose number requires that formulations of such compound be designed in such a way that dissolution of the full dose occur within the timeframe of the GI transit. The enhancement in oral bioavaibility with the use of ASDs has been widely published [3,

104-106]. It is apparent that the superior bioperformance displayed by ASDs is due to the inherent free energy advantage of the amorphous drug over the crystalline state [107]. However, it has been reported that the use of ASD alone does not guarantee an improved bioperformance [3], thus several factors associated with the development of ASD need to be appropriately understood and will be discussed in this review. It is acknowledged that bioperformance is a complex process and other factors such as lack of biorelevance or in vivo predictability using current in vitro methods [108-110] as well as biological transporter/metabolism interplay [111, 112] could significantly alter ASD bioperformance. These topics, however, are out of the scope of this review and will not be discussed further here. Instead, the Bioperformance section of this review focuses on the physical chemistry mechanisms by which ASDs improve the bioperformance of the API and highlights recent modeling work on these mechanisms.

Mechanisms for bioperformance enhancement by ASD:

1. Supersaturation (solubility enhancement)
2. Dissolution enhancement
3. Permeability enhancement

1.3.1 Supersaturation

The equilibrium solubility of a crystalline drug is a solid-liquid equilibrium and is reached when the chemical potential of the solid crystalline drug ($\mu_{D,crystal}$) equals the chemical potential of drug molecules present in solution ($\mu_{D,solution}$). In other words, the rate at which the crystalline solid dissolving is equal to that of crystallization from drug in solution; this is shown as Scenario A. Since majority of drug candidates exhibit very

low equilibrium solubility in water, one may add solubilizing excipients [113] to increase the drug concentration in solution. This addition of solubilizing excipients lowers $\mu_{D,solution}$ and allows more crystalline drug to dissolve. Although this solubilizing technique has been shown to increase drug oral bioavailability [114-116], readers should note that the use of solubilizing excipients may lead to undersaturation (Scenario B), which leads to decreased bioavailability. For instance, let us consider two formulations of the same drug at the same dose: formulation 1 containing drug suspension in water and formulation 2 containing a drug solution in a surfactant system such that the drug concentration is below its crystalline solubility. Although the total dissolved drug concentration is higher in formulation 2, the driving force for absorption (free drug concentration), $\mu_{D,solution}$, is lower compared to that of formulation 1. An analogous scenario may also occur with food intake, which perhaps may explain negative food effect phenomena. Furthermore, supersaturation (Scenario C) is a state where the chemical potential of the drug in solution is higher than that of the crystalline solid (note that supersaturation occurs in the absence of the crystalline solid), which is the desired scenario for maximal ASD bioperformance.

$\mu_{D,solution} = \mu_{D,crystal}$	A. Equilibrium solubility (saturation)
$\mu_{D,solution} < \mu_{D,crystal}$	B. Undersaturation
$\mu_{D,solution} > \mu_{D,crystal}$	C. Supersaturation

Although the use of chemical potential is a useful tool to understand the concept of supersaturation, it is difficult to measure the absolute value of a chemical potential. Thus, thermodynamic activity, which is a change in chemical potential with respect to a

standard state as shown in Eq. 1.1, is typically used instead. For simplicity of the discussion, the chemical potential of the crystalline drug dispersed in aqueous media at the crystalline solubility limit is used as the standard state. The extent of supersaturation can then be calculated by the activity ratio, a_R, as shown in Eq. 1.2. a_R represents the ratio between drug thermodynamic activity at a given concentration in solution ($a_{D,solution}$) to the activity at the crystalline solubility ($a_{D,saturation}$). In addition, each of the activity terms in both the numerator and denominator is a product of the activity coefficient (γ_D) and the drug concentration in solution ($C_{D,solution}$ or $S_{crystal}$). Unfortunately, laboratory measurement of the activity coefficient is not straightforward. Hence, the extent of supersaturation is often calculated by supersaturation ratio (SR), which is the ratio of drug concentration in solution to the crystalline solubility as shown in Eq. 1.3, which neglects the activity coefficient terms [2]. While this approach may be valid to calculate supersaturation for certain conditions such as that in dilute solution, where $\frac{\gamma_{D,solution}}{\gamma_{D,crystal}} \approx 1$ as shown in Eq. 1.4, this assumption may not be valid in environments where solubilizing additives are present. Recently, Setiawan et al. has developed a practical approach to measure a_R by utilizing diffusion cells as shown in Chapter 3. This approach was shown to effectively measure a_R in systems containing solubilizing additives.

$$a_{D,solution} = e^{\frac{\mu_{D,solution} - \mu_D^0}{RT}} \text{ where } \mu_D^0 = \mu_{D,crystal} \qquad [1.1]$$

$$a_R \equiv \frac{a_{D,solution}}{a_{D,saturation}} = \frac{\gamma_{D,solution} * C_{D,solution}}{\gamma_{D,crystal} * S_{crystal}} \qquad [1.2]$$

$$SR = \frac{C_{D,solution}}{S_{crystal}} \qquad [1.3]$$

$a_R \approx SR$ ($\frac{\gamma_{D,solution}}{\gamma_{D,crystal}} \approx 1$ for dilute solution) [1.4]

Supersaturation ($\mu_{D,solution}$) can only be increased up to a certain limit, i.e. its amorphous solubility. In other words, the amorphous solubility is the highest absorption driving force that may be achieved when ASDs are employed [117]. This limit is also known as a critical aggregation concentration [118-120]. Hence, it is critical to quantitatively measure and predict the amorphous solubility of a drug candidate. Assuming that the crystallization rate is slow, continued addition of drug in a supersaturated solution will result in an amorphous drug phase separation from the drug in solution. At this point, the chemical potential of supersaturated drug in aqueous solution is equal to that of the water-saturated drug amorphous phase ($\mu_{D,solution} = \mu_{D,amorphous}$). As noted previously, the absolute value of chemical potential is difficult to measure, thus the energetics advantage of the amorphous material over its crystalline counterpart may be calculated from the difference between the chemical potential of the amorphous and the crystalline materials. Hoffman initiated the development of equation describing this energetics advantage as shown in Eq. 1.5 [121]. Murdande et al. [122] recently extended this equation with correction for water activity and ionization as shown in Eq. 1.6. Note that it is quite challenging to produce a completely pure amorphous drug, since amorphous materials tend to be quite hygroscopic, thus a correction factor is necessary for a more accurate estimation of the amorphous solubility advantage over its crystalline counterpart.

$$\mu_{D,amorphous} - \mu_{D,crystal} = \Delta H_f \left(\frac{T_m - T}{T_m^2}\right) T \quad [1.5]$$

$$C_{amorphous} = C_{eq}\, x\, e^{\left[\frac{\mu_2^a - \mu_2^c}{RT}\right]}\, x\, e^{[-I(a_2)]}\, x\, \left(\frac{1-\alpha^c}{1-\alpha^a}\right) \quad [1.6]$$

where C_{eq} is crystalline solubility, $e^{\left[\frac{\mu_2^a-\mu_2^c}{RT}\right]}$ is free energy difference between the amorphous and crystalline forms and can be calculated using Hoffman approach in Eq. 1.5, $e^{[-I(a_2)]}$ is amorphous solute activity in solution, and $\left(\frac{1-\alpha^c}{1-\alpha^a}\right)$ is ionized fraction of amorphous solute (α^a) and of the crystalline solute (α^c), ΔH_f is melting enthalpy of the crystalline drug, T_m is melting temperature, and T is temperature of measurement.

From these equations, one needs to measure the crystalline solubility, melting point, melting enthalpy, water activity, and pKa (for ionizable compounds) to calculate amorphous solubility. Recently, Sadowski et al. [123] has developed a computational model utilizing perturbed-chain statistical associating fluid theory (PC-SAFT) that requires only few crystalline solubility data at different temperatures to estimate the amorphous solubility advantage. PC-SAFT treats organic molecules as a chain consisting spherical segments of a certain diameter with some fitted values from the experimentally determined crystalline solubility. The reported amorphous solubility for several drug compounds are in close agreement with the experimental values, which indicates that this approach may be beneficial in the early drug development pipeline where the amount of drug is quite limited.

In vitro tools to assess supersaturation limit

Several methods for laboratory measurement of amorphous solubility have been reported. One approach is to dissolve amorphous material in water as shown on the left of Figure 1.4 [122]. The maximum drug concentration achieved is taken as the amorphous solubility. The challenge with this approach is that it is difficult to produce a completely pure amorphous material, which is free from crystallization and defect. Thus, the

concentration observed may not accurately represent the true amorphous solubility. Another approach is solvent or pH shift where the drug is dissolved in a solvent or different pH, respectively, and titrated into an aqueous environment until an amorphous phase separation is observed as shown on the right hand side of Figure 1.4 [124]. This approach, however, requires a sensitive detection method and an impedance of crystallization if the drug is a rapid crystallizer. Nevertheless, a summary by Taylor et al. shown in Figure 1.5 demonstrated that the predicted amorphous solubility are in good agreement with the experimentally measured values regardless of the method [117].

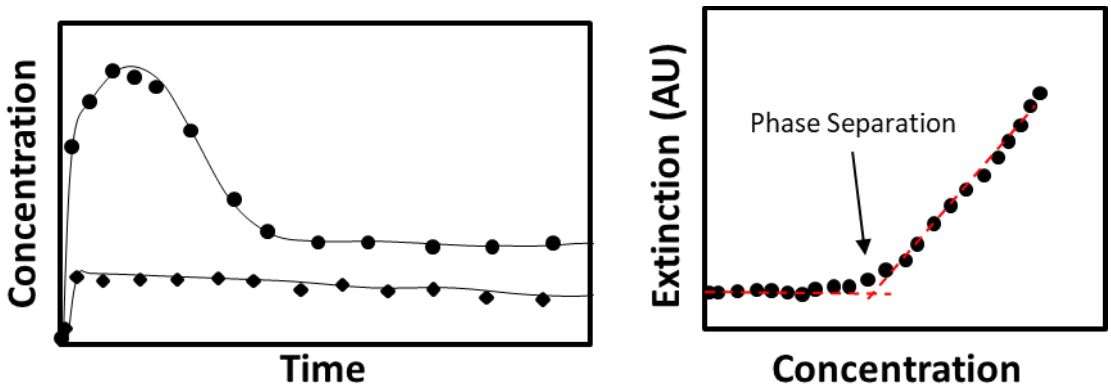

Figure 1.4 Cartoons showing in vitro methods for amorphous solubility determination. (Left) Dissolution of freshly prepared amorphous drug (filled circle) compared to its crystalline form (filled diamond) as illustrated by Murdande et al. [122] Amorphous solubility value is signified by the peak of the dissolution profile. (Right) Titration of dissolved drug in an organic solvent into an aqueous media as illustrated by Ilevbare et al. [124]. Amorphous solubility value is signified by the rise in absorbance in the high UV or visible range.

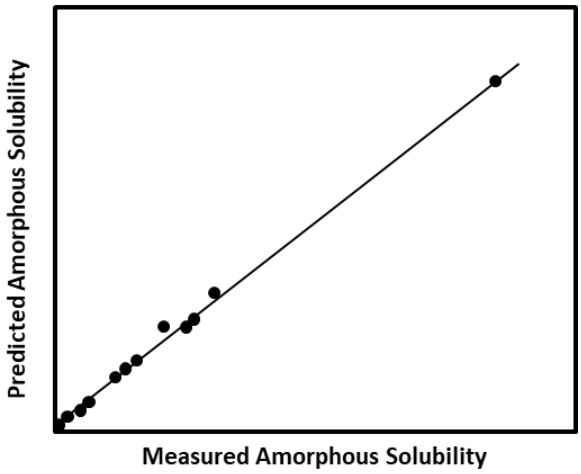

Figure 1.5 Cartoons of correlation plot between measured amorphous solubility of different compounds in vitro and its predicted values as calculated by the Hoffman equation. Adapted from Taylor et al. [117]

In vitro tools to assess the impact of excipients on supersaturation stability

To assess the impact of excipients on the stability of drug supersaturation, which will be referred to as 'parachute' in the following section, a "top-down" approach can be utilized (Figure 1.6). This approach can be accomplished by either solvent-shift or pH-shift methods. The goal is to dissolve the drug in a solvent or pH in which the drug is highly soluble then followed by a shift the media to an environment where the drug has a much lower solubility, thus creating a supersaturation state. Parachute effect due to excipients may be assessed by comparing the length of supersaturation to that in the absence of excipients. Various scales of volumes, from small (in the order of μL) to large (in the order of L), have been utilized depending on the available amount of the molecule tested [125, 126]. The length of supersaturation, which is also known as induction time, can be monitored by either measuring the drug concentration in solution or the formation of precipitate as a function of time. As precipitation is a kinetic process, it is best to use in

situ techniques that are capable of continuously monitoring drug supersaturation, such as UV dip probes [127, 128] or FBRM/PVM [129, 130]. While UV probes directly measure the drug concentration in solution, it may be difficult for these probes to distinguish UV absorbance of the dissolved drug from absorption and scattering due to particles formed when drug precipitation occurs. Second derivative technique may be used to eliminate this particle effect but submicron particles that scatter incident UV light may still obscure the concentration measurement [131-133]. Furthermore, FBRM/PVM technique may be used to directly observe the formation of particles in the media, but this technique is limited in that it does not provide any physicochemical properties of the formed particles besides particle size and morphology. Hence, FBRM/PVM technique is often coupled with a spectroscopy tool, such as Raman, IR, or near IR [130, 134, 135]. Ex-situ solid-state analyses of precipitate particles have also been used as a means to complement the results observed in solution. Techniques, such as scanning electron/polarized light microscopy, differential scanning calorimetry, or powder X-ray diffraction, may accommodate an understanding of the parachute mechanisms brought about by excipients [128, 136].

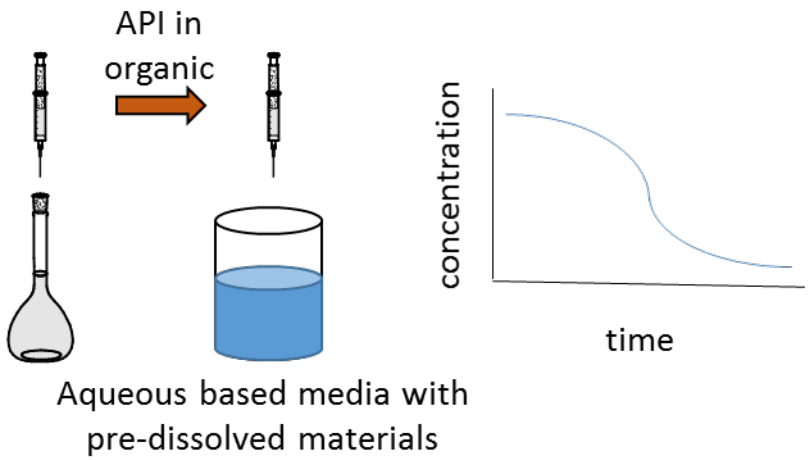

Figure 1.6 A “top-down” approach for evaluation of parachute effect from excipients.

1.3.2 Dissolution enhancement

The general dissolution process of ASDs follows the so-called “spring and parachute” concept [116]. ASDs contain a high-energy amorphous drug, which enable a rapid dissolution such that the intraluminal concentration reaches above the saturation solubility of the drug; this state is called the “spring.” For this strategy to be useful, the supersaturated solution must be stabilized for an adequate period to allow for significant absorption and thus enhance bioavailability. The stabilization of a supersaturated solution can be accomplished by adding precipitation inhibitors e.g. polymers, surfactants, which may act through a variety of mechanisms; this is called the “parachute.” Therefore, the success of ASDs depends on its ability to produce the spring and parachute effects.

Dissolution phenomenon may be described by the Noyes-Whitney equation below

$$\frac{dX}{dt} = \frac{\boldsymbol{A}\cdot D}{h}(\boldsymbol{C_s} - C_b) \qquad [1.7]$$

Here, X is the amount of dissolved drug, t is time, A is the surface area available for dissolution, D is the diffusion coefficient of the drug molecule, h is the thickness of

the boundary layer adjacent to the dissolving drug surface, C_s is the saturation solubility of the drug in a particular media, and C_b is the bulk drug concentration. Terms in bold indicate factors that may be modified by formulation approaches. ASDs typically demonstrate higher dissolution rate compared to crystalline API due to its higher solubility (i.e. amorphous solubility) [122, 124, 137] as indicated in the Supersaturation section above. ASDs will continue to dissolve until C_b is equal to C_s. Thus, the maximum achievable drug supersaturation in solution is the amorphous solubility where the amorphous drug in the ASD solid matrix is in "equilibrium" (assuming no crystallization occurs within the timeframe of GI transit) with the dissolved drug. Therefore, the amorphous-to-crystalline solubility, as discussed above, has a critical implication on bioperformance as this ratio dictates the extent of bioavailability enhancement possible by ASD. A wide range of amorphous-to-crystalline solubility ratios has been reported in the literature, e.g. 4 for ibuprofen and 65 for atazanavir [117, 138], indicating that formulating a drug as an amorphous product may not necessarily translate to the same bioavailability enhancement across different drug molecules.

Often the mechanism by which ASDs dissolve is probed using an empirical approach where the explanation around the phenomenon is inferred from the observation of the API dissolution profile. To date, we are not aware of any mathematical model that adequately describes the dissolution process of multicomponent ASDs, suggesting that our current understanding of ASD dissolution is still limited. In addition, although it is recognized that ASDs are multicomponent in nature, research has been mainly focused on the drug dissolution profile. We believe that the success of ASDs in achieving the desired bioperformance may be predicted by understanding the multiple events that are

simultaneously occurring when ASDs are introduced into an aqueous environment. In a simple case of an ASD consisting of a drug and a polymer, multiple events including water ingress, polymer chain relaxation with volume expansion or swelling, drug diffusion, drug dissolution, and polymer dissolution may occur. Higuchi [139] initiated the work to interrogate the release behavior of a drug out of a solid matrix where drug diffusion is the main motive of release. Although Higuchi equation is simple and practical, it has many inherent assumptions and limitations such that caution should be exercised with the application of this approach. Examples of these limitations, among many, are that it assumes a thin film (not a three-dimensional release), it does not consider the effects of polymer swelling, and it assumes a fixed boundary layer, which may not be true if the polymer dissolution is accounted for. Recently, a more comprehensive mathematical model has been developed by Peppas and co-workers to describe the drug dissolution phenomenon [140]. Although originally developed for HPMC-based matrix tablets and water-soluble drugs, this new model was claimed to be valid for poorly water-soluble drugs and other HPMC type and derivatives including HPMCAS, which has emerged to be a commonly used polymer in ASD formulations. Thus, we believe that extending this equation to ASDs coupled with *in situ* characterization tools [129, 131] will aid in a better understanding of the ASD dissolution process.

Formation of in-situ nanoparticles

Another term that is critical to the dissolution rate is the surface area, A term in Eq. 1.7. Particle size is a key determinant to surface area. It has been well documented

that dissolution of ASD leads to the generation of nanoparticles and such size reduction may further accelerate the dissolution process. For instance, recently Harmon et al. reported the formation of anacetrapib nanoparticles as a result of fast dissolution of copovidone out of the ASD solid matrix [141]. Interestingly, the authors found that the size of nanoparticles, which ranges between 50-200 nm, varies depending on the surfactant concentration present in the ASD. Friesen et al. also observed drug/polymer colloid nanoaggregates of 20-300 nm size, which the authors claimed to rapidly exchange with the free drug in solution [142]. Nanoparticles of 200-500 nm size were also observed by Alonzo et al. following a dissolution of low drug loading ASD (90:10 polymer/drug ratio) [133]. However, the authors observed that dissolution of high drug loading ASD (50:50 ratio) did not generate nanoparticles. The authors also noted that although the drug concentration generated by the two drug loadings was the same, the generation of nanoparticles with the low drug loading provided a faster dissolution rate. Other studies have also reported the generation of nanoparticles following ASD dissolution [22, 143-145], suggesting that formulators ought to be aware of this mechanism as another potential avenue to maximize ASD bioperformance.

Speciation

Another dimension of complexity in the dissolution of multicomponent ASDs is the potential formation of several drug species, such as dissolved/free drug, amorphous nanoparticles, micellized/complexed drug, and crystalline drug precipitates (Figure 1.7). Solution-state aggregates may be formed by both formulation excipients as well as by endogenous materials present in the body. Examples of these aggregates include micelles

created by surfactant above its critical micelle concentration [146, 147], aggregation of polymer with surfactant molecules to form “pearl-necklace shaped” aggregates [148, 149], polymer gelling/colloidal formation [142, 150], vesicle or mixed micelle formation by different types of surfactant molecules [151-153]. Although extensive research on the solubilization of poorly water-soluble drug molecules by the aforementioned aggregates has been studied, knowledge on the impact of these aggregates on the supersaturated state is still meager. Qi et al. [149] showed some degree of swelling by these aggregates as well as a change in the micelle shape from spherical to cylindrical form when spray dried particles are dissolved, although it was difficult to assess from this study whether the resulting drug concentration corresponds to supersaturation. Indulkar et al. recently reported micelle swelling phenomenon at high supersaturation, suggesting that more drug molecules are packed into the micelles at high supersaturation [154]. Micelle solubilization at the supersaturated state is also discussed in Chapter 3, which uses estradiol and polysorbate 80 as model compounds. Furthermore, the kinetics of solute solubilization into micelles are very rapid, in the order of milliseconds [155, 156]. Thus, one could expect that the rate at which these aggregates replenish the free drug molecule is faster than that of the dissolution out of the ASD matrix, which is in the order of minutes [122, 133, 141]. Therefore, speciation induced by excipients may provide additional bioperformance advantage.

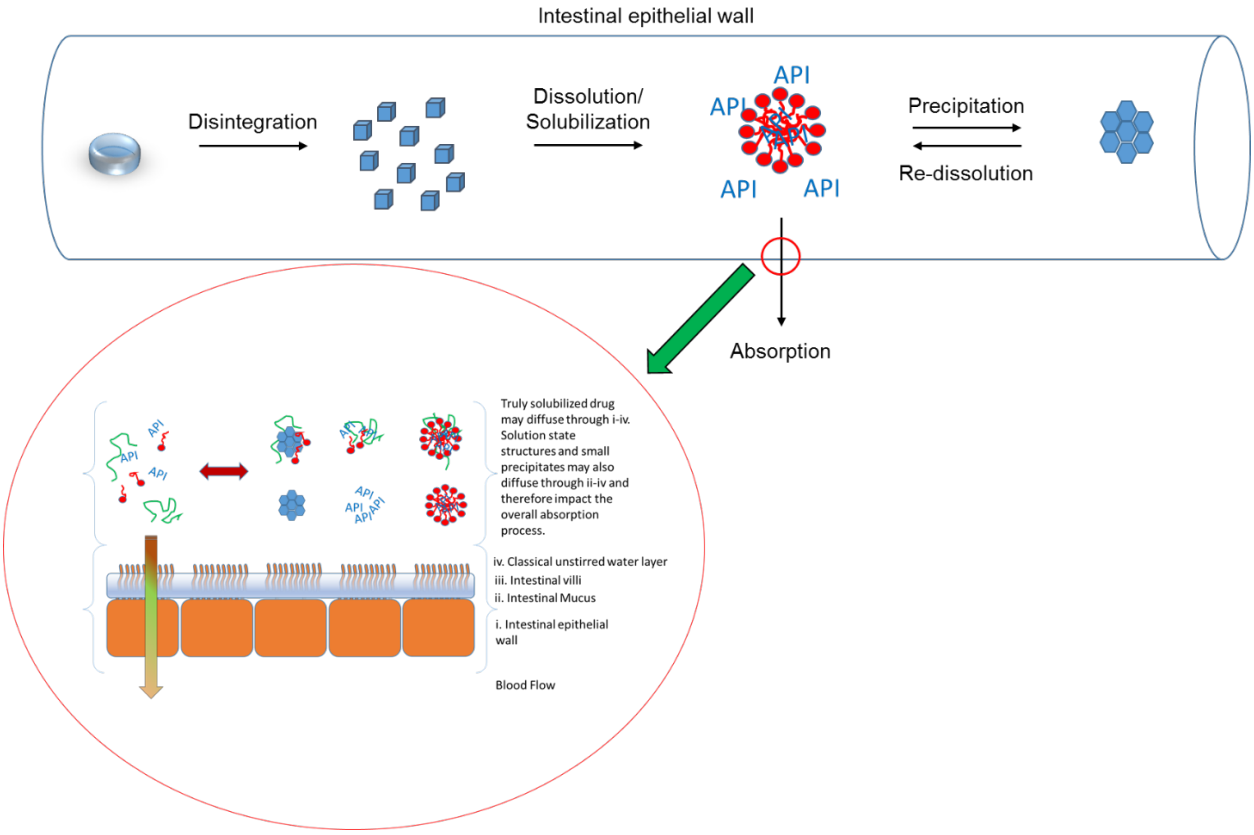

Figure 1.7 Illustration of various events experienced by an ASD formulation as it traverses through the GI tract prior to absorption to the systemic circulation.

In vitro tools to assess extent of "spring and parachute" of ASD

Given the importance of the attained supersaturation on the bioavailability enhancement, it is imperative that adequate in-vitro methodologies be designed to precisely measure the degree of supersaturation that are applicable for the prediction of in-vivo supersaturation. Dissolution experiments ('bottom up' approach in Figure 1.8) are usually performed to assess the extent of "spring and parachute" of ASD. Although USP type II dissolution apparatus has been traditionally used for dissolution measurements, Augustijns et al. pointed out a need for better harmonization among different institutions as well as a more biorelevant system for dissolution measurement [136]. The spring and

parachute may be monitored by either in situ measurement (e.g. UV probes) or ex situ (e.g. HPLC or NMR). Although the benefits of UV probes with online and less labor-intensive measurements are obvious, HPLC may be coupled with various kinds of detectors, which may offer other critical benefits such as simultaneous quantification of excipients concentration. As discussed above, not only the dissolution of the drug but also that of the excipients need to be considered in order to obtain a holistic understanding of ASD bioperformance. Unfortunately, most of the commonly used excipients lack UV chromophore, thus UV probes or detectors alone are insufficient. Several detectors, such as refractive index (RI), evaporative light scattering detector (ELSD), and charged aerosol detector (CAD) are available for detection of these non UV-absorbing compounds [157]. Therefore, utilization of these technologies needs to increase in the pharmaceutical arena.

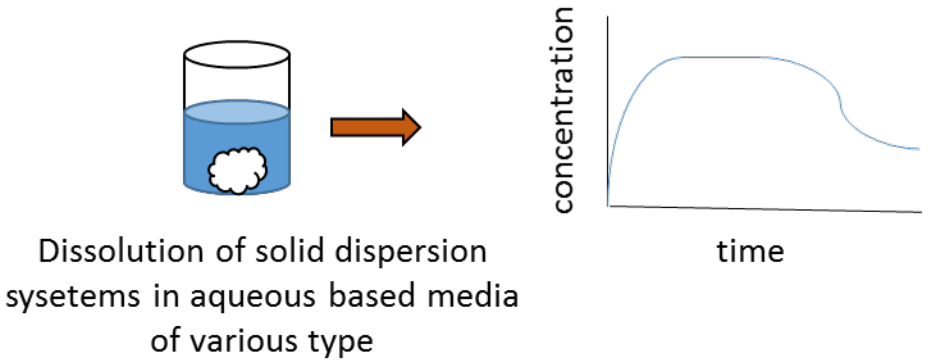

Figure 1.8 A “bottom-up” approach for evaluation of spring and parachute events from an ASD.

Impact of excipients on ASD dissolution

Various polymers, such as PVP, PVP-VA, HPMC, and HPMC-AS have been evaluated for their impact on the extent of spring and parachute [133, 158-160]. These studies suggest that an amphiphilic polymer generally provides superior performance of an ASD. The polymer amphiphilicity advantage can be thought of a balance between rapid dissolution provided by the hydrophilic portion coupled with supersaturation maintenance provided by the hydrophobic portion [145, 161]. For instance, several authors [142, 162] observed a correlation between compounds log P and melting temperature with their associated dissolution and crystallization kinetics, respectively. These authors suggested that an amphiphilic polymer with a slightly more hydrophilic or hydrophobic property be selected to compensate for a slow dissolution rate or a fast crystallizer, respectively. Qian et al. [159] observed a rapid "escape" of PVP-VA in the dissolution profile of BMS-A/PVP-VA, which resulted in the rapid crystallization of BMS-A in the solid matrix and the subsequent poor BMS-A dissolution. On the other hand, despite slower drug dissolution, HPMC-AS was able to maintain drug supersaturation in solution for over 24 hours, which in turn resulted in an increased bioavailability. DiNunzio et al. conducted a study on the supersaturation maintenance ability as well as the dissolution behavior of itraconazole ASD using three different grades of HPMC-AS [163]. The authors observed that the HF grade, which is the most hydrophobic out of the three grades, showed a superior maintenance of itraconazole supersaturation. However, the most hydrophilic grade, i.e. LF grade, provided the highest oral bioavailability among the three grades due to its faster dissolution. These results

pointed out that polymer amphiphilicity could bring a significant influence on ASD bioperformance.

Drug loading in the ASD matrix has also been shown to play an important role in the drug dissolution profile. Several reports [133, 143, 145, 164-168] have demonstrated drug-controlled and polymer-controlled regimes of dissolution at high and low/intermediate loading, respectively. Interestingly, in these studies, the drug dissolution rate at high drug loading is slower than that of low/intermediate drug loading. The proposed dissolution mechanism at low and intermediate drug loading is that the polymer dissolves rapidly which is then followed by drug dissolution into the viscous polymer-rich layer, such that the release of the drug is dependent on the polymer release. The polymer-rich layer may also lower the drug thermodynamic activity of the drug, allowing for rapid dissolution of drug out of the ASD matrix. In contrast, at higher drug loadings, the hydrophobic drug molecules are more likely to dominate the surface of ASD and thus the dissolution rate may be controlled by the properties of the drug itself. Therefore, in the absence of a large surface area drug dissolution may be slow despite the amorphous character of the drug in the ASD matrix.

1.3.3 Permeability enhancement

Although different solution-state aggregates may be present in solution as described by the inset in Figure 1.7, the driving force for absorption is the molecularly dissolved drug, i.e. drug thermodynamic activity. Absorption across a membrane is described by Fick's law (Eq. 1.8), where J is flux or mass transport per area per time, V is bulk volume, A is membrane surface area, C_b is bulk drug concentration (the same term

in Eq. 1.7), t is time, P_{eff} (Eq. 1.9) is effective permeability, a (Eq. 1.10) is drug thermodynamic activity, D is drug diffusion coefficient, K is membrane/water partition coefficient, h is membrane thickness, and γ is activity coefficient.

$$Flux(J) \equiv \frac{V}{A}\frac{dC}{dt} = \boldsymbol{P_{eff}x\ a} \quad [1.8]$$

$$P_{eff} = \frac{DK}{h} \quad [1.9]$$

$$a = \gamma C_b \quad [1.10]$$

As seen in Fick's law above, flux can be enhanced by not only an increase in thermodynamic activity, which has been discussed in the Supersaturation section, but also by an increase in drug intestinal permeability. Effective drug permeability consists of both permeability through the unstirred water layer (UWL) and permeability through the epithelial cell membrane. Sugano [169] developed equations to describe the aforementioned permeability as shown in Eq. 1.11-1.14 below.

$$\frac{1}{P_{eff}} = \left(\frac{1}{P_{ep}} + \frac{1}{P_{UWL}}\right)\frac{1}{FE} \quad [1.11]$$

$$\log P_{ep} = 1.1(\log P_{oct}) - 5.63 \quad [1.12]$$

$$P_{UWL} = \frac{D_{eff,UWL}}{h_{eff}} + P_{wc} \quad [1.13]$$

$$D_{eff,UWL} = D_{mono} \cdot f_{mono} + D_{bm} \cdot (1 - f_{mono}) \quad [1.14]$$

where P_{eff} is the effective permeability, P_{ep} is the epithelial cell membrane permeability, P_{UWL} is the UWL permeability, FE is the surface area expansion coefficient of the fold structures in the small intestine, P_{oct} is the drug octanol-water partition coefficient, $D_{eff,UWL}$ is the effective diffusion constant in UWL, h_{eff} is the effective thickness of UWL, and P_{wc} is the permeability coefficient by water convection, D_{mono} is the diffusion

coefficients of unbound monomer molecules, D_{bm} is the diffusion coefficient of bile micelle-bound molecules in the UWL, and f_{mono} is the fraction of free monomer. f_{mono} can be calculated as the ratio of solubility in blank buffer (S_{blank}) and bile micelle media ($S_{dissolv}$) ($f_{mono} = S_{blank}/S_{dissolv}$). D_{mono} can be calculated using Avdeef's method [170].

Epithelial permeability, P_{ep}, of a drug is generally a function of its hydrophobicity, P_{oct}, although the presence of permeation enhancers, including endogenous bile salt, may also increase epithelial permeability by the reversible process of intestinal cell abrasion and denudation [171-173]. UWL permeability, P_{UWL}, is dictated by the Brownian motion of drug molecule in UWL. Nanoparticles, which may be formed during ASD dissolution, may diffuse into the UWL and decrease the h_{eff}, thus increasing the P_{UWL} [174]. This phenomenon has been termed by Sugano as "particle drifting effect" [174].

An example of the effect of nanoparticles on P_{eff} is shown in Table 1.2. A hypothetical molecule with a molecular weight of 400, a logP of 4, FaSSIF solubility of 10 µg/mL and aqueous solubility of 1 µg/mL was used for illustration. Using the equations shown above, the calculated P_{eff} for this molecule is 1.70×10^{-4} cm/sec. As shown in the table below, depending on the dose administered the nanoparticles can provide significant enhancement in P_{eff} for this molecule as compared to the original P_{eff}.

Table 1.2 Hypothetical example of the effect of nanoparticle drifting on effective human permeability

Dose (mg)	% nanoparticles in formulation	Effective dose in nanoparticles (mg)	Particle size (nm, radius)	Calculated P_{eff} (x 10^{-4} cm/sec)
10	70	7	50	1.73
20	70	14	50	2.66
50	70	35	50	4.98
100	70	70	50	7.66

Other studies have also demonstrated P_{eff} enhancement due to nanoparticles. For example, Lenhardt et al. showed that nanoparticles increased the flux across Caco-2 monolayers [175]. Frank et al. and Lian et al also showed enhanced permeation through Caco-2 monolayers due to nanoparticles generated from ASD dissolution [176, 177]. Further, Yildiz et al. showed that nanoparticles in the order of hundreds of nanometers are capable of diffusing through the mucus in in vitro studies [178]. In the same study, Yildiz et al. also demonstrated that particle size, surface chemistry, and intestinal contents have a significant impact on diffusivity through mucus, which constitutes as the major component in the intestinal membrane UWL.

In vitro/in vivo tools to assess drug permeability

Several techniques available for the prediction and measurement of drug intestinal permeability include PAMPA or well plate with Caco-2 cells [170], diffusion cells (utilizing either synthetic membrane or excised tissue) [179-182], and in vivo perfusion [181, 183]. Avdeef [170] has shown a high correlation between Caco-2/PAMPA and human jejunal permeability (HJP) as shown in Figure 1.9, demonstrating the utility of these in vitro techniques. Although high correlation is observed, most of these studies were performed to measure the intrinsic drug permeability in the absence of excipients. Thus, it is intuitive to extend this work to systems containing potential excipients used in ASD and confirm the validity of these techniques in predicting intestinal permeability when excipients are present, especially at the supersaturated state. Recently, dissolution/permeation system (often called D/P system) has emerged as a tool to simulate the dissolution and permeation behaviors of a formulation simultaneously, which may serve as an additional bioperformance predictor in early drug development pipeline [184, 185].

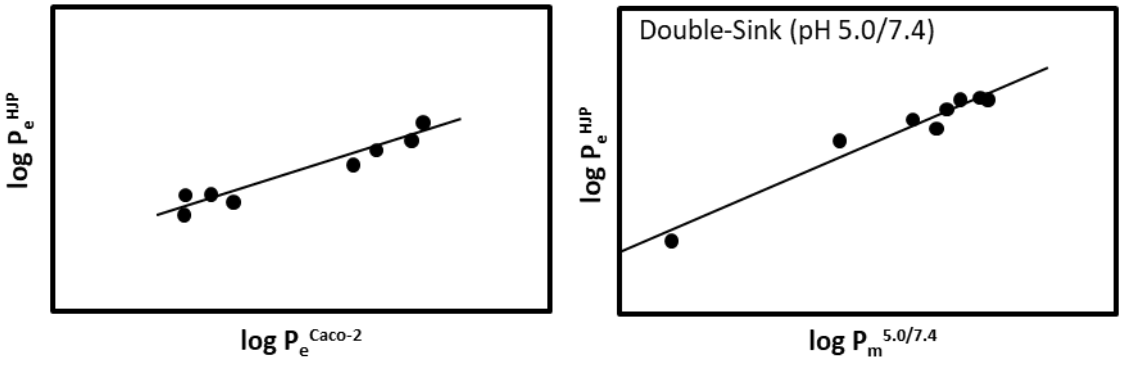

Figure 1.9 Cartoons showing summary of in vitro and in vivo permeability (P_e) data of several compounds by Avdeef et al. [170]. (Left) Correlation plot between in vitro Caco-

2 and in vivo human jejunal permeability (HJP) from compilation of Artursson's laboratory at Uppsala University. (Right) Correlation between double-sink PAMPA and HJP developed by Avdeef. Double sink PAMPA utilizes pH 5.0 and 7.4 as donor and acceptor media, respectively. P_m is the P_e value with UWL correction.

1.3.4 Physiologically based pharmacokinetic (PBPK) modeling for ASD

The complex dissolution characteristic of ASD and the disparate mechanisms by which ASD enhances bioperformance makes it essential that the factors impacting their bioperformance be clearly understood. Therefore, it will be beneficial to expand the application of physiologically based absorption modeling to these formulations since modeling can be performed early in drug development process without consuming the limited amount of API at this stage. However, to date there are not many published reports available on simulation of absorption ASD in particular. While the principles of absorption from supersaturated solutions have been studied [186], publications on applications of such models during product development are very limited. Gao et al. [187] examined the prediction of ASD performance, among other formulations, for rat toxicology studies, while more recently Zheng et al. [188] discussed the utility of PBPK models in the discovery space to drive utilization of ASD. In addition, physiologically based absorption modeling to predict ASD bioperformance in human have been recently published by Mitra et al. [189]. The authors highlighted three cases: 1) ASD with complete absorption, 2) ASD with decreased fraction absorbed with dose escalation and 3) ASD with incomplete and low absorption. These examples covered a wide spectrum of ASD bioperformance and strategies to model each of the case scenarios were discussed.

Thus, these examples demonstrated the utility of these models in providing early forecast of ASD bioperformance, which will provide mechanistic understanding of critical factors affecting ASD bioperformance and thereby aid the development of a drug product that will deliver the optimal benefit to patients. Furthermore, it is expected that the impact of speciation towards ASD bioperformance be part of future studies in PBPK modeling area to provide a holistic view of ASD absorption.

1.4 Objectives

The overarching goal of this dissertation is to gain a molecular level understanding of factors affecting the drug thermodynamic activity in both the solid and solution state. In the solid state, a hypothesis around the relative impact of manufacturing and storage conditions on ASD bioperformance, i.e. drug activity, was tested. In the solution state, the hypotheses on how drug activity changes with speciation and the impact of this activity change on crystallization were evaluated. As such, the following specific aims were conducted to test these hypotheses:

1. Perform literature survey to gauge the relative thermodynamics magnitude of each processes in which ASDs may be exposed to (Chapter 2)
2. Evaluate the change in drug activity in solution in the presence of solubilizing excipient with the use of side-by-side diffusion cells (Chapter 3)
3. Assess the impact of drug activity change resulted from the use of solubilizing excipient towards drug crystallization kinetics (Chapter 4)

Chapter 2 - The Amorphous Energy Landscape

2.1 Introduction

Delivering poorly soluble active pharmaceutical ingredient (API) via the amorphous form may improve the kinetic drug solubility, dissolution rate, and oral bioavailability [20]. Although amorphous materials have a higher free energy compared to the associated crystalline form, little work has been done to understand the changes in chemical potential of the API throughout formulation and delivery processes. Specifically, the change in chemical potential resulting from mixing the API with polymer and in the presence of moisture at room temperature is particularly difficult to measure and, therefore, is largely unexplored with the exception of a few recent publications [26, 190, 191]. Further, API-polymer interactions and API chemical potential will be a function of the processing conditions (mechanical stress, exposure to various solvents, thermal stresses, etc.). For instance, if an amorphous composite is produced via the spray drying process or via the co-precipitation process, it is important to understand the potential for formation of solvates as a function of solvent/co-solvent activities and or pH [192]. Alternatively, if an amorphous composite is produced via hot-melt extrusion, the chemical potential as a function of temperature becomes an important aspect towards understanding phase behavior and the resulting impact on finished product [19].

In order to maintain the API in its amorphous state, typically excipients such as polymers are mixed with the drug to create an amorphous solid dispersion (ASD). ASDs have been shown to sustain the physical stability of the disordered API in the amorphous

composite when the glass transition temperature is well above the storage temperature [193] and when processing spaces do not provide kinetic access to failure modes such as crystallization [194] or amorphous-amorphous phase separation [195]. Thermodynamically, the physical stability of ASDs is dictated by the miscibility and solubility limits. A system is said to be miscible when a mixture is homogeneous where the drug concentration is below the crystalline solubility limit or below spinodal decomposition limit. Between the spinode and the binode, amorphous-amorphous phase separation may occur via a process of nucleation of a discontinuous amorphous phase and a continuous amorphous phase. Practically speaking, producing an ASD in the thermodynamically stable region is ideal since in this region the API is truly "dissolved" in the polymer solid matrix. However, a high drug loading is often desired to reduce the manufacturing cost via increased throughput as well as to increase patient compliance, i.e. a smaller dosage form is desired. In addition, the performance of amorphous composites is a strong function of composition – some ASDs may gel when exposed to aqueous based media [141], some compounds may dissolve via different mechanisms as a function of composition [133, 145], and ultimately a change in bioavailability as a function of composition may occur [196]. The demand for high drug loading ASDs requires formulators to seek for ways to produce metastable ASDs that are stable during processing, storage, and GI transit. Ultimately, thermodynamic limits define the driving force for the observed kinetic processes. This chapter provides a summary of literature survey containing thermodynamic limits of each process experienced by ASDs and evaluate the relative thermodynamic values of each process.

2.2 Crystallization Energetics

As mentioned above, amorphous materials possess higher free energy than its crystalline counterpart does, which ultimately result in higher solubility and dissolution rate when the molecule is dissolved. In the same token, this high free energy places the molecules in a metastable state wherein the molecules possess some driving force for crystallization. For crystallization process to occur, molecules have to not only diffuse and coagulate but also be oriented such that the resulting orientation represents the crystal lattice. Due to the sluggish molecular diffusion in the glassy state [33] as well as the probability of achieving the correct orientation [197], crystallization rate may greatly vary depending on the experimental condition and the physicochemical properties of the molecule tested. Although the kinetics of crystallization is an important subject, this discussion will only focus on the thermodynamic factors affecting crystallization.

The calculation of crystallization driving force was initiated by Hoffman wherein the amorphous material is assumed to be a supercooled liquid at the temperature of interest [121]; this is shown in Eq. 2.1:

$$\Delta G_{a-c} = \Delta H_f \left(\frac{\Delta T \cdot T}{T_m^2}\right) \qquad [2.1]$$

where ΔH_f is the heat of fusion, $\Delta T = T_m - T$, T_m is the melting point, and T is the measurement temperature.

From this equation, it is clear that compounds with high heat of fusion will have a high crystallization free energy. This is exemplified in a study of hexitols crystallization conducted by Siniti et al. [198]. Eq. 2.1 has been shown to provide accurate prediction of the free energy change in small molecular weight organic molecules [199]. Hancock et al.

and, most recently, Sousa et al. followed up Hoffman's work with heat capacity correction that provides a more accurate prediction of the crystallization free energy [137, 138]. Note that free energy for crystallization is equivalent to the solubility advantage of amorphous materials over their crystalline counterpart (Section 2.5). Although the impact of enthalpy on crystallization is obvious, entropy effect is more difficult to assess. Zhou et al. observed that compounds with lower configurational entropy exhibit a faster crystallization process [197]. Configurational entropy can be assumed to be related to the number of assessable molecular conformations in the amorphous state and, thus, lower configurational entropy would result in higher probability to find the correct molecular orientation appropriate for the crystal lattice. However, this argument is counterintuitive when applied to the Gibbs free energy equation ($\Delta G = \Delta H - T\Delta S$) as both high enthalpy and entropy are required to result in high (crystallization) free energy, as opposed to having lower entropy. Hence, the entropy effect on crystallization may not be straightforward.

In an ASD, polymer interacts with API in such a way that there is a measurable solubility (ΔG_M in Section 2.4) of API in the polymer. Although it has been shown that miscibility can be achieved in the absence of strong API-polymer interactions such as hydrogen bonding [200], it is likely that higher solubility or miscibility at higher drug loading is more achievable with systems exhibiting strong API-polymer interactions than those in the absence of significant interaction. In a hypothetical system with a strong API-polymer interaction, the chemical potential of the API is significantly lower compared to the neat amorphous API and the crystallization driving force is no longer represented by the calculated value in Eq. 2.1. Therefore, it is intuitive to select polymer

system that would offer significant intermolecular interactions with the API to increase the level of mixing as well as reduce the drug crystallization energetics. Further, the presence of water as either moisture in storage or bulk water in dissolution process may significantly alter this level of mixing. These topics will be discussed further in Section 2.5.

2.3 Relaxation Energetics

If we produce an amorphous solid by quenching from the molten state at a temperature just below the melting temperature, without crystallization of the amorphous solid, the molecular mobility is high enough for the system to remain equivalent. However, as the temperature drops near or below the glass transition temperature (T_g), the molecular motion becomes so sluggish that an amorphous solid is created containing higher free energy compared to the equilibrium supercooled liquid (Figure 2.1). Upon annealing at a certain temperature below T_g, glasses will continue to relax into a lower energy state with gradual loss of enthalpy and free volume. The enthalpy lost upon annealing can be recovered by reheating to reach the equilibrium supercooled liquid state, the amount of which can be measured by thermal analysis techniques such as differential scanning calorimetry [201, 202]. Relaxation of the amorphous material can have an impact on the crystallization through both the change in thermodynamic driving force and the kinetic effect due to loss of molecular mobility upon relaxation.

The total enthalpy change that is required for the glass to relax to a supercooled liquid can be calculated by Eq. 2.2 [203]:

$$\Delta H_\infty = \Delta C_p\left(T_g - T_a\right) \qquad [2.2]$$

Among it, ΔC_p is the heat capacity difference between the glass and the supercooled liquid. T_g is the glass transition temperature, and T_a is the annealing temperature.

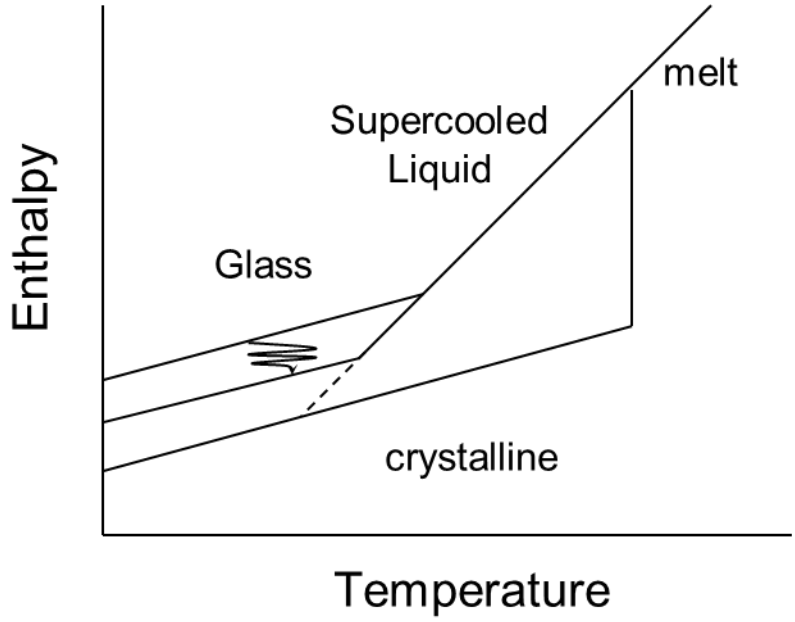

Figure 2.1 Enthalpy vs temperature diagram for a typical polymer, in the amorphous and crystalline states.

ΔH_∞ represents the theoretical highest recovery enthalpy that an amorphous glass can achieve at T_a. The relaxation kinetics of an amorphous material in the glassy state are non-linear in most of the pharmaceutical systems [201, 204] and expected to decrease with decreasing temperature and longer annealing time below T_g, which may sometimes make the measurement of the enthalpy of recovery challenging. ΔH_∞ is used here for comparison, to estimate the maximum thermodynamic impact relaxation can have on the crystallization process.

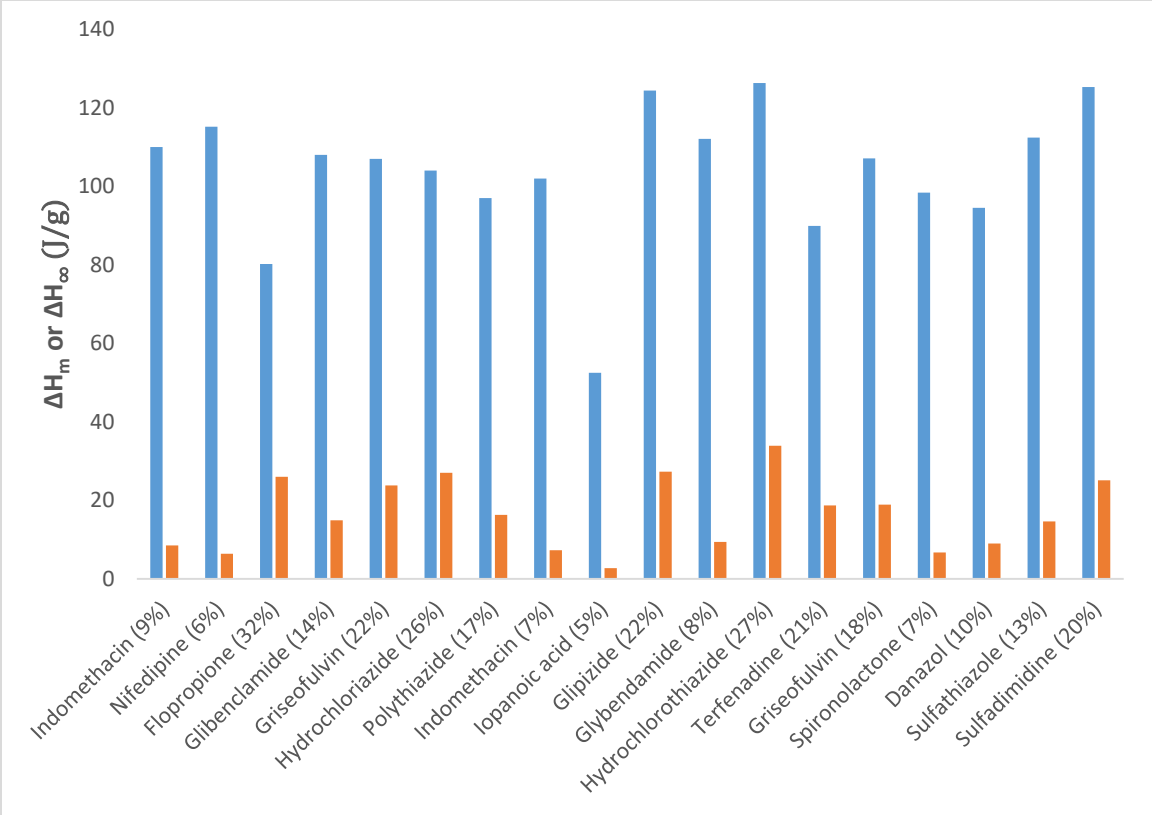

Figure 2.2 Values of melting (blue) and maximum theoretical recovery (orange) enthalpy of various API. Percent value in parentheses represents the relative percent of theoretical maximum enthalpy recovery to the melting enthalpy.

A survey of drug and drug-like compounds reveals that the theoretical maximum enthalpy of relaxation associated with neat amorphous materials ranges between 3-35 J/g at temperatures near room temperature (Figure 2.2). The enthalpy of relaxation counts for 5-30% of the enthalpy of fusion in the systems included in the survey. After correction of the enthalpy of crystallization is corrected to the temperature of interest (annealing temperature of 298K in most cases, see table C.1), the enthalpy of relaxation could represent an even larger overall change in the energetics of the system. This observation suggests that during annealing, some amorphous solids, especially those with steep heat capacity change upon glass formation, may lose significant driving force for

crystallization upon relaxation. This loss of driving force, combined with the lower molecular mobility of a relaxed glass, can reduce the risk of crystallization by a large extent. It is worth noticing, however, that some of the high enthalpy of relaxation is rooted in the big difference between the glass transition temperature and the annealing temperature. The molecular mobility in these systems at the annealing temperature could be too slow for the pharmaceutical relevant time window, and the effect might not be as significant. For example, it has been experimentally demonstrated that molecular processes that occur in a drug at a temperature of at least 50 K lower than its glass transition temperature are too slow to be significant over the entire lifetime of a typical pharmaceutical product [201, 202]. It also needs to be pointed out that the systems compared above could be potentially biased towards moderate to slow crystallizers, as it is challenging to render a strong crystallizer to the amorphous state, to gather the enthalpy of relaxation data [205].

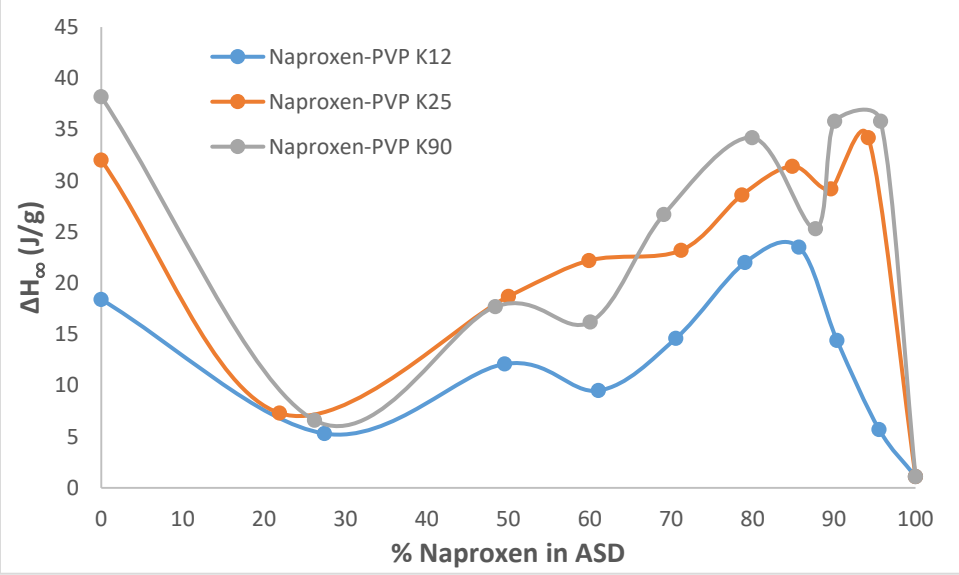

Figure 2.3 Relaxation enthalpy of naproxen ASDs with different PVP polymers as a function of naproxen ratio in the ASD.

In the presence of polymer as additive, the enthalpy of relaxation is mostly increased, as the total enthalpy change for polymer is generally higher than that of the small molecule due to the larger difference between the glass transition temperature and the annealing temperature (*Figure 2.3* and Table C.2). This suggests that the relaxation enthalpy of the API in the dispersion is miniscule compared to its own relaxation enthalpy as neat amorphous. The increase in the relaxation enthalpy is not likely the main reason for the improved physical stability of amorphous API in solid dispersion, however, as the increase is not very significant especially at high drug loading. It has been shown that even a small amount of polymer additive can effectively inhibit crystallization [206-208]. Further, a significant alteration in molecular mobility can also be observed when a small amount of polymer additive is added (Figure 2.4 and Table C.3). Valdecoxib and Etoricoxib solid dispersions with PVP K29/32 were annealed for 24 hours, and recovery enthalpy was reduced with 1% of polymer addition and minimal T_g change.

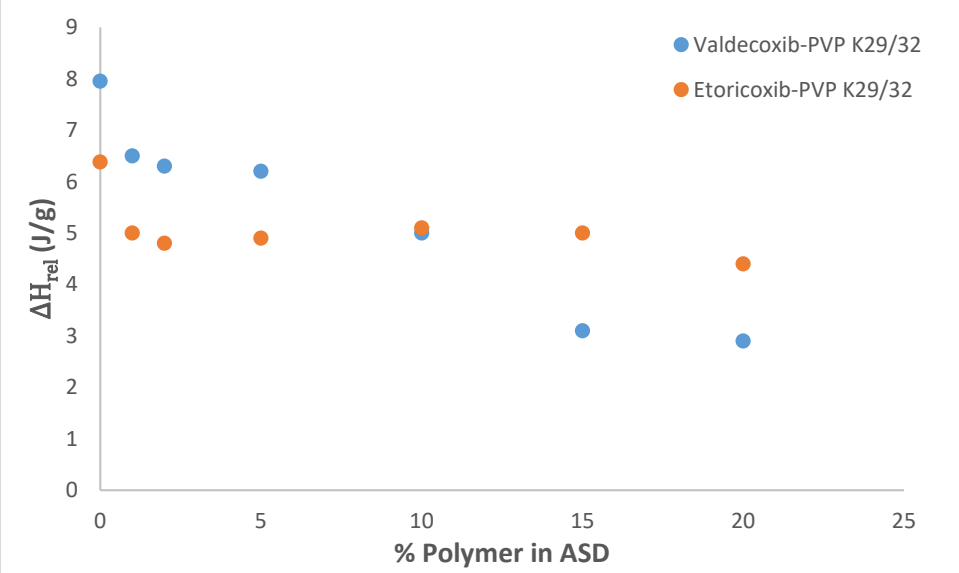

Figure 2.4 Relaxation enthalpy of valdecoxib and etoricoxib ASDs with PVP K29/32 polymer as a function of polymer ratio in the ASD.

2.4 Mixing Energetics

Countless papers have been published with the aim of understanding the energetics of ASDs [209]. Sample preparation method must be taken into consideration when evaluating ASD energetics. Specifically, although it is understood that mixing requires favorable free energy of interactions, the phase behavior as a function of processing, e.g. spray drying or hot-melt extrusion, must be considered in that the number of phases in equilibrium will be a function of the temperature and composition. Application of thermodynamic principles requires an understanding of whether the system is kinetically trapped or truly miscible (Figure 2.5).

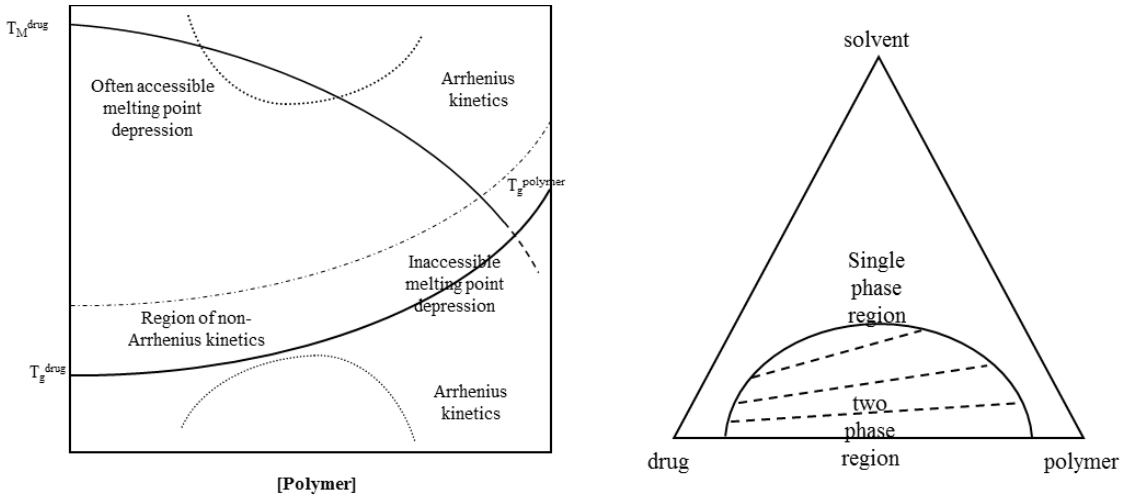

Figure 2.5 Example temperature vs composition (left) and ternary (right) phase diagrams of polymer-API dispersions.

Although improved physical stability of ASD compared to the neat amorphous API has been documented in the literature, the mechanism is not well understood [207, 208, 210-220]. Assuming a single-phase ASD is achieved, there are some attempted explanations proposed in the literature for the improved physical stability. For example, it was proposed that in most cases, polymer has a higher T_g compared to the API, therefore the T_g of the amorphous solid dispersion would be elevated, and the molecular mobility needed for crystallization will be reduced. Alternatively, if the chemical potential of the API is lowered through mixing with a polymer, the crystallization driving force, and hence crystallization nucleation rate, will thereby be reduced (Figure 2.6). Furthermore, if favorable intermolecular interactions between API and polymer reduces the intermolecular distances, the resulting loss of free volume will also reduce mobility needed for crystallization.

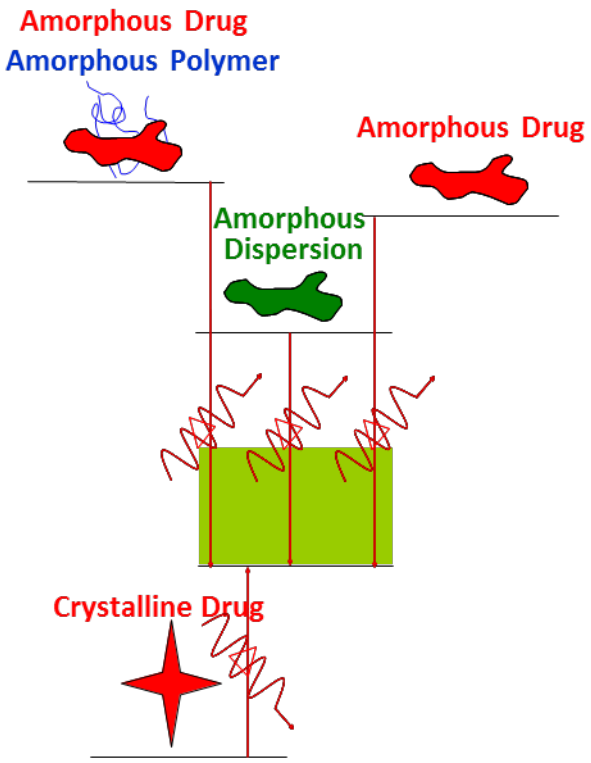

Figure 2.6 Example energy diagram of an API-polymer dispersion and its pure components.

Flory-Huggins lattice theory has been used as a good starting point to understand the thermodynamics of API-polymer systems with molecular size in consideration [221, 222], as shown in Eq. 2.3.

$$\Delta G_M = RT\left(n_{drug} \ln \Phi_{drug} + n_{polymer} \ln \Phi_{polymer} + n_{drug}\Phi_{polymer}\chi\right) \quad [2.3]$$

Here, n_{drug} is the number of moles of drug, $n_{polymer}$ is the number of moles of polymer, Φ_{drug} is the volume fraction of the drug, $\Phi_{polymer}$ is the volume fraction of the polymer, R is the gas constant, and T is the absolute temperature. χ is the Flory-Huggins interaction parameter, which describes the enthalpy change of bonding a monomer unit with an API molecule.

The enthalpy of mixing for a drug-polymer binary system can be given by the van Laar expression in Eq. 2.4.

$$\Delta H_M = \chi RT n_{drug} \Phi_{polymer} \quad [2.4]$$

The Flory-Huggins interaction parameter χ is the determining factor in terms of enthalpy contribution to the free energy of mixing: a negative or slightly positive value of χ will be needed to lead to a negative value of free energy of mixing, and thereby facilitate mixing. On the other hand, a highly positive χ indicates strong cohesive interaction within drug or polymer, and therefore the mixtures are less likely to form a single-phased amorphous system. The χ value can be determined through model fitting of experimental data, for example gathered from melting-point depression measurements [221], solution calorimetry measurements or theoretical calculation [223]. Depending on the experimental method that is used to measure the miscibility between amorphous API and polymer, the χ value can vary. In Table 2.4, the χ value in addition to the enthalpy and free energy of mixing calculated based on χ are summarized. Fifty percent drug loading was used for the calculation as this usually corresponds to the highest degree of API-polymer interaction. It can be seen that when the χ value is small, the enthalpy of mixing is relatively insignificant compared to the enthalpy of fusion. When χ has a large negative value, which indicates strong adhesive interaction between API and polymer, the mixing enthalpy and free energy effects are on the other hand quite significant. Similarly, a large positive χ value renders a high positive free energy of mixing, indicating a poor mixing between API and polymer.

Table 2.1 Calculated enthalpy and free energy of mixing values based on given χ values when drug content is 50 vol-% in various drug-polymer systems.

API	**Polymer**	**χ**	**ΔH_{mix}, J/g**	**ΔG_{mix}, J/g**	**ΔH_m, J/g**
Nifedipine	PVPK12	-2.5	-6.6	-11.4	115.2
Nifedipine	VA64	-1.8	-4.7	-9.5	115.2
Nifedipine	PVAc	0.0	-0.1	-4.8	115.2
Indomethacin	PVPK12	-8.2	-28.9	-35.4	110.0
Indomethacin	PVPK25	-8.0	-28.2	-34.5	110.0
Indomethacin	VA64	-4.5	-15.8	-22.2	110.0
Indomethacin	PVAc	-0.4	-1.4	-7.8	110.0
Felodipine	PVP K12	-0.1	-0.1	-2.9	80
Nifedipine	PVP K12	0.0	0.0	-2.9	115.2
Ketoconazole	PVP K12	-0.1	-0.1	-2.2	
Sucrose	PVP K12	0.0	0.0	-3.2	
Indomethacin	PVP K12	-0.8	-1.6	-4.6	110.0
Sucrose	Dextran	0.2	0.4	-3.9	
Ibuprofen	Dextran	0.4	1.2	-4.6	130.0
Indomethacin	Dextran	0.7	1.4	-2.7	110.0
Itraconazole	Eudragit E100	0.1	0.1	-1.3	85
Phenyl butazone	PEG6000	0.1	0.1	-2.8	
Nifedipine	PEG6000	0.1	0.1	-2.8	115.2
Indomethacine	PEG6000	0.4	0.7	-2.1	110.0
Phenobarbital	PEG6000	1.4	4.0	-0.1	

Table 2.1 (continued)

API	Polymer	χ	ΔHmix, J/g	ΔGmix, J/g	ΔHm, J/g
Acetophenone	PEG6000	0.4	2.2	-6.7	
Aspirin	PEG6000	0.1	0.3	-5.1	
Paracetamol	PEG6000	0.9	2.9	-1.5	
Phenyltoin	PEG6000	0.6	1.8	-2.6	
Sucrose	PEG6000	22.3	45.8	42.7	

Solution calorimetry is a very useful tool that can be used to directly measure the mixing energy in solid dispersion [224-226]. In the solution calorimetry method, a solvent that readily dissolves both drug and polymer serves as the thermodynamic reference state. A physical mixture of an amorphous drug and an amorphous polymer is dissolved into the specified solvent and the heat of solution is measured. A single-phase solid dispersion of the same total composition as the physical mixture is then measured and the difference gives the heat of mixing the drug and the polymer. The enthalpy of mixing can hence be calculated with Eq. 2.5:

$$\Delta H_{drug-polymer} = \left(x_{drug}\Delta H_{drug} + x_{polymer}\Delta H_{polymer}\right) - \Delta H_{dispersion} \qquad [2.5]$$

The advantage of solution calorimetry is that it provides access to the activity coefficient at any composition and at the temperature of interest. In addition, enthalpy difference between amorphous and crystalline materials measured by solution calorimetry has been demonstrated to be more accurate than differential scanning calorimetry technique [227]. The solution calorimetry data presented here allows for calculation of the reduced chemical potential of the API through processing with a miscible polymer. Consider the magnitude of the heat of mixing of the compounds in

comparison to the heat of crystallization at room temperature. Generating these data across composition allows for direct measurement of the chemical potential.

The energetics of mixing of diverse compounds, which are listed in Figure 2.7, are shown Figure 2.8 and as follows: itraconazole/eudragit system shows a near zero enthalpy of mixing, compound A/PVP-VA64 system shows a shallow heat of mixing and contains only dispersive interactions, compound B exhibits a weak hydrogen bond with HPMCAS, felodipine/PVP system displays a stronger interaction with a more negative mixing enthalpy, and indomethacin/PVP shows the most favorable mixing. The enthalpy of mixing in Figure 2.8 ranges from -3 to -40 J/g, which correlates well with the range seen in Table 2.1. Figure 2.9 further shows the free energy of mixing of these systems, which were obtained by combining the heat of mixing values shown in Figure 2.8 and the entropy contributions to mixing (i.e. $-T*\Delta S_{mix}$) estimated from the Flory-Huggins equation (Eq. 2.2), as a function of polymer content. Furthermore, Figure 2.9 allows for calculation of API solubility in the amorphous polymer matrix by drawing a tangent line from the API heat of mixing curve to its corresponding polymorphic melting free energy, $\Delta G_{a\text{-}c}$, value (i.e. at 0% polymer).

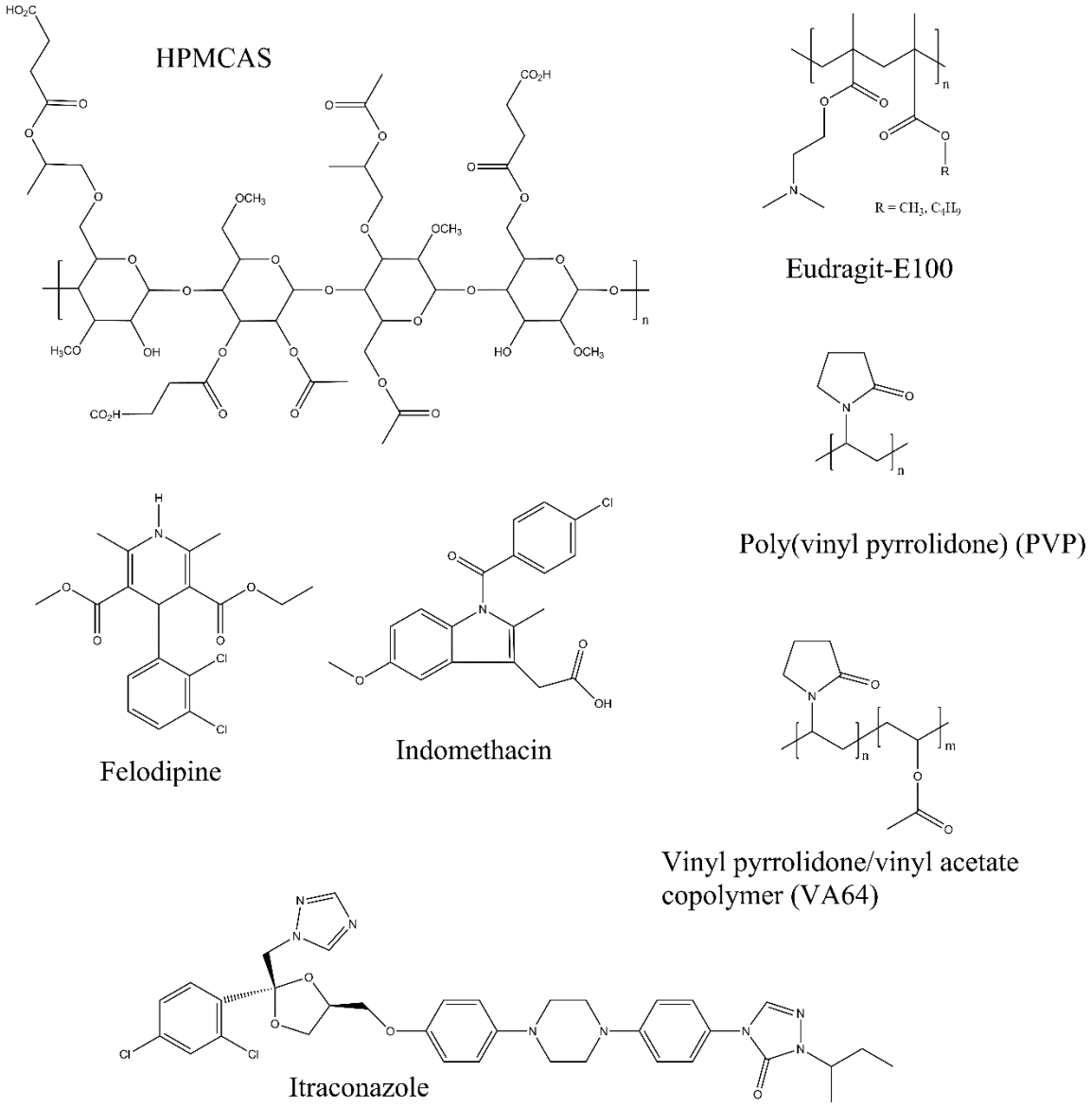

Figure 2.7 Chemical structures of the compounds used in solution calorimetry analysis.

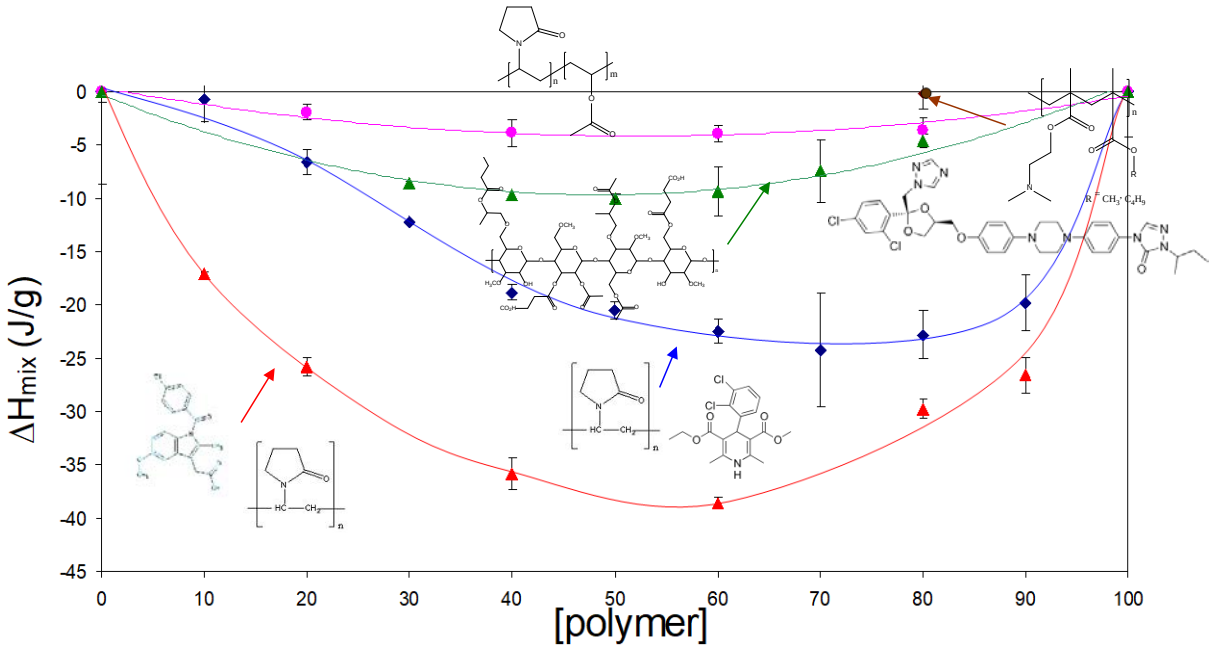

Figure 2.8 Enthalpy of mixing of several API-polymer model systems as a function of polymer content (%). Itraconazole/eudragit (brown), compound A/vinyl acetate-PVP copolymer (VA64) (pink), compound B/hypromellose acetate succinate (HPMCAS) (green), felodipine/PVP (blue), and indomethacin/PVP (red).

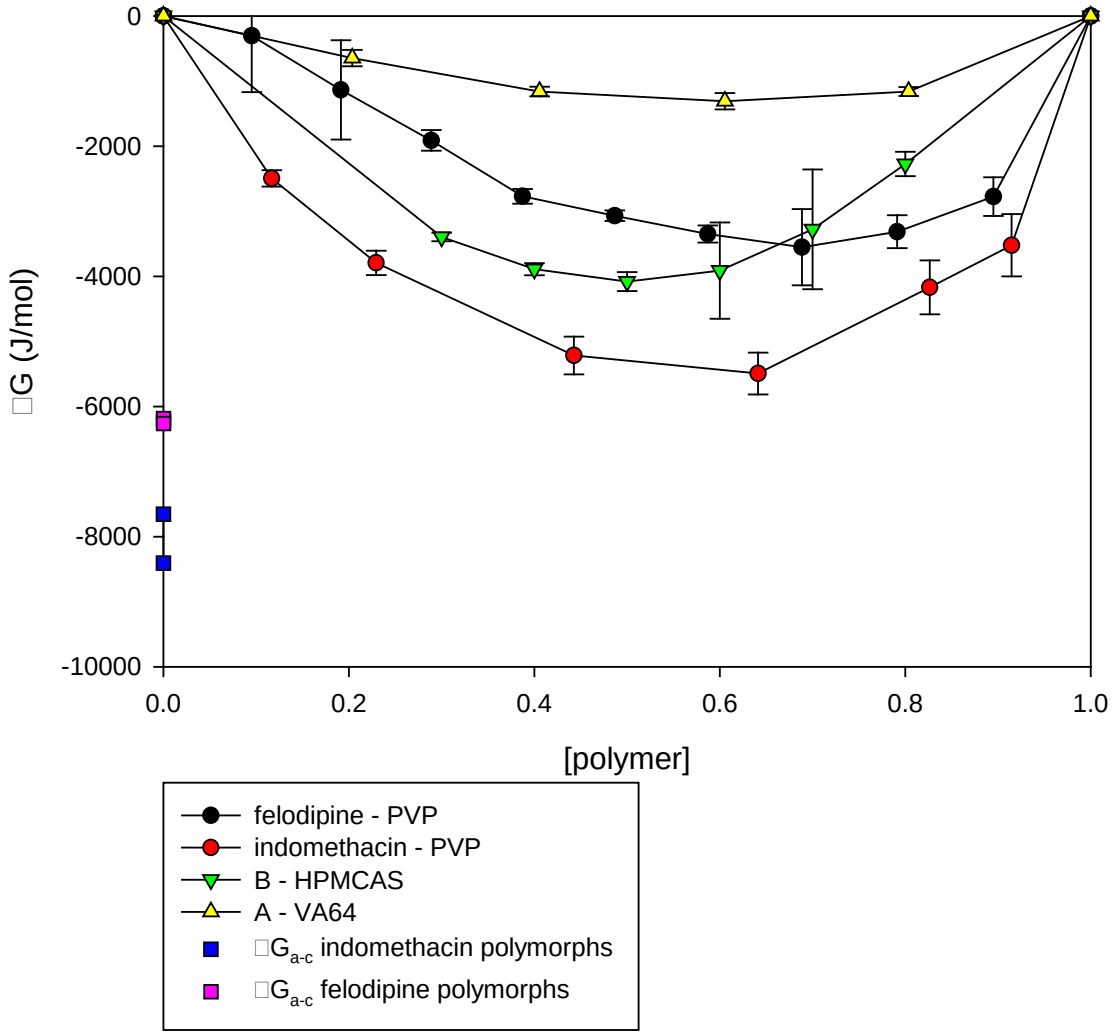

Figure 2.9 Free energy (ΔG) of mixing of several API-polymer model systems as a function of polymer volume fraction calculated by estimating the entropic contribution to mixing (ΔS_{mix}) from the Flory-Huggins model. Free energy of crystallization values (ΔG_{a-c}) for the different crystal polymorphs of felodipine and indomethacin are shown as points on the y-axis.

As discussed in the previous section, an amorphous glass will relax to the equilibrium supercooled liquid line with annealing below T_g. In the solution calorimetry work performed by Marsac et al., the excess enthalpy of mixing which originates from relaxation was measured. The correction is shown for the indomethacin/PVP and felodipine/PVP systems. In the case of the felodipine/PVP, the heat of mixing is significantly reduced from -6.7 J/g in the glassy state to -1.9 J/g in supercooled liquid at the 80:20 (drug:polymer) composition [227]. Alternatively, the measured heat of mixing of glassy indomethacin with PVP at the same 80:20 composition is -25.8 J/g while the calculated heat of mixing the supercooled liquids is -22.7 J/g. The relaxation correction for these two particular systems is similar in magnitude but significantly different in their relative enthalpy change.

In addition, the kinetics by which ASD approaches the equilibrium liquid line needs to be taken into consideration. Polymer additives tend to reduce the relaxation rate and the glass might not have the opportunity to relax fully within pharmaceutical relevant time frame. For example, measured enthalpy of neat amorphous felodipine gives a value of about 6 J/g while enthalpy relaxation with addition of 10 wt% PVP gives a value of only 3 J/g [17]. Thus, it is reasonable to conclude that the impact of relaxation may be more significant at high drug loading.

2.5 Impact of Water on ASD Energetics

The measurement of amorphous API solubility can be quite challenging due to its metastable nature. The ratio of amorphous to crystalline solubility ($\sigma_{amorphous}/\sigma_{crystalline}$) can be written as the following [228, 229]:

$$\frac{\sigma_{amorphous}}{\sigma_{crystalline}} = \exp\left(\frac{\Delta G_{a-c}}{RT}\right) \quad [2.6]$$

where $\Delta G_{a\text{-}c}$, the difference in the free energy of the crystalline and amorphous material at a temperature T can be estimated using the Hoffman equation in Eq. 2.1.

As shown in Eq. 2.6, the free energy difference between the amorphous and crystalline API is directly related to the solubility difference between the two species. However, the measurement of amorphous API solubility is not straightforward especially when the API has a strong crystallization tendency [228]. Therefore, there may be some discrepancies shown in the experimental solubility ratio compared to the calculated value. Table 2.2 shows the experimental and theoretical amorphous-to-crystalline solubility ratios in literature. Most of the experimental solubility ratios are lower than their theoretical solubility prediction, due to the difficulty in measuring the amorphous solubility of compounds [228].

Table 2.2 Theoretical and experimental amorphous/crystalline solubility ratios of various drugs [124, 228], compared to their free energies of crystallization ($\Delta G_{a\text{-}c}$) at 25 °C, estimated by Eq. 2.6.

Compound	**Experimental solubility ratio**	**Theoretical solubility ratio**	**T (°C)**	**$\Delta G_{a\text{-}c}$, J/g**
Indomethacin	4.5	25-104	25	21.4, 23.5[a]
Indomethacin	2.8	16-41	45	21.4, 23.5[a]
Gibenclamide	14	112-1652	23	
Glucose	24	16-53	20	
Griseofulvin	1.4	38-441	21	
Hydrochlorthiazide	1.1	21-113	37	

Table 2.2 (continued)

Compound	Experimental solubility ratio	Theoretical solubility ratio	T (°C)	Δ Ga-c, J/g
Iopanoic acid	3.7	12-19	37	
Polythiazide	9.8	48-455	37	
Felodipine	7-10 with polymer	9	37	16.2, 16.1, 16.3[b]
Indomethacin	4.9	7	25	21.4, 23.5[a]
Iopanoic acid	1.5	6	25	11.0
Glipizide	9.2	11	25	21.8
Glybenclamide	22.6	18	25	24.5
Hydrochlorothiazide	4.9	33	25	35.3
Terfenadine	10	13	25	19.9
Griseofulvin	1.4	29	25	24.4
Spironolactone	2.1	111	25	31.4
Danazol	3	26	25	26.1
Ritonavir	14.5	15.8	37	
Efavirenz	2.2	2.4	37	
Loratadine	4.8	4.3	37	
Ketoconazole	14.7	15.3	37	
Indomethacin	10.1	8.9	37	
Felodipine	10.4	9.0	37	
Clotrimazole	13.0	10.0	37	
Clozapine	15.4	15.1	37	

[a] Crystal form α and γ, respectively. Enthalpy difference of the indomethacin polymorphs obtained from: [137].

[b] Crystal form I, II and III, respectively. Differences in free energies between the felodipine polymorphs obtained from: [230].

2.5.1 ASD Dissolution Energetics

Dissolution process is often described by the Nernst-Brunner equation below

$$\frac{dM}{dt} = \frac{DA}{h}(C_S - C) \approx \frac{DAC_S}{h} \qquad [2.7]$$

M is the mass of solute dissolved, dM/dt is the dissolution rate, D is the diffusion coefficient of solute, A is the surface area of the exposed solid, h is the thickness of the diffusion layer, Cs is the solubility of solute in dissolution medium, and C is the concentration of solute in the dissolution medium. Under sink condition, C can be approximated to zero resulting in a simplified version of this equation.

In this equation, the quantities of D and h are dictated by the physicochemical properties of the API as well as the anatomy and physiology of the absorption site, i.e. small intestine. This leaves surface area (A) and solubility (Cs) as variables controllable via formulation approaches. As discussed in Section 1.3.2, surface area can be increased by the generation of nanoparticles when ASD dissolve [133, 141, 159]. In addition, amorphous material possesses higher "solubility," albeit it is a kinetic phenomenon, as a result of having a higher free energy than the crystalline counterpart. Hence, the amorphous solubility provides another means of enhancement in dissolution rate. Solubility of the amorphous material can be calculated by re-arranging Eq. 2.6 and adding correction factors for water activity and ionization constant proposed by Murdande et al. [122], as shown in Eq. 2.8 below:

$$C_{amorphous} = C_{eq} \cdot e^{[-I(a_2)]} \cdot e^{\left[\frac{\Delta G_{a\to c}}{RT}\right]} \cdot \left(\frac{1-a^c}{1-a^a}\right) \qquad [2.8]$$

Considering the fact that amorphous API chemical potential can be significantly reduced in an ASD, immense stability advantage in polymer can be achieved via increased API solubility especially when the magnitude of the free energy of

crystallization is comparable with the free energy of mixing. As seen in Table 2.2, the free energy of crystallization (ΔG_c) for different compounds is similar in magnitude to the free energy of mixings of various drug-polymer disperisons (ΔG_{mix}), shown in Table 2.1. For example, 50% indomethacin and 50% PVP shows a ΔG_{mix} of -35 J/g. This value is even lower than the reduction in chemical potential the pure indomethacin undergoes when crystallizing from the amorphous phase (-23.5 J/g, Table 2.2). Of course, an exact estimation of the thermodynamic stability enhancement can only be made by comparing the drug chemical potential in the dispersion to the one in the neat amorphous phase. Furthermore, solubility of drug in polymer at an arbitrary drug loading can be calculated by generating a ΔG_{mix} curve across the whole composition range (albeit the value of χ parameter may differ across composition) and solving for the chemical potentials by the graphical tangent intercept method as shown in Figure 2.9 [227].

For the thermodynamic aspects, consider a Flory-Huggins treatment of a binary amorphous API-polymer dispersion. The reduction of the chemical potential of the API in this system ($\mu_{dispersion,API}$) relative to its pure amorphous form ($\mu^0_{a,API}$) is given by [231]

$$\mu_{dispersion,API} - \mu^0_{a,API} = RT\left\{\ln \Phi_{a,API} + \left(1 - \frac{1}{DP}\right)\Phi_{a,polymer} + \chi\Phi^2_{a,polymer}\right\} \quad [2.9]$$

where the Φ terms indicate volume fractions of respective compound in the amorphous phase and DP is the degree of polymerization. For most polymers, DP is much larger than one, so this equation can be expressed approximately as

$$\mu_{dispersion,API} - \mu^0_{a,API} = RT\left(\ln \Phi_{a,API} + \Phi_{a,polymer} + \chi\Phi^2_{a,polymer}\right) \quad [2.10]$$

At the amorphous solubility limit of the dispersion, the chemical potential of the API in the solution ($\mu_{as,API}$) is equal to the chemical potential of the API in the amorphous dispersion ($\mu_{dispersion,API}$),

$$\mu_{as,API} = \mu_{dispersion,API} \quad [2.11]$$

and accordingly, at the crystal solubility limit the chemical potential in the solution ($\mu_{cs,API}$) would equal the one in the pure crystal phase ($\mu^0_{c,API}$),

$$\mu_{cs,API} = \mu^0_{c,API} \quad [2.12]$$

The difference in the chemical potential of the API in the pure crystal phase relative to the one in the pure amorphous phase ($\mu^0_{a,API}$), is

$$\mu^0_{a,API} - \mu^0_{c,API} = \Delta G_{a-c} \quad [2.13]$$

where ΔG_{a-c} is the difference in free energy between the pure amorphous and pure crystalline API. Eq. 2.10-2.13 can be combined to show the chemical potential difference between the amorphous solubility limit of the API in the dispersion, and the pure API crystal phase solubility limit:

$$\mu_{as,API} - \mu_{cs,API} = \Delta G_{a-c} + RT\left(\ln \Phi_{a,API} + \Phi_{a,polymer} + \chi \Phi^2_{a,polymer}\right) \quad [2.14]$$

and so, the ratio of the activities of the two solutions at their respective limits (or the amorphous dispersion/crystal solubility ratio) becomes

$$\frac{\sigma_{amorphous}}{\sigma_{crystalline}} = e^{\frac{\Delta G_{a-c}}{RT} + \ln \Phi_{a,API} + \Phi_{a,polymer} + \chi \Phi^2_{a,polymer}} \quad [2.15]$$

which can be compared to the solubility ratio in the pure amorphous form (Eq. 2.6), which contains only ΔG_{a-c} in the exponent. It can be seen in Eq. 2.15 that the more negative the value for χ is the more adhesive the API-polymer interactions are, and the lower the API loading in the dispersion is (lower Φ_{API}) the greater is the reduction of the

amorphous solubility ratio by dispersion formulation. For example an indomethacin-PVP dispersion (χ = -6.88 and ΔG_{a-c}= 7800 J/mol [227]) at a drug loading of 50%, gives an amorphous/crystalline solubility ratio of only 3.4 at 25 °C, as estimated by Eq. 2.15, while the solubility ratio in the pure amorphous form estimated by Eq. 2.6, is 23. Since the crystal solubility is the same in both cases (pure crystal phase), this reduction of the ratio is due only to the reduction of the amorphous solubility of the dispersion. By formulating an indomethacin-PVP dispersion, the amorphous solubility of indomethacin is hence reduced by a factor of almost 7. Therefore, although the stability of the API's amorphous phase is improved by dispersing it in a polymer by reducing the kinetics of crystallization, the thermodynamic amorphous solubility might also be reduced.

The above description covers a simplified case assuming that the solid immediately dissolves from the dry state into water, while the actual dissolution into aqueous media might be gradual. Consider for example a case where an initially stable API-polymer dispersion gradually dissolves into water, where the solubility of API in water is very low. This process could be illustrated in the phase diagram shown in Figure 2.10. The initially stable API-polymer dispersion is indicated by the black dot. The dissolution of water into the dispersion could then follow the gradient outlined by the arrow. Because the miscibility between water and API is low, the chemical potential of the API in the dispersion would likely be increased as water is introduced into the system [232]. As the water content further increases the chemical potential of the API is also increasing, so that the composition is at some point found to be outside the region of stable composition (given by the crystalline solubility), which could cause crystallization at an early stage in the dispersion. Further, as more water is absorbed, the mixture

crosses the spinodal line, which would cause amorphous phase separation before it would be diluted enough to remain outside the spinodal region (below the amorphous solubility limit) in the aqueous phase.

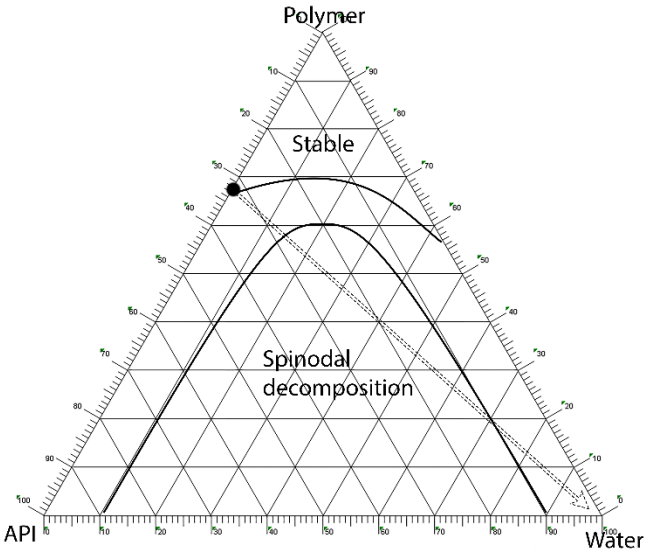

Figure 2.10 Hypothetical ternary phase diagram of a miscible polymer-API system together with water, where water-API has limited miscibility. The arrow shows a route of increasing water content in the dispersion as it gradually dissolves into water.

2.5.2 Impact of Water on the Activity Coefficient and Chemical Potential of the API in ASD

The impact of water on ASDs, either storage moisture or dissolution process, can be described by Flory-Huggins model. The activity of a compound in a mixture or solution is defined as $a = \gamma x = \exp\left(\frac{\mu-\mu^0}{RT}\right)$, where γ is the compound's activity coefficient, x is its molar fraction, μ is the chemical potential and μ^0 is the chemical potential at the standard state. Flory-Huggins approach can be expanded to a mixture of API, water, and polymer to give the activity coefficient of the API [222, 232] in the dispersion:

$$\ln \gamma_{API} = \left(\ln \frac{v_{API}}{x_{API}} + v_{pm} - \frac{v_{pm}}{DP} + \chi_{API-pm} v_{pm}(1 - v_{API}) + \chi_{API-H2O} v_{H2O}(1 - v_{API}) - \chi_{pm-H2O} v_{pm} v_{H2O}\right) \quad [2.16]$$

where x_{API} is the molar fraction of API. As seen by the signs preceding each interaction term containing the $\chi_{a\text{-}b}$ parameters, unfavorable API-water miscibility (i.e. positive $\chi_{API\text{-}H2O}$) increases the activity coefficient and chemical potential of the API, while unfavorable polymer-water interaction (i.e. positive $\chi_{pm\text{-}H2O}$) instead decreases the activity coefficient and chemical potential of the API in the mixture. Given the high hygroscopicity / hydrogen bonding potential of polymers that are often used as excipients or carriers in drug formulations (characterized by both a high T_g and a negative value for $\chi_{pm\text{-}H2O}$), together with API's poor aqueous solubility in general (positive $\chi_{API\text{-}H2O}$), water will raise the chemical potential through both terms. Therefore, the chemical potential of the API in the dispersion could be raised with increasing water content when polymers with hydrogen bonding characteristics are used.

2.6 Conclusion

Historical work has focused on theoretical and experimental approaches to understand individual processes that may lead to changes in the energy landscape of amorphous materials, but little work has focused on the relative magnitude of each process. This paper has summarized and discussed the relative energy contributions from environmental storage (i.e. relaxation), formulation, and crystallization tendency in the amorphous phase, as well as stability of the amorphous form when the dispersion is exposed to moisture or introduced into aqueous media.

Literature survey performed in this chapter revealed that relaxation can be significant, i.e. 5-30%, relative to the drug melting energetics. It was observed that the higher the change in heat capacity as glassy materials are formed the more significant the relaxation energetics will be. In addition, a significant change in the relaxation enthalpy was observed even with addition of small amount of polymers, indicating the importance of polymer addition in ASDs. It is more difficult, however, to compare relaxation enthalpy of the composite to the neat API melting energetics since the polymer significantly raises the relaxation enthalpy of ASD. Energy associated with mixing was found to be similar in magnitude as that of relaxation process. Further, the extent of mixing is strongly dependent on the χ parameter between the drug and the polymer used in an ASD. Mixing energetics could be significant when χ is large in magnitude, suggesting the importance of polymer selection in which mixing is highly favorable in such ASD. Amorphous drug-polymer dispersions not only reduce the mobility of the drug and drug crystallization kinetics, but also greatly reduce the chemical potential of the drug if the interactions between drug and polymer are favorable. If the reduction in chemical potential by mixing with polymer is of the same order of magnitude as the free energy of crystallization at room temperature, an increased solubility and stability of drug in polymer can be obtained. On the other hand, the presence of water in the dispersion, either storage moisture or GI aqueous environment, will increase the chemical potential of the drug. Furthermore, drug chemical potential could be further inflated by the potential polymer-water interaction. Understanding the favorability extent of drug-polymer interaction will aid formulators in deciding the drug loading in ASDs, where higher drug loading can be utilized for a more favorable drug-polymer combination.

Overall, generation of a complete thermodynamic description of an ASD is possible and critical to the success of ASD performance.

Chapter 3 - What is the True Driving Force for Absorption of Poorly Water-Soluble Drugs in the Presence of Solubilizing Additives?

3.1 Introduction

Research shows that approximately 70% of new chemical entities may be classified as Biopharmaceutics Classification System (BCS) Class II compounds, which have low solubility and high permeability characteristics in its most stable crystalline form [107, 233, 234]. When delivered orally, drug molecules must first dissolve in the gastrointestinal (GI) environment in order for permeation and absorption to occur. Consequently, drugs with poor aqueous solubility and/or low dissolution rate have minimal driving force for absorption. Supersaturating drug delivery systems (SDDS) [2], such as amorphous solid dispersions (ASDs) [3, 235], have been demonstrated to promote absorption of poorly soluble compounds. The use of SDDS leads to a generation of drug supersaturation whereby the drug free energy is higher than that of the crystalline state, resulting in an increased driving force for absorption.

In vivo absorption phenomenon is often simulated in vitro by diffusion cells and mathematically described by Fick's law (Eq. 3.1). The rate of absorption per unit area, represented as flux (J), is a product of the effective permeability (P_{eff}) and the drug solution thermodynamic activity ($a_{D,solution}$). Experimentally, volume (V) and membrane surface area (A) along with the change in drug concentration as a function of time in the acceptor ($\frac{dC}{dt}$) terms can be measured to determine the flux across a membrane.

$$Flux(J) \equiv \frac{V}{A}\frac{dC}{dt} = P_{eff} \cdot a_{D,solution} \qquad [3.1]$$

P_{eff} is the effective permeability of the drug molecule through the unstirred water layer, which is dictated by the physicochemical properties of the drug molecule. Therefore, P_{eff} is relatively constant as long as the drug is chemically stable, and the extent of absorption is thus governed by the drug's thermodynamic activity.

Unfortunately, the measurement of thermodynamic activity is not straightforward and, thus, flux is often evaluated based on the bulk drug concentration in the donor side. While the use of bulk concentration may adequately estimate thermodynamic activity in certain conditions, such as dilute or ideal solution, the application of this assumption to describe in vivo absorption could be erroneous because the drug concentration may not necessarily be dilute and that the total drug concentration may not represent the true absorption driving force [117]. For instance, drug molecules may be solubilized by endogenous surfactants present in the intestinal lumen and these molecules entrapped in the micelles may not readily be absorbed via passive diffusion, contrary to those 'free' molecules [179, 182]. In such non-ideal conditions, the effective concentration, i.e. thermodynamic activity, is a product of the drug concentration ($C_{D,solution}$) and the thermodynamic activity coefficient ($\gamma_{D,solution}$) as shown in Eq. 3.2. Furthermore, non-ideal flux (Eq. 3.3) can be calculated by combining Eq. 3.1 and Eq. 3.2.

$$a_{D,solution} = \gamma_{D,solution} * C_{D,solution} \quad [3.2]$$

$$J = P_{eff} \cdot \gamma_{D,solution} * C_{D,solution} \quad [3.3]$$

Due to analogous reason of difficulty in thermodynamic activity measurement, supersaturation is often measured by supersaturation ratio (SR) in Eq. 3.4, which is a ratio between the total drug concentration, $C_{D,solution}$, and the crystalline solubility, $S_{crystal}$ [2]. However, the total concentration may not be representative of the true

absorption driving force for the same reason noted above. Therefore, the true extent of supersaturation should be calculated as the activity ratio ($\boldsymbol{a_R}$), which is a ratio between the drug solution activity, $a_{D,solution}$, to the drug solution activity at the crystalline solubility limit, $a_{D,saturation}$, as shown in Eq. 3.5. The drug solution activity coefficient and the drug solution activity coefficient at the crystalline solubility are represented as $\gamma_{D,solution}$ and $\gamma_{D,crystal}$, respectively. Note that the $\frac{\gamma_{D,solution}}{\gamma_{D,crystal}}$ term in Eq. 3.5 serves as the correction factor for supersaturation in non-ideal conditions. Furthermore, Eq. 3.5 can be combined with Eq. 3.1 to yield Eq. 3.6, which allows for calculation of $\boldsymbol{a_R}$. In other words, flux at any non-dilute condition can be compared to the flux at the crystalline solubility in a surfactant-free system to attain the true extent of supersaturation. This approach assumes that the drug concentration at the crystalline solubility is dilute, which is applicable for most BCS class II compounds.

$$SR = \frac{C_{D,solution}}{S_{crystal}} \quad [3.4]$$

$$a_R \equiv \frac{a_{D,solution}}{a_{D,saturation}} = \frac{\gamma_{D,solution} * C_{D,solution}}{\gamma_{D,crystal} * S_{crystal}} = \frac{\gamma_{D,solution}}{\gamma_{D,crystal}} * SR \quad [3.5]$$

$$a_R \equiv \frac{a_{D,solution}}{a_{D,saturation}} = \frac{J_{D,solution}/P_{eff}}{J_{D,saturation}/P_{eff}} = \frac{J_{D,solution}}{J_{D,saturation}} \quad [3.6]$$

This paper aims to examine $\boldsymbol{a_R}$ and the ideality $\left(\frac{\gamma_{D,solution}}{\gamma_{D,crystal}}\right)$ of estradiol (E2), a poorly water-soluble compound, in the absence and presence of a surfactant model. Furthermore, the loci of estradiol molecules, i.e. unbound or bound/micellized, will be determined in the presence of the surfactant based on the $\boldsymbol{a_R}$ obtained.

3.2 Materials and Methods

3.2.1 Materials

17β-Estradiol (E2), polysorbate 80 (PS80), and tris maleate were purchased from Sigma-Aldrich (St. Louis, MO). Sodium hydroxide, methanol, and dimethyl sulfoxide (DMSO) were purchased from Fisher Scientific (Fair Lawn, NJ). Hydroxypropyl methylcellulose (HPMC) K4M grade was obtained from Colorcon (West Point, PA). Deionized water was obtained from a MilliQ water purification device (Milli-Q Synthesis, Millipore, Bedford, MA) and filtered through a 0.22 μm filter (Millipak 40, Millipore, Bedford, MA) before use. Polytetrafluoroethylene (PTFE) syringe filters with a diameter of 13 mm (0.22 μm pore size) were purchased from Tisch Scientific (Cleves, OH). Regenerated cellulose dialysis membrane with 6-8 kDa MWCO was obtained from Spectrum Laboratories (Rancho Dominguez, CA). All materials were used as received.

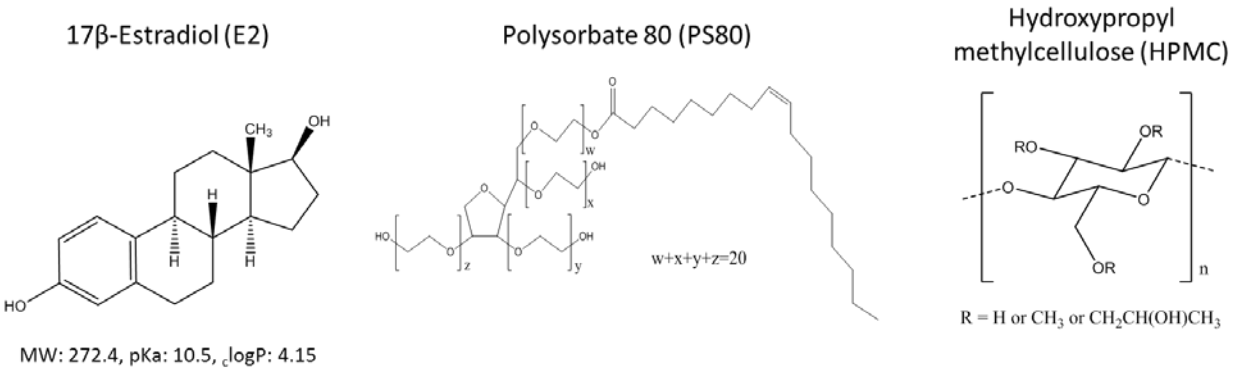

Figure 3.1 Chemical structures of estradiol (E2), polysorbate 80 (PS80), and hydroxypropyl methylcellulose (HPMC)

3.2.2 Crystalline Solubility Measurement

Crystalline solubility of E2 was determined by placing an excess amount of E2 into a glass vial containing 50 mM tris maleate buffer at pH 7.4 in the absence and presence of excipients (for media containing excipients, excipients were pre-dissolved in the buffer prior to the solubility measurement). The mixture was rotated by a vial rotator in an incubator at 37°C for 72 hours, which was subsequently filtered through a 0.22 μm syringe filter. The syringe filter was saturated by discarding the first 3 mL of the filtrate. The concentration of E2 was determined by a high-performance liquid chromatography (HPLC) equipped with a UV detector (HPLC and UV detector by Waters, Milford, MA) and a Symmetry C18 column (4.6 mm internal diameter, 150 mm length, 5 μm particle size; Waters, Milford, MA). The mobile phase consisted of methanol and water in the ratio 70:30 v/v and was used isocratically. Detection wavelength was set at 280 nm. All solubility measurements were performed in triplicate.

3.2.3 Flux Measurement

Flux experiments were performed using side-by-side diffusion cells (PermeGear, Inc., Hellertown, PA). A regenerated cellulose membrane (MWCO 6-8 kDa) was inserted between the donor and acceptor sides of each diffusion cells. The surface area of the exposed membrane was 7.065 cm^2. Diffusion cells were stirred at 100 rpm and immersed in a water bath to keep a constant temperature of 37°C. The volume of solution was 30 mL in each side of the diffusion cells. For experiments at SR=1 (i.e. suspension), the donor compartment was filled with buffer solution containing an excess of crystalline drug whereas the acceptor compartment was filled with a blank buffer solution. Drug

concentration in the acceptor compartment was monitored as a function of time to determine flux. The drug effective permeability can be calculated from this flux value using Eq. 5.1 and P_{eff} was assumed constant throughout the rest of the flux experiments.

For experiments at higher SR, a solvent shift approach was utilized, where a highly concentrated E2 solution in DMSO was transferred to the aqueous solution at t=0. DMSO content in the donor compartment was kept below 1% v/v. Experiments in the presence of surfactant was performed similarly as described above where suspension was used for SR=1 and solvent shift approach for higher SR experiments. The concentration of surfactant in the acceptor compartment was kept the same as that in the donor to avoid osmosis process.

3.3 Results

3.3.1 Crystalline Solubility

The solubility of crystalline E2 in various media is shown in Figure 3.3. In the absence of excipients, E2 crystalline solubility was 2.2 ± 0.0 μg/mL in buffer. The addition of 1% w/v PS80 increased E2 crystalline solubility 30-fold to 60.2 ± 1.3 μg/mL. The addition of 100 μg/mL HPMC did not alter the crystalline solubility of E2 in either buffer or PS80 solution.

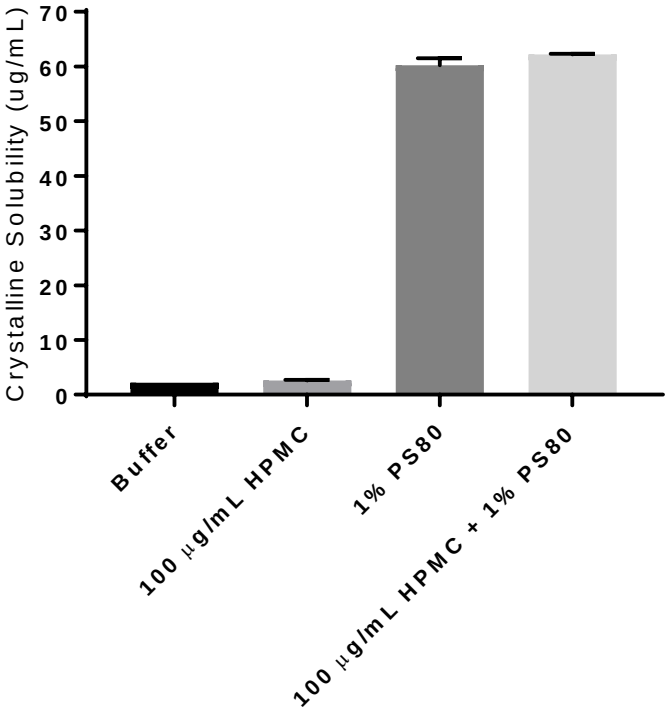

Figure 3.2 E2 crystalline solubility in different media. Error bars indicate standard deviation with n=3.

3.3.2 $J_{D,saturation}$, a_R, and $\frac{\gamma_{D,solution}}{\gamma_{D,crystal}}$ in Buffer

Based on Eq. 3.6, $J_{D,saturation}$ must first be determined to evaluate the true supersaturation, $\boldsymbol{a_R}$. Figure 3.4 shows the acceptor E2 concentration versus time at the crystalline solubility limit, in which excess solids were added to exceed the E2 crystalline solubility value, in the buffer media. $J_{D,saturation}$ can be calculated by Eq. 3.1 with the slope of Figure 3.4 as $\frac{dC}{dt}$ term and the surface area and volume values are listed in Materials and Methods section. Thus, a value of 0.312 ug/cm^2/hr was obtained for $J_{D,saturation}$.

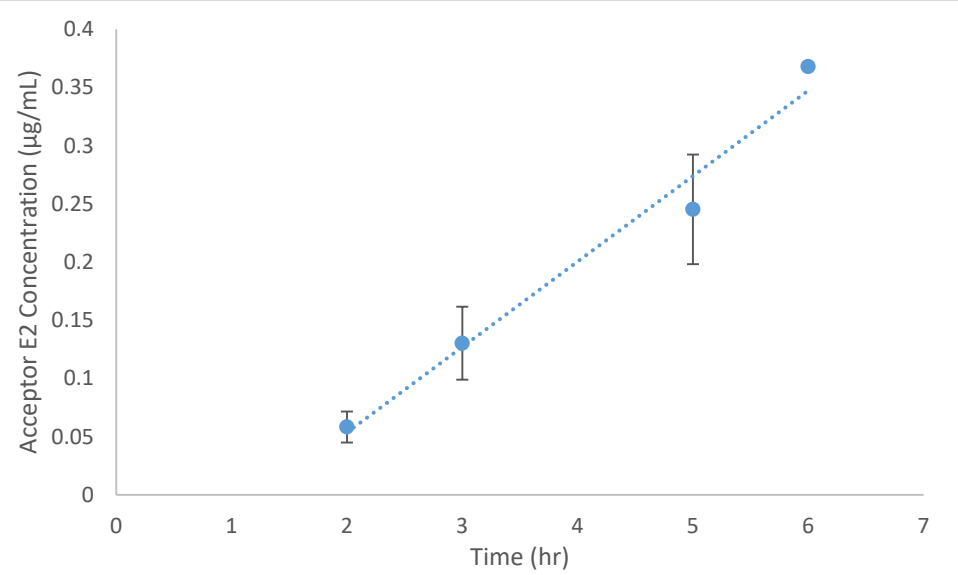

Figure 3.3 Acceptor E2 concentration versus time at the crystalline solubility limit.

Once $J_{D,saturation}$ is determined, $\boldsymbol{a_R}$ can be determined by comparing the flux at any supersaturation level to $J_{D,saturation}$. Herein, different degree of supersaturation was created on the basis of SR by multiplication of the equilibrium solubility, as noted in Eq. 3.4. The resulting flux associated with each SR can then be compared to $J_{D,saturation}$ to determine $\boldsymbol{a_R}$ via Eq. 3.6 and, subsequently, $\frac{\gamma_{D,solution}}{\gamma_{D,crystal}}$ via Eq. 3.5. In the absence of surfactant (Figure 3.5), SR and $\boldsymbol{a_R}$ correlate linearly and behave ideally with $\frac{\gamma_{D,solution}}{\gamma_{D,crystal}} \approx 1$ up to the maximum $\boldsymbol{a_R}$ of 6. Above the maximum $\boldsymbol{a_R}$, increase in SR did not further increase $\boldsymbol{a_R}$ and, thus, $\frac{\gamma_{D,solution}}{\gamma_{D,crystal}}$ decreases to satisfy Eq. 3.5.

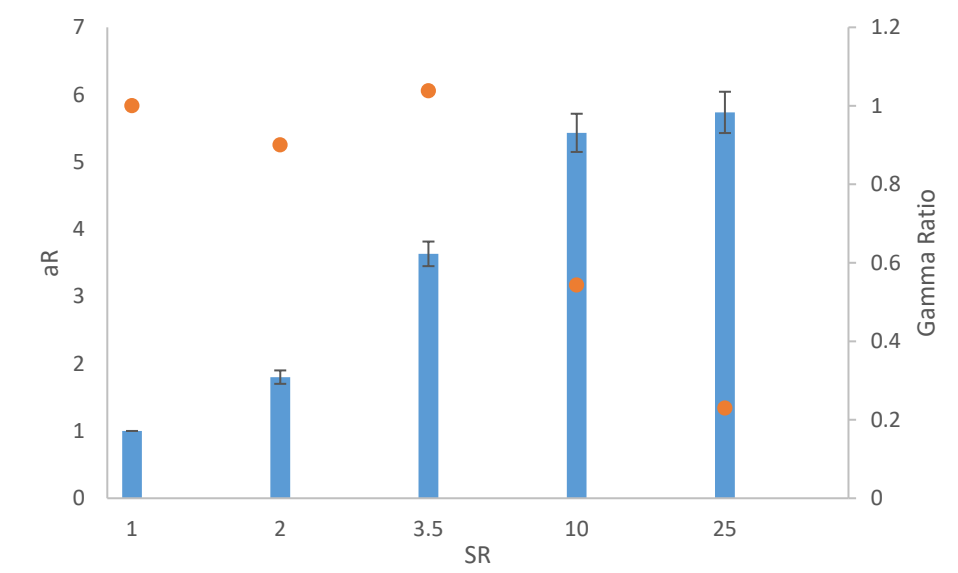

Figure 3.4 Relationship between SR, a_R (blue bar), and $\frac{\gamma_{D,solution}}{\gamma_{D,crystal}}$ (orange circle, represented as 'Gamma Ratio') in buffer. Error bars represent standard deviation with n=3.

3.3.3 a_R and $\frac{\gamma_{D,solution}}{\gamma_{D,crystal}}$ in PS80 solutions

To illustrate the impact of PS80 surfactant on $\mathbf{a_R}$, experiments with the same dissolved E2 amount of 20 μg/mL were performed in the buffer and two different concentrations of PS80 solution as shown in Figure 3.6. This figure shows that E2 crystalline solubility increases while $\mathbf{a_R}$ decreases with increasing PS80 concentration. At the highest PS80 concentration, $\mathbf{a_R}$ was less than 1 indicating that the solution was no longer supersaturated.

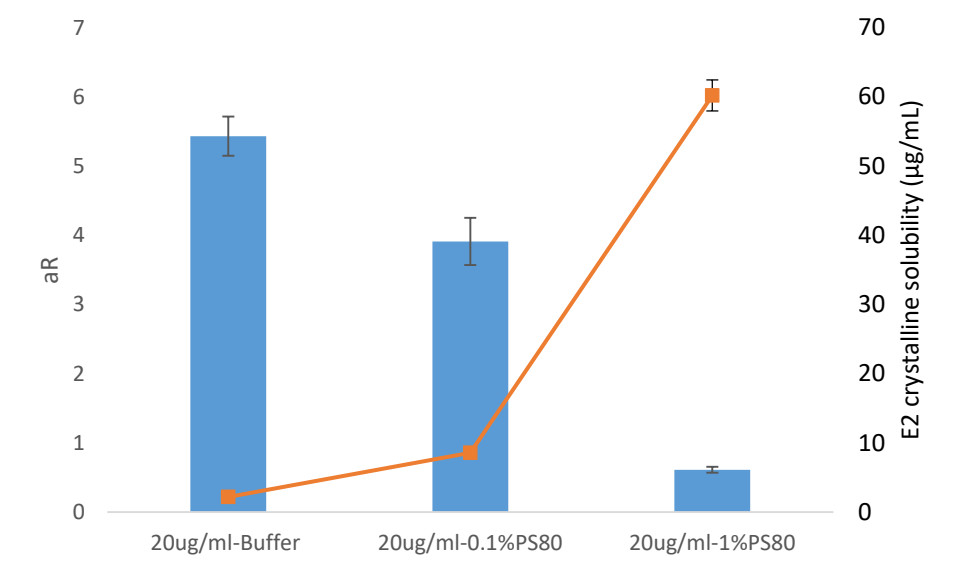

Figure 3.5 a_R (blue bar) and crystalline solubility (orange square) in buffer, 0.1% PS80 and 1% PS80 at the same E2 dissolved concentration. Error bars represent standard deviation with n=3.

Although addition of 1% PS80 led to a subsaturated E2 solution at 20 µg/mL concentration, supersaturation can still be achieved by further increasing the initial E2 concentration beyond its crystalline solubility limit of 60 µg/mL. Analogous to Figure 3.5, $\boldsymbol{a_R}$ and $\frac{\gamma_{D,solution}}{\gamma_{D,crystal}}$ values at different SR can be measured as shown in Figure 3.7. This figure shows that $\boldsymbol{a_R}$ is higher than SR, especially for points before $\boldsymbol{a_R}$ reaches the maximum. For instance, at SR=1, which is at the crystalline solubility, the flux is higher than that at the crystalline solubility in buffer. $\boldsymbol{a_R}$ continues to increase with increasing SR up to the maximum $\boldsymbol{a_R}$ of 6, which is the same to that in buffer. The values of $\frac{\gamma_{D,solution}}{\gamma_{D,crystal}}$ indicate that there is a positive deviation in the presence of PS80, which is followed by a decrease after maximum $\boldsymbol{a_R}$ is achieved.

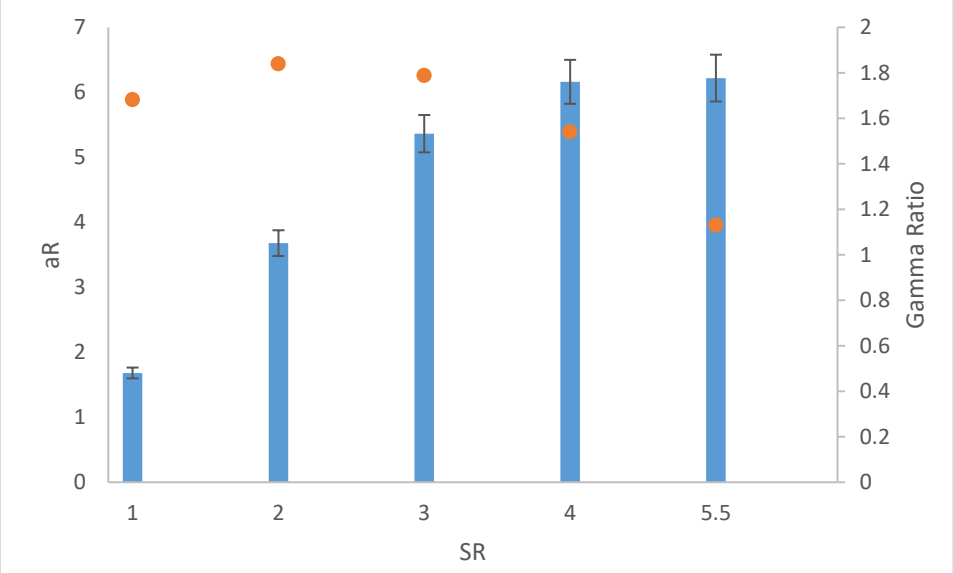

Figure 3.6 Relationship between SR, a_R (blue bar), and $\frac{\gamma_{D,solution}}{\gamma_{D,crystal}}$ (orange circle, represented as 'Gamma Ratio') in 1% PS80. Error bars represent standard deviation with n=3.

3.4 Discussion

SDDS are an attractive approach to overcome poor aqueous solubility demonstrated by the majority of new chemical entities, owing to their ability to increase drug dissolution rate and generate high apparent solubility. Although supersaturation is not a new concept, the term supersaturation can be misleading. By definition, supersaturation is the increase in drug thermodynamic activity over that of the crystalline state, which is termed $\boldsymbol{a_R}$ in this study. However, oftentimes it is difficult to directly measure thermodynamic activity in complex systems, such as when the drug is present in an environment with excipients and endogenous materials. Consequently, it is often more practical and convenient to define supersaturation as the ratio of total drug concentration over the crystalline solubility, i.e. SR. Herein, a mathematical approach was developed to

allow a rapid determination of $\boldsymbol{a_R}$ by comparing the flux of any drug solution to its flux at the crystalline solubility in surfactant-free system, albeit that the crystalline solubility should be in the dilute region.

Application of the derived mathematical equations on supersaturation in buffer is shown in Figure 3.5. A linear correlation between $\boldsymbol{a_R}$ and SR was observed with $\frac{\gamma_{D,solution}}{\gamma_{D,crystal}}$ close to unity, which indicates that dilute or ideal condition assumed here is reasonably valid in buffer. At high SR, however, $\boldsymbol{a_R}$ plateaus at a maximum value. The point at which $\boldsymbol{a_R}$ reaches a plateau is also known as liquid-liquid phase separation or amorphous phase separation in the literature [124]. The measured E2 amorphous solubility in buffer was 14 μg/mL, which gives SR of 6, exactly where the $\boldsymbol{a_R}$ plateau occurs (keep in mind that $\boldsymbol{a_R}$ and SR correlate linearly at low SR). Above this limit, there is no further increase in the true supersaturation and, thus, no increase in flux or absorption is observed. Subsequently, maintaining the drug concentration at this limit in the intestinal lumen throughout the duration of GI transit has been thought of as a strategy to maximize intestinal absorption [117].

The first comparison of $\boldsymbol{a_R}$ in the buffer and PS80 solutions is shown in Figure 3.6. This figure demonstrates that at the same total drug concentration, $\boldsymbol{a_R}$ is considerably lower in PS80 solutions than in buffer. Although E2 may be in the supersaturated state in the surfactant-free system, addition of surfactant could cause a lower the degree of supersaturation to even an undersaturated state. This result suggests that the measure of performance of any dosage form, such as dissolution or flux, ought to be performed in simulated intestinal media containing bile salts and other potential formulation solubilizing agents. Such approach will then allow formulators to select an appropriate

dose that will generate a drug concentration that provides maximum driving force for absorption. The same practice could also be done in the presence of simulated food content to assess the potential negative food effect in drug absorption.

In 1% PS80 solution, $\boldsymbol{a_R}$ value is higher than SR for each SR point (Figure 3.7). For example, $\boldsymbol{a_R}$ is almost 2 at SR=1, which suggests that supersaturation is observed even at the crystalline solubility limit in PS80 solution. This observation could potentially explain positive food phenomena. Similar to that in buffer, $\boldsymbol{a_R}$ reaches a plateau at high SR, indicating that amorphous phase separation occurring between SR of 3 and 4. The measured E2 amorphous solubility in 1% PS80 was 220 μg/mL, which would give an SR of 3.7, confirming the observation in Figure 3.7. The values of $\frac{\gamma_{D,solution}}{\gamma_{D,crystal}}$ in this figure showed that there is a positive deviation from ideality, which indicates that the effective concentration (i.e. activity) is higher than the measured concentration.

Table 3.1 Summary of E2 thermodynamic activity, free drug concentration, and number of E2 molecules per micelle as a function of SR in 1% PS80 solution. Error values are standard deviation with n=3.

SR	a_R	[Free Drug] (µg/mL)	#Drug/#Micelle	$K_{m/w}$
1	1.73 ± 0.03	3.80	1.6	14.8
2	3.78 ± 0.17	8.31	3.2	13.4
3	5.51 ± 0.37	12.11	4.8	13.9
4	6.33 ± 0.48	13.92	5.9	14.8
5	6.38 ± 0.60	14.04	5.9	14.7

Furthermore, using the a_R values found in Figure 3.7 combined with a mass balance of $[E2]_{total} = [E2]_{free} + [E2]_{micelle}$, the free drug concentration, the $K_{m/w}$, and the number of drug molecules per micelle can be calculated. Herein, the value of $K_{m/w}$ was found to be constant at approximately 14 at 1<SR<6 (Table 3.1). Assuming a constant PS80 aggregation number of 60 [236], the amount of E2 molecules contained in each PS80 micelle can further be calculated. As shown in Table 3.1, the number of E2 molecules contained per PS80 micelle increases from approximately 1-2 E2 molecules at the crystalline solubility limit to six E2 molecules at the amorphous solubility limit (i.e. maximum a_R, indicating that micelles can sequester more drug molecules at the supersaturated state than that at the crystalline solubility limit. As more drug molecules are packed inside micelles, the size of these micelles increases. Others have also reported examples of "swollen" micelles as high as 2-3 fold increase in their hydrodynamic size at

the supersaturated state in surfactant-containing systems [149, 154]. Furthermore, the microenvironment of a micelle in which a solute may reside can be divided into two regions: hydrophobic core and palisade region, with the latter also known as the core-corona interface [237]. Indulkar et al. observed that drug molecules mostly reside in the palisade region of micelles when the concentration is between the crystalline solubility limit and low levels of supersaturation, whereas at high supersaturation these drug molecules occupy both the core and palisade regions [154]. We suspect that the same phenomena is observed with E2 local environment at the supersaturated state where E2 populates the palisade region at low supersaturation and both palisade and the core at high supersaturation.

3.4.1 Pharmaceutical Implications

The mathematical equations developed in this study provided a rapid determination of $\boldsymbol{a_R}$ and, thus, the absorption driving force. Although this technique was successfully applied to E2, which is a non-ionizable molecule within the gastrointestinal pH, application of this technique to other drug candidates requires a careful consideration on the membrane selection. A regenerated cellulose dialysis membrane was used in this study, which sufficed the need of separating free drug from both the amorphous aggregate and micellized drug molecules as previously demonstrated by others [154, 179, 238]. However, we acknowledge that other drug molecules may very well have ionizable groups, may form dimers, or perhaps may be complexed with cyclodextrin, all of which would be “recognized” as a free drug species using the dialysis membrane. From the physiology standpoint of the oral absorption process, it is *only* the free neutral species

that drives the absorption across the intestinal membrane. Thus, in the more complex case described above, e.g. ionizable compounds, those that may form dimers, or cyclodextrin-containing formulations, other membranes such as excised animal intestinal tissue or Ussing chamber [181] or those utilized in perfusion experiments [181, 183] among others should be employed and validated. In addition, the approach developed in this study requires a dilute condition, which can only be satisfied using poorly soluble compounds or BCS class II compounds. Nevertheless, the same approach of comparing the solution flux to the flux at the crystalline solubility in surfactant-free system as demonstrated in this study combined with an appropriate membrane selection based on the drug molecules tested would enable one to calculate the dynamic change in the drug thermodynamic activity necessary to maximize oral absorption.

3.5 Conclusions

The use of solubilizing agents in a formulation can significantly alter the supersaturated state by changing the thermodynamic driving force for drug absorption. Herein, a comparison of flux of a drug solution to the flux at the crystalline solubility limit in surfactant-free system allowed for calculation of the true supersaturation, $\boldsymbol{a_R}$. In addition, this approach enabled the mechanism elucidation by which surfactant micelles modulate supersaturation, whereby there is an increase of E2 molecules contained per micelle from approximately two molecules at the crystalline solubility limit to six molecules at the amorphous solubility limit. The exercise performed here is a useful approach to determine the true driving force for absorption in complex systems

containing various solubilizing excipients without prior knowledge of the thermodynamics of the system itself.

Chapter 4 - Impact of Drug-Excipient Intermolecular Interactions on Estradiol Crystallization Kinetics

4.1 Introduction

Although classical nucleation theory has been utilized to describe drug crystallization events arising from supersaturating drug delivery systems (SDDS) [2, 107, 239, 240], often the crystallization processes, especially in complex systems where formulation excipients and endogenous materials are present during the gastrointestinal (GI) transit, are very stochastic in nature and hence difficult to predict. This challenge stems from the fact that the crystallization process is convoluted by both thermodynamic driving forces of the drug as well as kinetic effects from interactions between drug molecules and additives (either excipients or endogenous materials). The thermodynamic driving force for crystallization of an amorphous material is commonly described by the Hoffman equation [121] and the recent variation thereof with improved heat capacity correction [138]. This crystallization driving force is also the amorphous energetic advantage over the crystalline form for drug absorption across a membrane. Hence, the thermodynamic driving force is a “double-edged sword” where a high driving force results in high absorption rate with a high crystallization risk.

For drug delivery purposes, excipients are added to minimize the high crystallization risk while still maintaining a high absorption rate. The use of excipients in SDDS has been ubiquitously illustrated in the literature, but the results observed may not necessarily produce the desired crystallization inhibition effect. In fact, some excipients actually accelerate drug crystallization. In the case of surfactants, sodium dodecyl sulfate

(SDS) and dodecyl trimethyl ammonium bromide (DTAB) were found to maintain supersaturation of γ-aminobutyric acid by delaying nucleation [241]. Guzman et al. also showed the supersaturation maintenance of celecoxib by SDS, tocopherol polyethylene glycol 1000 succinate (TPGS), and cremophor EL among other surfactants tested in their formulation screening [116]. Another interesting study showed that bile salts, which are commonly found in the intestinal fluids, delayed the crystallization of several poorly soluble compounds tested [242]. On the other hand, celecoxib crystal growth was shown to be accelerated by SDS and TPGS [243]. In yet another example, carbamazepine crystallization was promoted by SDS and sodium taurocholate (STC) [244]. When studying polymer excipients, Chauhan et al. ranked polymers as PVP>Eudragit>HPMC for the inhibition of indomethacin crystallization [245] whereas the same types of polymers were ranked as HPMC>PVP>Eudragit for griseofulvin and danazol supersaturation [246]. Ilevbare et al. proposed that solubility parameter could be used as a predictive tool for drug-excipient compatibility, where polymers with similar solubility parameter to the drug would provide the longest induction time [127]. Although many of the systems analyzed in Ilevbare et al. study were observed to follow the solubility parameter criteria, there were deviations of this ‘rule’ observed. As seen in the examples above, observations around the impact of excipients on the supersaturated state tend to be valid case by case and are difficult to be generalized. In addition, formulation excipients are usually added not only for maintaining drug supersaturation but also for manufacturing purposes. Hence, despite the primary motivation for including a particular excipient, secondary effects might be realized. A seemingly infinite other combinations

of functional excipients might be added with various ends in mind but may lead to an impact on the kinetics of crystallization.

As mentioned above, the observed induction time may be affected by the thermodynamic and kinetics factors, thus it is difficult to extrapolate the crystallization kinetics results to other systems. For instance, some excipients/additives, such as surfactants or bile salts, are capable of solubilizing hydrophobic drug molecules and could further change the drug thermodynamic activity in solution [154, 179, 247]. Therefore, it is difficult to distinguish whether a maintenance of supersaturation is due to a reduced thermodynamic activity caused by such solubilizing excipients or whether excipients provide a kinetic stabilization via drug-excipient intermolecular interactions. Previously, Setiawan et al. developed a mathematical model that allows for calculation of thermodynamic activity in the supersaturated state (Chapter 3). This chapter combines the mathematical model built in Chapter 3 with induction time experiments to probe the kinetics aspect of induction time due to excipients by keeping a constant thermodynamic activity. Specifically, this project aims to investigate the influence of hydroxypropyl methylcellulose (HPMC) and polysorbate 80 (PS80) on estradiol (E2) induction time.

4.2 Materials and Methods

4.2.1 Materials

17β-Estradiol (E2), polysorbate 80 (PS80) and tris maleate were purchased from Sigma-Aldrich (St. Louis, MO). Sodium hydroxide, methanol, and dimethyl sulfoxide (DMSO) were purchased from Fisher Scientific (Fair Lawn, NJ). Hydroxypropyl methylcellulose (HPMC) K4M grade was obtained from Colorcon (West Point, PA).

Deionized water was obtained from a MilliQ water purification device (Milli-Q Synthesis, Millipore, Bedford, MA) and filtered through a 0.22 μm filter (Millipak 40, Millipore, Bedford, MA) before use. Polytetrafluoroethylene (PTFE) syringe filters with a diameter of 13 mm (0.22 μm pore size) were purchased from Tisch Scientific (Cleves, OH). Regenerated cellulose dialysis membranes with 6-8 kDa MWCO were obtained from Spectrum Laboratories (Rancho Dominguez, CA). All materials were used as received. The chemical structures of E2, PS80, and HPMC are shown in Figure 4.1.

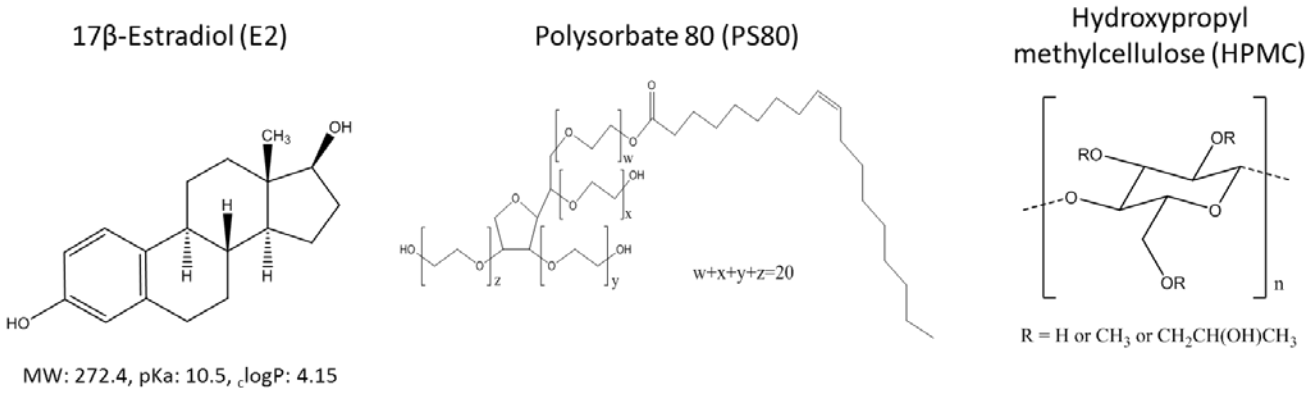

Figure 4.1 Chemical structures of estradiol (E2), polysorbate 80 (PS80), and hydroxypropyl methylcellulose (HPMC).

4.2.2 Crystalline Solubility Determination

The equilibrium solubility values of E2 in various test media were determined by placing an excess amount of E2 solid powder into a glass vial with a PTFE-lined screw cap containing the appropriate media, e.g. 50 mM tris maleate buffer pH 7.4 or buffer containing excipient(s). The mixture was rotated by a vial rotator in an incubator at 37°C for 72 hours and then filtered through a 0.22 μm syringe filter. The syringe filter was

saturated by discarding the first 3 mL of the filtrate. The concentration of E2 was determined using high-performance liquid chromatography (HPLC) with a UV detector (Waters, Milford, MA) and a Symmetry C18 column (4.6 mm internal diameter, 150 mm length, 5 μm particle size; Waters, Milford, MA). The mobile phase consisted of 70:30 methanol/water and was used isocratically. The detection wavelength was set at 280 nm. All solubility measurements were performed in triplicate.

4.2.3 Amorphous Solubility Measurement

The amorphous solubility measurement was performed via a solvent shift method. Highly concentrated E2 stock solutions in DMSO were prepared and each of these solutions was added into a cuvette containing 3 mL solution of buffer in the absence and presence of excipients. The addition of E2 stock solution was repeated several times to obtain several points below and above the amorphous solubility. The final concentration of DMSO was less than 1% v/v. After each E2 stock solution addition, the solution was stirred at 300 rpm for at least 1-2 minutes before measurement using a UV-Vis spectrometer. UV-Vis absorption was monitored by a Shimadzu UV-1800 spectrometer (Columbia, MD) at a wavelength of 700 nm. The onset of the rise in UV absorbance was taken as the amorphous solubility point [124]. An aliquot of each solution was placed under polarized light microscope (Olympus, Waltham, MA) to confirm the absence of birefringence.

4.2.4 Flux measurement

Flux experiments were carried out by following a method developed previously by Setiawan et al. (Chapter 3) to correct for the true extent of supersaturation, i.e. activity ratio (a_R). Variables in Eq. 4.1 are bulk volume (V), membrane surface area (A), acceptor

concentration (C), and effective permeability of drug molecules through the membrane (P_{eff}). Herein, a_R is the ratio of the drug activity in solution ($a_{D,solution}$) to the activity of the drug in solution at the crystalline solubility limit ($a_{D,saturation}$) as shown in Eq. 4.2. Thermodynamic activity is a product of the drug activity coefficient (γ_D) and the corresponding solution concentration ($C_{D,solution}$) or the crystalline solubility ($S_{crystal}$). Chemical potential of the crystalline solid drug dispersed in buffer at the saturation limit was used as the reference state for the activity measurement throughout this study. Supersaturation ratio (SR in Eq. 4.3) is a concentration-based measure of supersaturation where the ratio of the activity coefficients is neglected. Combination of Eq. 4.1 and 4.2 provides a direct means to measure a_R as shown in Eq. 4.4 where a_R is a ratio of flux at any drug concentration ($J_{D,solution}$) to the flux of drug at its crystalline solubility limit in surfactant-free system ($J_{D,saturation}$).

$$Flux(J) \equiv \frac{V}{A}\frac{dC}{dt} = P_{eff} \cdot a_{D,solution} \quad [4.1]$$

$$a_R \equiv \frac{a_{D,solution}}{a_{D,saturation}} = \frac{\gamma_{D,solution} * C_{D,solution}}{\gamma_{D,crystal} * S_{crystal}} = \frac{\gamma_{D,solution}}{\gamma_{D,crystal}} * SR \quad [4.2]$$

$$SR = \frac{C_{D,solution}}{S_{crystal}} \quad [4.3]$$

$$a_R \equiv \frac{a_{D,solution}}{a_{D,saturation}} = \frac{J_{D,solution}/P_{eff}}{J_{D,saturation}/P_{eff}} = \frac{J_{D,solution}}{J_{D,saturation}} \quad [4.4]$$

4.2.5 Induction Time Measurement

Desupersaturation of E2 was performed via a solvent shift method and analyzed by μDiss UV probes (Pion Inc., Billerica, MA). A highly concentrated stock solution of E2 was prepared in DMSO at varying concentrations depending on the initial supersaturation. A 100 μL Hamilton gas-tight syringe (Reno, NV) was used to inject the

drug stock solution into an experiment vial within approximately 20 s. The experiment vial was pre-filled with 20 mL of the corresponding media and stirred at 100 rpm. A thermal block was used to maintain a solution temperature of 37°C. A UV absorbance scan of E2 desupersaturation was generated and converted into its second derivative profile. The second derivative data at $\lambda = 280$ nm was then plotted against time as shown in Figure 4.2. Second derivative approach has previously been shown as a means to eliminate scattering effect from precipitate particles formed during a desupersaturation experiment, which in turn allows for a direct analysis of the drug concentration in solution [240, 248]. GraphPad Prism (La Jolla, CA) software was used to determine induction time from the second derivative data using the "plateau followed by one phase decay" model.

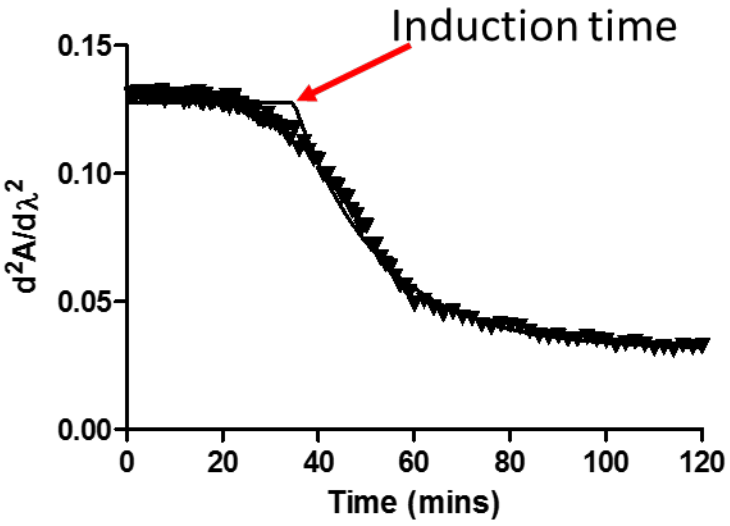

Figure 4.2 Example of a typical second derivative of UV absorbance plotted as a function of time for determination of E2 induction time. Data points (triangle) are taken with

intervals of 30 s or 1 min. Solid line represents the Prism fitted curve to determine the induction time.

4.2.6 Scanning Electron Microscopy (SEM) Analysis

Morphology of the solid precipitates in each induction time experiment was triple-washed with 5 mL of cold water stored in a 4°C (this washing step was performed before all of the post induction time analysis) and then analyzed with an FEI Quanta 250 Environmental SEM (FEI, Hillsboro, OR). Samples were mounted onto an aluminum stub using double-sided carbon tape. The sample surface was coated with a thin layer of gold/palladium using standard techniques. Micrographs were collected using a secondary electron detector and an accelerating beam voltage of 2 kV.

4.2.7 Powder X-Ray Diffraction (PXRD) Analysis

Precipitate samples at the end of induction time were analyzed using a powder X-ray diffractometer (Miniflex 600, Rigaku, The Woodlands, TX) at room temperature. X-ray diffractograms were obtained by exposing the sample to Cu K_α radiation (40 kV, 15 mA) with scanning speed of $2°2\theta\ min^{-1}$ and step size of $0.02°2\theta$.

4.2.8 Solid State Nuclear Magnetic Resonance (ssNMR) Analysis

Room temperature ssNMR was acquired using a Tecmag Redstone spectrometer (Tecmag, Inc., Houston, TX) operating at 75.6 MHz for ^{13}C (7.05 T static magnetic field). Samples were packed into 7.5 mm zirconia rotors and sealed with Teflon or Kel-F end caps (Revolution NMR, LLC, Fort Collins, CO). Experiments were performed using

a 7.5 mm double resonance MAS probe (Varian, Palo Alto, CA). All ^{13}C spectra were acquired under MAS [249] at 4 kHz at ambient conditions. ^{13}C chemical shifts are reported relative to 3-methylglutaric acid referenced to 18.84 ppm [250] with an accuracy of ±0.4 ppm. ^{13}C spectra were collected using ramped-CP [251], TOSS [252], and SPINAL64 decoupling [253] with ^{1}H decoupling field about 63 kHz. All spectra were acquired with a 5 s recycle delay and a 51.2 ms acquisition time. All spectra were processed without line broadening.

^{1}H T_1 relaxation values were measured using the saturation-recovery experiment through ^{13}C observation. In the Fourier-transformed spectrum, the intensity of the peak of interest was plotted against recovery delay times and the values were fitted to the following equation within the TNMR software:

$$M = M_0 \cdot \left(1 - e^{-\tau/T_1}\right) \qquad [4.5]$$

where M is the integrated signal intensity and τ is the recovery delay time. M_0 is an amplitude parameter obtained from the fit and T_1 is the obtained spin-lattice relaxation time.

4.3 Results

4.3.1 Crystalline and Amorphous Solubility

Crystalline and amorphous solubility of E2 as a function of PS80 concentration are shown in Figure 4.3. In the absence of excipients, crystalline solubility is 2 μg/mL. This crystalline solubility value increases linearly with increasing PS80 concentration to 60 μg/mL at 1% PS80. Addition of up to 0.05% HPMC (data not shown) did not affect the crystalline solubility in both the absence and presence of PS80. Amorphous solubility

measured at each PS80 concentration will be used to identify E2 concentrations that would provide the same a_R of 6 at each PS80 level (recall from Chapter 3 that a_R=6 at the amorphous solubility limit regardless of the PS80 presence). Comparisons of induction time at a_R=6 is shown in Figure 4.5.

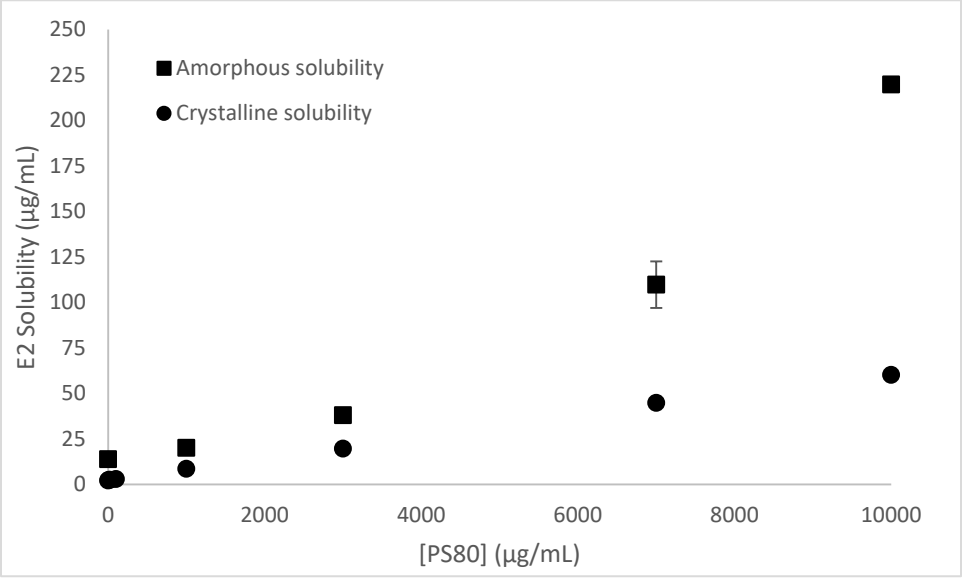

Figure 4.3 E2 crystalline (circle) and amorphous (square) solubility as a function of PS80 concentration. Error bars indicate standard deviation (n=3).

4.3.2 Induction Time

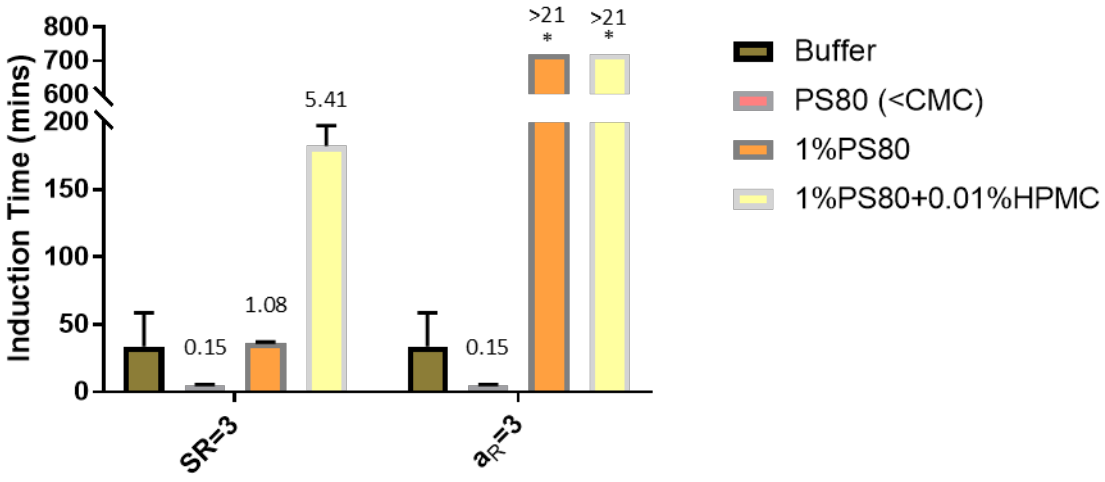

Figure 4.4 E2 induction time in buffer, PS80 in both the absence and presence of HPMC at SR and a_R of 3. The symbol "*" indicates induction time of longer than 12 hours. Number above each bar represents induction time in the presence of excipient(s) relative to that in buffer, $\frac{t_{i,e}}{t_{i,0}}$. Each value represents the mean ± SD (n=3). CMC is critical micelle concentration.

To illustrate the importance of correcting for the true extent of supersaturation (a_R) in place of SR, induction time experiments were compared side by side at the same a_R and SR as shown in Figure 4.4. Relative induction time, $\frac{t_{i,e}}{t_{i,0}}$, was used to indicate excipients impact on induction time as compared to the induction time in buffer. Induction time is accelerated by excipients when $\frac{t_{i,e}}{t_{i,0}} < 1$ and, conversely, delayed when $\frac{t_{i,e}}{t_{i,0}} > 1$. Induction time of 25 minutes was observed in buffer at SR=3. At the same SR, $\frac{t_{i,e}}{t_{i,0}}$ is equal to 0.15, 1.08, and 5.41 in low PS80 (below its critical micelle concentration, CMC, of 78 μg/mL), 1% PS80, and 1% PS80+0.01% HPMC systems, respectively.

When compared at the same a_R=3, $\frac{t_{i,e}}{t_{i,0}}$ is equal to 0.15 in low PS80 system while it is greater than 21 in both 1% PS80 and 1% PS80+0.01% HPMC systems. Induction times in buffer and low PS80 system were equal at SR and a_R of 3 because SR and a_R were shown in Chapter 3 to correlate linearly in unity in the absence of solubilizing excipients or micelles. However, it is clearly demonstrated that induction time profile, especially in the presence of solubilizing excipients, differ significantly depending on whether SR or a_R comparison is used.

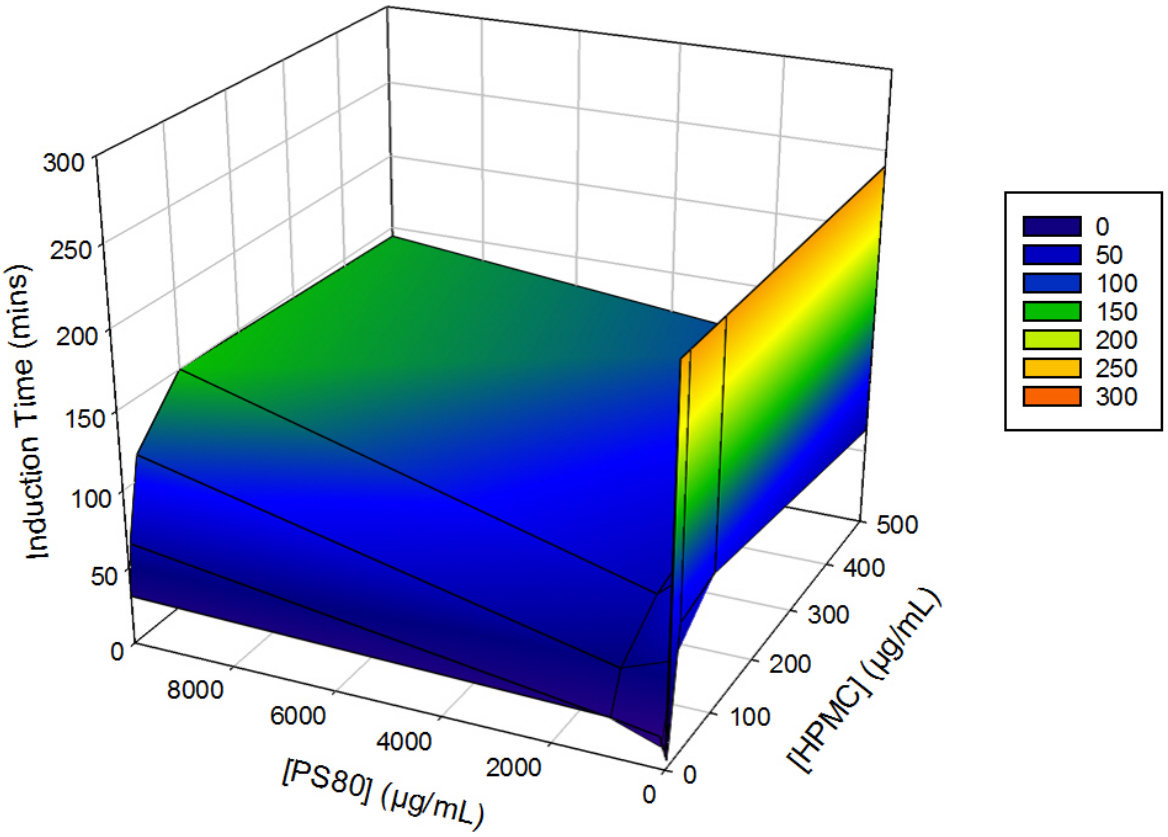

Figure 4.5 E2 induction time as a function of PS80 and HPMC concentrations at a_R of 6, which corresponds to the respective amorphous solubility limit.

Since the goal of this study was to isolate the kinetics factor of induction time, comparisons were done at the same a_R to ensure that drug thermodynamic activity remains the same. Figure 4.5 shows a 3D plot of induction time as a function of excipient concentrations at a_R=6, which corresponds to the maximum drug activity at the amorphous solubility limit (see Figure 4.3). Induction time was 15 minutes in buffer. Addition of HPMC, even at a low concentration, significantly prolongs induction time where E2 did not precipitate within the 4 hours of experiment. On the other hand, interestingly, the shortest induction time was observed in low PS80 system (below its CMC), consistent with observations in Figure 4.4. Induction time, however, increased with increasing PS80 concentration. At the highest PS80 concentration of 1%, induction time was 60 minutes. When HPMC is added, induction time was prolonged at each PS80 concentration. In addition, Figure 4.5 suggests that there is an induction time maxima at each PS80 concentration, and the higher the PS80 concentration the less HPMC concentration is needed to reach this maxima.

4.3.3 Characterizations of Solid Precipitates

Solid precipitates generated at the conclusion of each induction time experiment were analyzed by several techniques to understand the mechanisms by which excipients affect induction time. Figure 4.6 shows the SEM images of solid precipitates generated at the end of induction time experiments in buffer, 1% PS80, and 1% PS80+0.01% HPMC. All precipitates from this study were crystalline in nature as confirmed by polarized light microscope (data not shown) and powder X-ray diffraction (Figure 4.7). Rod-shaped E2 crystals were observed in precipitates from both buffer and 1% PS80+0.01% HPMC,

whereas irregular shape with mixtures of rod-like and plate-like crystal habits were observed in precipitates from 1%PS80. The X-ray diffractograms suggest that E2 crystallized to its original hemihydrate crystal form in all media. Interestingly, precipitates from 1% PS80+0.01% HPMC exhibit a halo pattern in the 2-theta region between 35-45°, which suggests that there exists an amorphous co-precipitate in the collected sample.

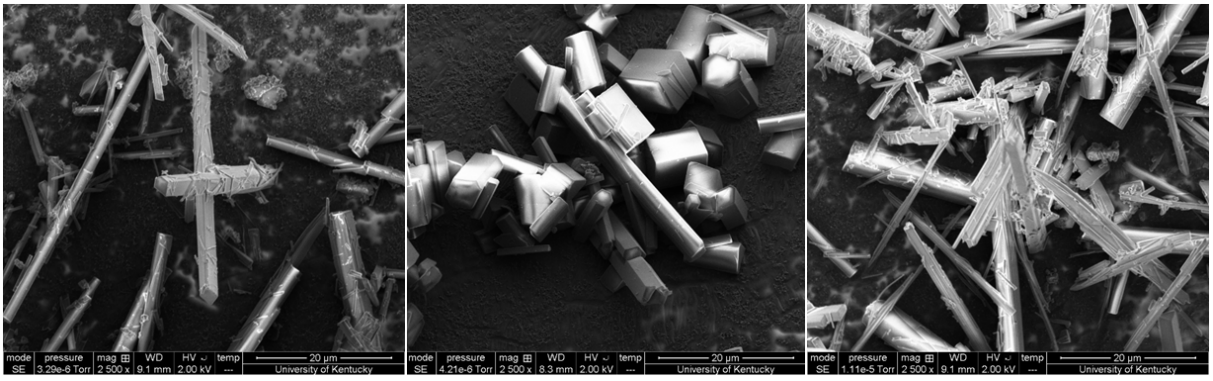

Figure 4.6 SEM images of solid precipitates obtained from (left to right): Buffer, 1% PS80, 1%PS80 + 0.01%HPMC.

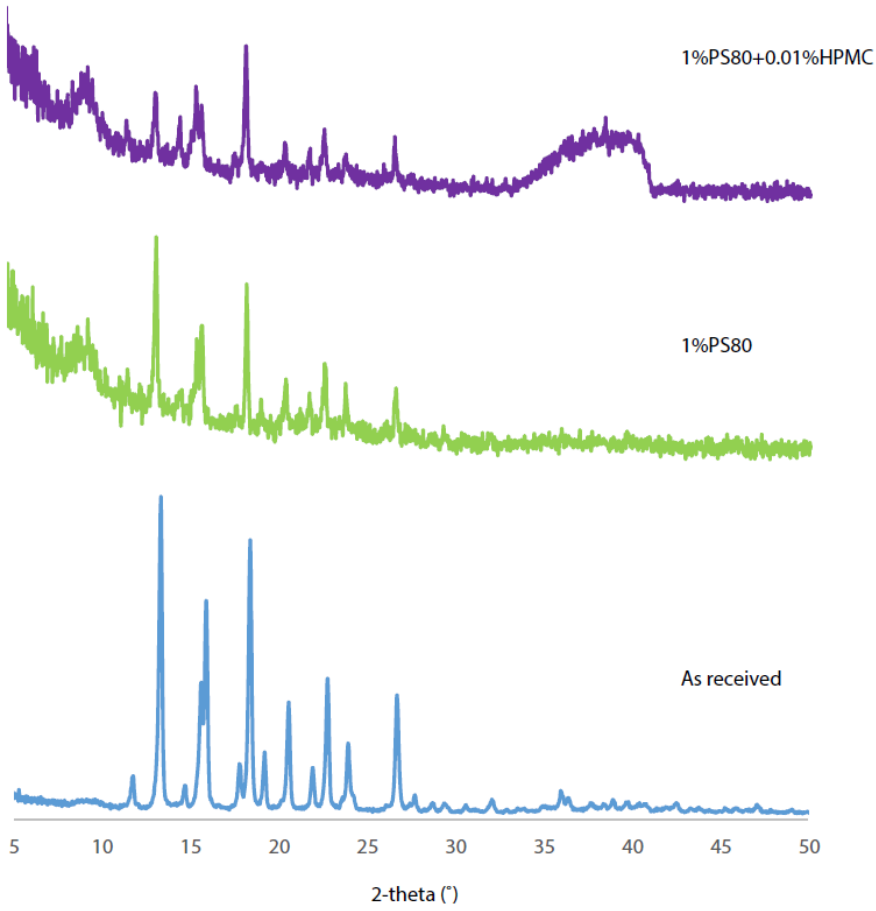

Figure 4.7 Powder X-ray diffractograms of (from bottom up) as received E2, solid precipitates in 1%PS80 and 1%PS80 + 0.01%HPMC.

To further investigate the precipitate sample from 1%PS80 + 0.01%HPMC, solid-state NMR 1D scan was performed as shown in Figure 4.8. In addition, 1D NMR scan was performed on as received E2 and HPMC materials for comparison purposes. The precipitate sample showed broad peaks between 50-110 ppm region (indicated by arrows in the figure), which belong to HPMC. In addition, T_1 relaxation times of E2 and HPMC in the precipitate sample were analyzed to investigate whether the two components are miscible in the sample [28]. The results in Table 4.1 showed that the T_1 relaxation time of HPMC in the precipitate differs from that of E2 crystal, suggesting that the two

components are immiscible. Furthermore, the T_1 value of HPMC in the precipitate sample is statistically different from the as-received HPMC, suggesting that there is some level of interaction between HPMC and E2 in the precipitate sample albeit they are immiscible.

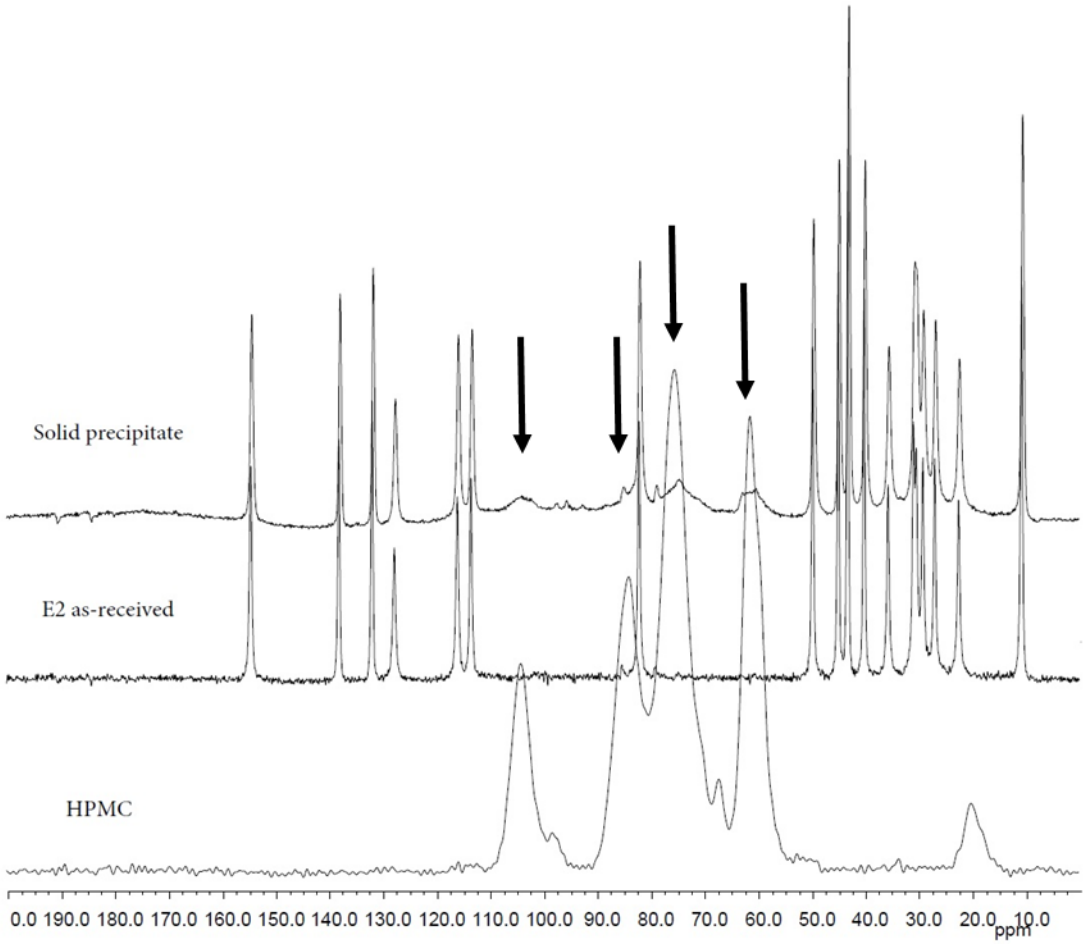

Figure 4.8 From bottom to top are the solid-state NMR ^{13}C spectra of HPMC, as-received E2, and the solid precipitate obtained at the end of induction time experiment in 1%PS80 + 0.01%HPMC media. Arrows indicate the presence of HPMC molecules in the E2 solid precipitate.

Table 4.1 T_1 relaxation times for E2 and HPMC in the precipitate sample and HPMC as received.

Component	**T_1 (s)**
E2 in precipitate	>15
HPMC in precipitate	3.16 ± 0.30
HPMC as received	1.26 ± 0.02

4.4 Discussion

SDDS rely on their ability to generate the 'spring and parachute' effect in the GI tract within the GI transit time to enhance the oral bioavailability of poorly soluble crystalline drugs [2]. The extent of 'spring' is key towards oral bioavailability enhancement where high 'spring' is needed to drive absorption, but low 'spring' is more favorable in maintaining supersaturation in general. Concentration-based SR has often been used to measure the extent of 'spring' term because of the practicality in laboratory measurement [2]. In a study conducted by Setiawan et al. in Chapter 3, however, demonstrated that SR could deviate from the true supersaturation, a_R. Therefore, a_R was used in this study for induction time comparisons. Figure 4.4 illustrates the impact of the deviation between SR and a_R on E2 induction time where the greatest disparity in induction time was observed especially in the non-dilute systems containing high PS80

concentration. These results suggest that while it is practical to use SR for induction time comparisons, significantly different results may be observed when a_R is considered especially in systems containing solubilizing excipients.

By means of comparing induction time at the same a_R, the impact of excipients ('parachute' term) on induction time kinetics can be evaluated. Figure 4.5 shows the impact of PS80 and HPMC concentrations on induction time at a_R=6. Low concentration of PS80 (below its CMC) was shown to accelerate induction time. Nucleation process is dictated by the sum total of competing free energy gain from creating a volume that creates a more stable state for the system and the free energy cost of creating an interface [254]. These nuclei undergo a reciprocating process of dissolution and crystallization until stable nuclei are formed, which is then followed by the subsequent crystal growth process. For every interface, a potential difference across the interface, which is also known as interfacial tension, is present. Interfacial tension is magnified when the degree of dissimilarity between the two species is high at the interface. Herein, hydrophobic E2 nuclei are surrounded by hydrophilic aqueous environment, creating a high interfacial tension. Surfactant, abbreviated from 'surface-active agent', molecules tend to occupy these surfaces (liquid-gas) or interfaces (liquid-liquid or liquid-solid) and orient themselves in such a way that will reduce the surface/interfacial tension [255]. Hence, it is hypothesized that the short induction time in low PS80 system is due to the reduced interfacial tension, allowing a more facile transport of E2 molecules onto the nuclei. Although there is no direct evidence on this hypothesis, the surface tension data (not shown) suggest that there was a 40% reduction in the surface tension at the CMC of PS80 compared to that in absence of PS80. Although surface tension (liquid-gas) is different

from interfacial tension (liquid-solid), it is reasonable to expect that a decrease in the surface tension be accompanied by a decrease in the interfacial tension. The hydrophilicity/hydrophobicity between the two interfaces, liquid-gas and liquid-solid, can be argued to be similar in nature. In addition, adsorption of surfactant molecules onto E2 nuclei could also offer an explanation for the rapid E2 crystallization via 'poisoned' E2 nuclei surfaces [256]. Based on the computational prediction of the E2 hemihydrate crystal structure, water molecules are shared between the hydroxyl groups attached to both benzene ring and the 5-membered ring of E2 molecule in a head-to-tail fashion [257]. Hence, if surfactant adsorption were to occur, hydrophobic tail of PS80 would have covered the hydrophobic face of E2 lattice and precipitate particles produced would have shown a uniform crystal habit. Instead, precipitates from PS80 solution exhibited random crystal habits, and thus surfactant adsorption may be ruled out or at least it may not be the primary factor for the short induction time observed.

Above the CMC, surface tension remains constant. In other words, only the surfactant monomer brings about the change in surface tension. If interfacial tension were the primary factor for E2 induction time, then it is reasonable to expect that induction time be the same in PS80 systems both below and above the CMC. However, induction time is longer at higher PS80 concentration as observed in Figure 4.4 and 4.5. Although micelle adsorption could occur, the bulkiness (aggregation number of 60) of the PS80 micelle along with its bulky PEGylated hydrophilic surface make it unlikely for PS80 micelles to adsorb onto small E2 nuclei. In the presence of micelles, E2 molecules located in free aqueous environment and those in micelles are continuously exchanging. Thus, it is reasonable to observe a slower crystallization kinetic because this competing

effect would reduce the likelihood of free drug being available for nucleation, especially at low a_R shown in Figure 4.4 where induction time in 1% PS80 is significantly longer than that in buffer. At higher a_R=6, induction time in 1% PS80 is shorter and close to the value observed in buffer (Figure 4.5). The fast crystallization at high a_R could be due to micellar catalysis [258]. Micellar catalysis phenomena have been reported in the literature where a substrate is localized in the micelle such that the reactive site is available to the attacking reagent [259]. Nucleation is a physical reaction process, which could be catalyzed in micelles. At the amorphous solubility limit, there are 6 E2 molecules contained per PS80 micelle as shown in Chapter 3. Therefore, it would be interesting to evaluate whether this number corresponds to the minimum number of molecules required to form a stable E2 nuclei to support micellar catalysis hypothesis.

In all studies performed herein, the addition of HPMC always extends E2 induction time. HPMC is known to increase the solution viscosity, which has been proposed as one of the mechanisms by which crystallization is delayed [260, 261]. However, our viscosity data (not shown) suggests that no significant change in viscosity is observed when HPMC is added, at least in the concentration range employed here. From the SEM data in Figure 4.6, needle-like crystal habits from 1% PS80+0.01% HPMC were observed. This needle-like habits is similar to that obtained from buffer but different from that obtained from 1% PS80 media, which has a random plate-like habits. Although similar in crystal habits, precipitates from buffer may differ in the lattice growing face compared to that in 1% PS80+0.01% HPMC. In other words, in buffer E2 may grow on the fastest growing site along the hydroxyl terminal of the molecule whereas the presence of HPMC may block this site causing E2 to grow via a slower

growing site/axis. The fact that there is a change in crystal habits and a significantly longer induction time in 1% PS80+0.01% HPMC compared to 1% PS80 to suggests that there is an adsorption of HPMC on the surface of E2 precipitates. Indeed, this phenomenon is supported by the PXRD (Figure 4.7) and solid-state NMR (Figure 4.8) data, both of which showed the presence of HPMC in the precipitate samples. Quantitative analysis of HPMC in the precipitate sample using ssNMR was difficult due to the limited amount of sample generated and the long relaxation time of the E2 crystalline. However, the precipitate sample was able to be quantitatively analyzed using charged aerosol detector HPLC system. The results suggest that the precipitate contained 10% of HPMC. Although it is possible that the presence of HPMC in the precipitate is due to the residual water (since HPMC is pre-dissolved in the media) after filtration, this can be ruled out because analysis on the mass change between precipitate after filtration versus dried precipitate corresponds to less than 1% of water mass. If any of the HPMC from this residual water were "arrested" in the precipitate, its mass would have corresponded to less than 1 ppm mass of the sample (HPMC concentration was 100 μg/mL in the media), which is miniscule compared to the 10% value observed in the HPLC data. Further, the fact that there is a significant change in T_1 relaxation times (Table 4.1) between as-received HPMC and HPMC in the precipitate suggests that there is some degree of intermolecular interaction, such as surface adsorption, between HPMC and E2 molecules in the precipitate sample. A depletion experiment, where controlled size (0.4-22 μm) particles of E2 as-received crystals were dispersed in solution containing pre-dissolved HPMC, was also performed to identify whether HPMC adsorbs onto E2 solid surfaces at the later portion of crystal growth step. The result showed that there was

no depletion of HPMC from the solution, which suggests that adsorption occurred at the early stage of nucleation when the nuclei size is in the low nanometers range or less.

4.5 Conclusions

Excipients, such as polymers and surfactants, are key components to successful supersaturated formulations as they are intended to provide the ‘parachute effect’ throughout the GI transit. However, the excipient screening process, which is typically performed in the pre-formulation step of the drug development, may often be performed at different thermodynamic activity and hence erroneous conclusions about the impact of excipients on induction time may be obtained. Coupling flux with induction time studies allows for measurement of crystallization kinetics at the same thermodynamic activity, which permits formulators to isolate the kinetics factor of induction time. This approach is a beneficial and useful application in excipient screening process, which provides information on the parachute effect while uncompromising the maximum spring effect.

APPENDIX A - Impact of Different Polymers on the Crystallization Kinetics of Structurally Diverse Drug Molecules

A.1. Purpose

The purpose of this exercise was to observe the influence of different polymers on the induction time of several drug molecules.

A.2. Methods

Induction time experiments were performed via a solvent shift method and analyzed by μDiss UV probes (Pion Inc., Billerica, MA). A highly concentrated drug stock solution was prepared in DMSO or methanol at varying concentrations depending on the initial supersaturation. A 100 μL Hamilton gas-tight syringe (Reno, NV) was used to inject the drug-in-organic solution into the experiment vial and the solution was injected within approximately 20 s. The experiment vial was pre-filled with 20 mL of the corresponding media and stirred at 100 rpm. Excipients of 100 μg/mL each were pre-dissolved in the media. The vial was placed in a thermal block to maintain a solution temperature of 37°C. A UV absorbance scan of the drug was generated and converted into its second derivative profile. The second derivative data was then plotted against time to determine induction time. Amorphous solubility was determined following Ilevbare et al. method [124].

A.3. Results

Estradiol (E2) induction time data in Chapter 6 showed that, in general, E2 crystallized quite rapidly and the addition of HPMC helped sustain supersaturation. It was then our interest to explore other commonly used polymers on E2 supersaturated

solution. All the experiments herein were performed at the drug amorphous solubility limit. Figures A.1 (top) and (bottom), which show E2 induction time in the absence and presence of 10 mg/mL PS80, respectively, suggest that there is no difference between the polymers used in maintaining E2 supersaturation, at least within the 2 hours experiment time.

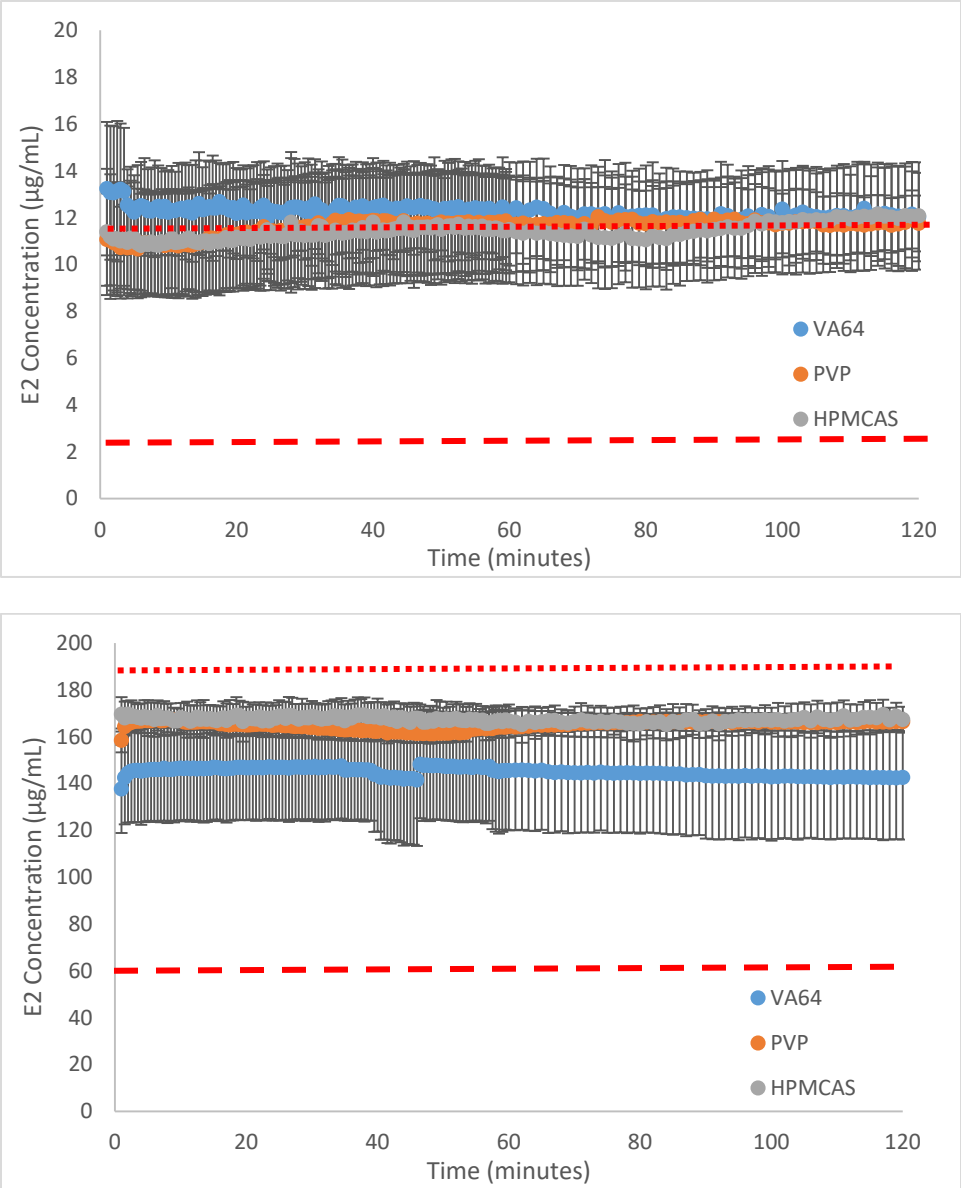

Figure A.1. E2 concentration profile as a function of time starting with supersaturation at the amorphous solubility limit of the drug in the absence (top) and presence (bottom) of

10 mg/mL PS80. Dotted line represents amorphous solubility limit and dashed line represents crystalline solubility limit.

On the other hand, different polymers conferred very distinct induction time profiles when tested on other drug molecules, i.e. indomethacin and telaprevir, as shown in Figures A.2 and A.3. Interestingly, in some cases the concentration of indomethacin was able to exceed the amorphous solubility limit.

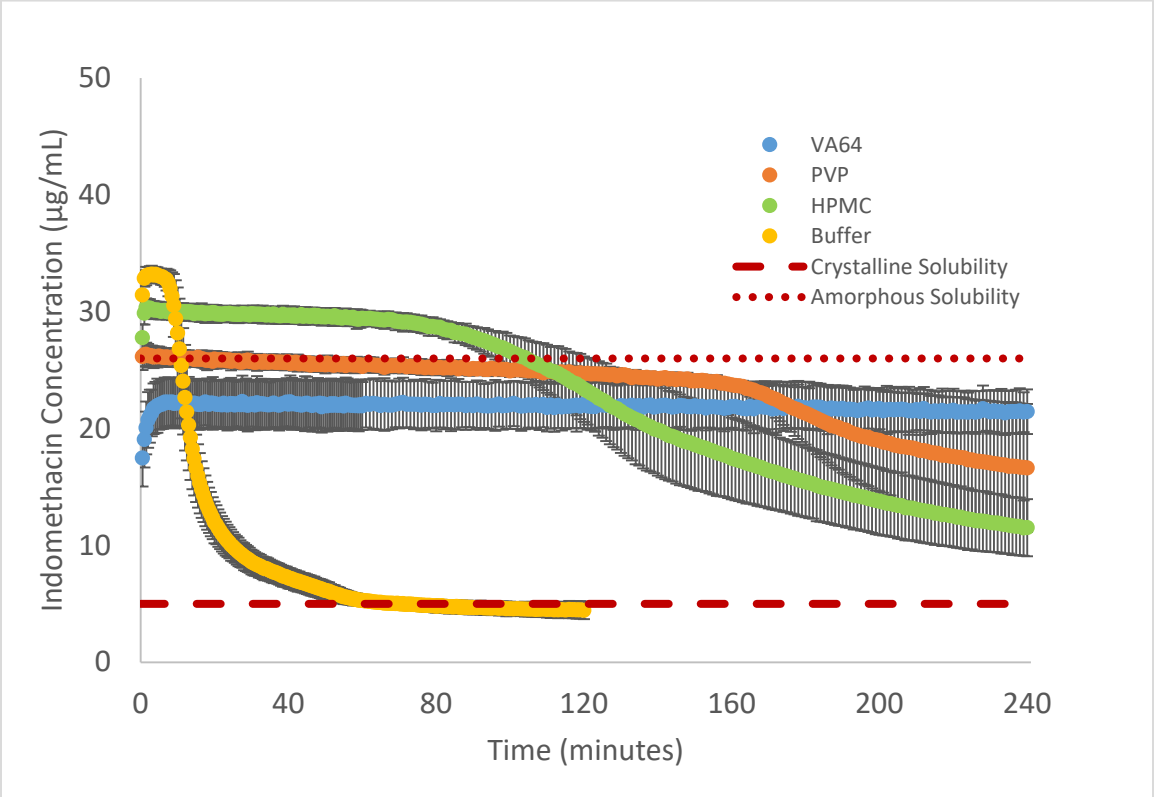

Figure A.2. Indomethacin concentration profile as a function of time starting with supersaturation at the amorphous solubility of the drug in the presence of various polymers. Dotted line represents amorphous solubility limit and dashed line represents crystalline solubility limit.

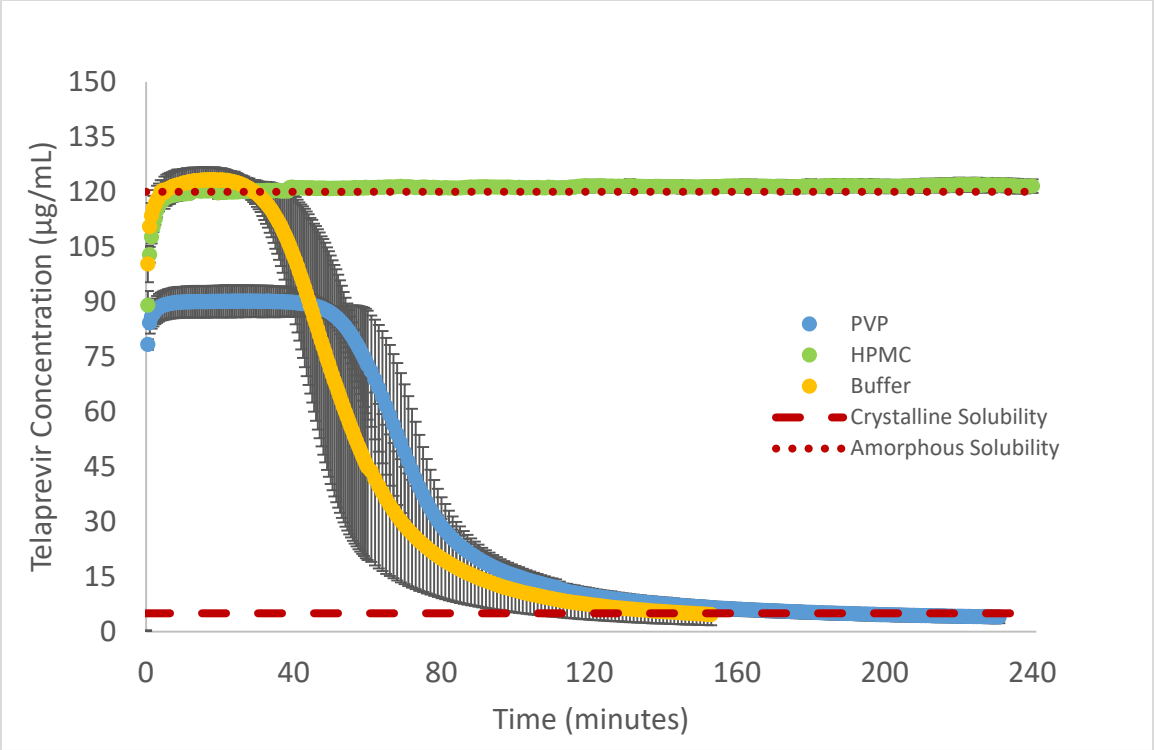

Figure A.3. Telaprevir concentration profile as a function of time starting with supersaturation at the amorphous solubility of the drug in the presence of various polymers. Dotted line represents amorphous solubility limit and dashed line represents crystalline solubility limit.

APPENDIX B – Preformulation Screening of Structurally-Similar Abuse Deterrent Molecules

B.1 Purpose

The purpose of this exercise was to determine several important parameters useful for preformulation screening process of structurally similar JPC molecules. JPC molecules were recently developed to treat methamphetamine abuse [262].

B.2. Methods

Solid-state crystallization rate was determined following Baird et al. [10]. Solution-state crystallization rate was determined by a solvent shift method, where initially the drug was dissolved in DMSO and the solution was transferred into FaSSIF such that the final drug concentration was 1 mg/mL. The drug concentration was monitored every 30 minutes by HPLC with a UV detector (analysis performed at 272 nm) and a Symmetry C18 column (4.6 mm internal diameter, 150 mm length, 5 μm particle size). The mobile phase consisted of 85:15 methanol/water each containing 0.1% phosphoric acid and was used isocratically. Amorphous solubility was determined following Ilevbare et al. method [124]. The structures of JPC molecules are not shown for confidential purposes.

B.3. Results

Several important parameters (i.e. solid-state and solution-state crystallization rates as well as amorphous solubility) of JPC molecules are listed in Table B.1. From this table, it is clear that these parameters, which subsequently dictate the drug bioperformance, can vary greatly even with a subtle variation of functional groups

attachment from the parent molecule structure. In general, the solid-state crystallization kinetics correspond to those in the solution state, except in the case of JPC-078 where the two kinetics significantly differed. The amorphous solubility also greatly varies within compounds, indicating that not all compound is suitable for amorphous formulation. Although it can be argued that the difference between the amorphous solubility to the crystalline solubility is an important parameter when one utilizes amorphous formulation, the amorphous solubility value itself is also critical in determining the maximum absorbable dose as low solubility would result in low absorption, assuming all other factors are constant.

Table B.1. Solid-state and solution-state crystallization rates as well as amorphous solubility values of various JPC compounds.

Compound	Crystallization rate (solid)	Crystallization rate (solution)	Amorphous solubility (ug/mL)
JPC-068	intermediate	fast	13.90
JPC-077	fast	fast	12.00
JPC-078	fast	slow	7.37
JPC-089	intermediate	slow	4.39
JPC-109	fast	fast	1.95
JPC-141	intermediate	slow	212.05

APPENDIX C – Tables of Chapter 2

Table C.1 Thermodynamic properties of various drugs [205, 228, 263]. T_g: glass transition temperature, T_m: melting temperature, ΔH_m: enthalpy of fusion, ΔC_p: heat capacity difference between the glass and super cooled liquid, ΔH_∞: equilibrium/maximum relaxation enthalpy, T_a: annealing temperature.

Compound	**T_g, K**	**T_m, K**	**ΔH_m, J/g**	**ΔC_p, J/g/K**	**ΔH_∞, J/g**	**$\Delta H_\infty/\Delta H_m$, %**	**T_g-T_a, K**
Indomethacin	321.0	434.0	110.0	0.37	8.5	9	23.0
Nifedipine	321.6	445.3	115.2	0.27	6.4	6	23.6
Flopropione	335.1	414.8	80.2	0.7	26.0	32	37.1
Glibenclamide	331.0	450.0	108.0	0.45	14.9	14	33.0
Griseofulvin	364.0	494.0	107.0	0.36	23.8	22	66.0
Hydrochloriazide	385.0	547.0	104.0	0.31	27.0	26	87.0
Polythiazide	346.0	493.0	97.0	0.34	16.3	17	48.0
Indomethacin	317.6	435.2	102.0	0.37	7.3	7	19.6
Iopanoic acid	315.4	425.6	52.5	0.15	2.7	5	17.4
Glipizide	331.3	471.5	124.4	0.82	27.3	22	33.3
Glybendamide	321.6	446.9	112.1	0.40	9.4	8	23.6
Hydrochlorothiazide	387.3	539.4	126.3	0.38	33.9	27	89.3
Terfenadine	332.6	423.2	89.9	0.54	18.7	21	34.6
Griseofulvin	363.3	494.2	107.1	0.29	18.9	18	65.3
Spironolactone	353.6	480.4	98.4	0.12	6.7	7	55.6
Danazol	348.0	492.8	94.5	0.18	9.0	10	50.0
Sulfathiazole	331.1	473.8	112.4	0.44	14.6	13	33.1
Sulfadimidine	347.3	470.6	125.3	0.51	25.1	20	49.3

Table C.2 Maximum relaxation enthalpy and glass transition data for drug/PVP dispersions of various compositions annealed at constant temperature (T_g: glass transition temperature, T_a: annealing temperature, ΔC_p: heat capacity difference between the glass and supercooled liquid, ΔH_∞: equilibrium relaxation enthalpy) [264].

System	**Drug Loading, %**	**T_g, K**	**T_a, K**	**ΔC_p, J/(g*K)**	**ΔH_∞, J/g**
Naproxen/PVPK12	100	279.3	278	0.79	1.1
Naproxen/PVPK12	95.53	309.4	278	0.18	5.7
Naproxen/PVPK12	90.36	338.1	278	0.24	14.4
Naproxen/PVPK12	85.68	345.1	278	0.35	23.5
Naproxen/PVPK12	79.07	339.2	278	0.36	22.0
Naproxen/PVPK12	70.58	316.4	278	0.38	14.6
Naproxen/PVPK12	61.06	305.9	278	0.34	9.5
Naproxen/PVPK12	49.54	314.6	278	0.33	12.1
Naproxen/PVPK12	27.43	294.5	278	0.32	5.3
Naproxen/PVPK12	0	370.1	278	0.2	18.4
Naproxen/PVPK25	100	279.3	278	0.79	1.1
Naproxen/PVPK25	94.22	414.6	278	0.25	34.2
Naproxen/PVPK25	89.61	404.8	278	0.23	29.2
Naproxen/PVPK25	84.87	390.1	278	0.28	31.4
Naproxen/PVPK25	78.69	380.2	278	0.28	28.6
Naproxen/PVPK25	71.22	360.7	278	0.28	23.2
Naproxen/PVPK25	59.91	341.5	278	0.35	22.2

Table C.2 (continued)

System	Drug Loading, %	Tg, K	Ta, K	Δ Cp, J/(g*K)	ΔH∞, J/g
Naproxen/PVPK25	50.02	330.1	278	0.36	18.7
Naproxen/PVPK25	21.9	298.3	278	0.36	7.3
Naproxen/PVPK25	0	430.2	278	0.21	32.0
Naproxen/PVPK90	100	279.3	278	0.79	1.1
Naproxen/PVPK90	95.72	433.8	278	0.23	35.8
Naproxen/PVPK90	90.08	415.8	278	0.26	35.8
Naproxen/PVPK90	87.72	404.7	278	0.2	25.3
Naproxen/PVPK90	79.94	391.9	278	0.3	34.2
Naproxen/PVPK90	69.1	370.2	278	0.29	26.7
Naproxen/PVPK90	60.06	351.5	278	0.22	16.2
Naproxen/PVPK90	48.41	333.4	278	0.32	17.7
Naproxen/PVPK90	26.21	295.4	278	0.38	6.6
Naproxen/PVPK90	0	451.8	278	0.22	38.2

Table C.3 Recovery enthalpy (ΔH) and glass transition (T_g) changes in polymer-drug dispersions annealed at constant time (t_a) and temperature (T_a) [265].

System	Drug Loading, %	T_g, K	T_a, K	t_a, hr	ΔH, J/g
Valdecoxib	100	331.9	313	24	7.95
Valdecoxib/PVP K29/32	99	332	313	24	6.5
Valdecoxib/PVP K29/32	98	332.5	313	24	6.3
Valdecoxib/PVP K29/32	95	333	313	24	6.2
Valdecoxib/PVP K29/32	90	337	313	24	5
Valdecoxib/PVP K29/32	85	339.5	313	24	3.1
Valdecoxib/PVP K29/32	80	344	313	24	2.9
Etoricoxib	100	333.5	314	24	6.38
Etoricoxib/PVP K29/32	99	334	313	24	5
Etoricoxib/PVP K29/32	98	334	313	24	4.8
Etoricoxib/PVP K29/32	95	335.5	313	24	4.9
Etoricoxib/PVP K29/32	90	336	313	24	5.1
Etoricoxib/PVP K29/32	85	338	313	24	5
Etoricoxib/PVP K29/32	80	342	313	24	4.4

REFERENCES

1. Lipp, R., *The Innovator Pipeline: Bioavailability Challenges and Advanced Oral Drug Delivery Opportunities.* American Pharmaceutical Review, 2013.
2. Brouwers, J., M.E. Brewster, and P. Augustijns, *Supersaturating drug delivery systems: the answer to solubility-limited oral bioavailability?* J Pharm Sci, 2009. **98**(8): p. 2549-72.
3. Newman, A., G. Knipp, and G. Zografi, *Assessing the performance of amorphous solid dispersions.* J Pharm Sci, 2012. **101**(4): p. 1355-77.
4. Yu, L., *Amorphous pharmaceutical solids: preparation, characterization and stabilization.* Advanced Drug Delivery Reviews, 2001. **48**(1): p. 27-42.
5. Bhugra, C. and M.J. Pikal, *Role of thermodynamic, molecular, and kinetic factors in crystallization from the amorphous state.* Journal of Pharmaceutical Sciences, 2008. **97**(4): p. 1329-1349.
6. Mahmah, O., et al., *A comparative study of the effect of spray drying and hot-melt extrusion on the properties of amorphous solid dispersions containing felodipine.* Journal of Pharmacy and Pharmacology, 2014. **66**(2): p. 275-284.
7. Marsac, P.J., et al., *Effect of temperature and moisture on the miscibility of amorphous dispersions of felodipine and poly(vinyl pyrrolidone).* J Pharm Sci, 2010. **99**(1): p. 169-85.
8. Rumondor, A.C., et al., *Understanding the tendency of amorphous solid dispersions to undergo amorphous-amorphous phase separation in the presence of absorbed moisture.* AAPS PharmSciTech, 2011. **12**(4): p. 1209-19.
9. Lakshman, J.P., et al., *Application of melt extrusion in the development of a physically and chemically stable high-energy amorphous solid dispersion of a poorly water-soluble drug.* Mol Pharm, 2008. **5**(6): p. 994-1002.
10. Baird, J.A., B. Van Eerdenbrugh, and L.S. Taylor, *A classification system to assess the crystallization tendency of organic molecules from undercooled melts.* J Pharm Sci, 2010. **99**(9): p. 3787-806.
11. Zhang, G.G., et al., *Phase transformation considerations during process development and manufacture of solid oral dosage forms.* Adv Drug Deliv Rev, 2004. **56**(3): p. 371-90.
12. Poozesh, S., et al., *Understanding the process-product-performance interplay of spray dried drug-polymer systems through complete structural and chemical characterization of single spray dried particles.* Powder Technology, 2017. **320**(Supplement C): p. 685-695.
13. Ayenew, Z., A. Paudel, and G. Van den Mooter, *Can compression induce demixing in amorphous solid dispersions? A case study of naproxen–PVP K25.* European Journal of Pharmaceutics and Biopharmaceutics, 2012. **81**(1): p. 207-213.
14. Ke, P., et al., *Investigation of preparation methods on surface/bulk structural relaxation and glass fragility of amorphous solid dispersions.* International Journal of Pharmaceutics, 2012. **422**(1–2): p. 170-178.
15. Leane, M.M., et al., *Formulation and process design for a solid dosage form containing a spray-dried amorphous dispersion of ibipinabant.* Pharmaceutical Development & Technology, 2013. **18**(2): p. 359-366.

16. Wu, T. and L. Yu, *Surface Crystallization of Indomethacin Below T g.* Pharmaceutical Research, 2006. **23**(10): p. 2350-2355.
17. Marsac, P.J., H. Konno, and L.S. Taylor, *A comparison of the physical stability of amorphous felodipine and nifedipine systems.* Pharm Res, 2006. **23**(10): p. 2306-16.
18. Rumondor, A.C., L.A. Stanford, and L.S. Taylor, *Effects of polymer type and storage relative humidity on the kinetics of felodipine crystallization from amorphous solid dispersions.* Pharm Res, 2009. **26**(12): p. 2599-606.
19. Qian, F., et al., *Is a distinctive single Tg a reliable indicator for the homogeneity of amorphous solid dispersion?* International Journal of Pharmaceutics, 2010. **395**(1): p. 232-235.
20. Hancock, B.C. and G. Zografi, *Characteristics and significance of the amorphous state in pharmaceutical systems.* J Pharm Sci, 1997. **86**(1): p. 1-12.
21. Kim, J., et al., *Uniquely Broad Glass Transition Temperatures of Gradient Copolymers Relative to Random and Block Copolymers Containing Repulsive Comonomers*. Macromolecules, 2006. **39**(18): p. 6152-6160.
22. Matteucci, M.E., et al., *Design of Potent Amorphous Drug Nanoparticles for Rapid Generation of Highly Supersaturated Media.* Molecular Pharmaceutics, 2007. **4**(5): p. 782-793.
23. Pikal, M.J., et al., *Quantitative crystallinity determinations for beta-lactam antibiotics by solution calorimetry: correlations with stability.* J Pharm Sci, 1978. **67**(6): p. 767-73.
24. Kayaert, P. and G. Van den Mooter, *Is the amorphous fraction of a dried nanosuspension caused by milling or by drying? A case study with Naproxen and Cinnarizine.* European Journal of Pharmaceutics and Biopharmaceutics, 2012. **81**(3): p. 650-656.
25. Marsac, P. and L. Taylor, *Thermodynamics of mixing drugs and polymers*, in *AAPS National Meeting* 2008.
26. Alin, J., et al., *Solution Calorimetry for Determination of Room Temperature Miscibility and Solubility of a Drug in a Polymer Matrix*. 2017: Polymer.
27. Ilevbare, G., P. Marsac, and A. Mitra, *Performance and Characterization of Amorphous Solid Dispersions: An Overview*, in *Discovering and Developing Molecules with Optimal Drug-Like Properties*, A.C. Templeton, et al., Editors. 2015, Springer New York. p. 287-343.
28. Yuan, X., D. Sperger, and E.J. Munson, *Investigating Miscibility and Molecular Mobility of Nifedipine-PVP Amorphous Solid Dispersions Using Solid-State NMR Spectroscopy*. Molecular Pharmaceutics, 2014. **11**(1): p. 329-337.
29. Shah, B., V.K. Kakumanu, and A.K. Bansal, *Analytical techniques for quantification of amorphous/crystalline phases in pharmaceutical solids.* Journal of Pharmaceutical Sciences, 2006. **95**(8): p. 1641-1665.
30. Venkatesh, G.M., et al., *Detection of Low Levels of the Amorphous Phase in Crystalline Pharmaceutical Materials by Thermally Stimulated Current Spectrometry.* Pharmaceutical Research, 2001. **18**(1): p. 98-103.
31. Williams, R.O., A.B. Watts, and D. Miller, *Formulating Poorly Water Soluble Drugs*. 2016: Springer International Publishing.

32. Evans, C.L. and X.S. Xie, *Coherent Anti-Stokes Raman Scattering Microscopy: Chemical Imaging for Biology and Medicine.* Annual Review of Analytical Chemistry, 2008. **1**(1): p. 883-909.
33. Ediger, M.D., C.A. Angell, and S.R. Nagel, *Supercooled Liquids and Glasses.* The Journal of Physical Chemistry, 1996. **100**(31): p. 13200-13212.
34. Marsac, P.J. and E.J. Munson, *Advanced Characterization of Solid Oral Dosage Forms: Linking Physical Changes to Measures of Performance and Quality*. 2016: AAPS NewsMagazine.
35. Archana Kumar, P.D., et al., *Fast Non-Destructive Detection of Low Level Crystalline Forms in Amorphous Spray Dried Dispersion Using Transmission Raman Spectroscopy and Comparison to Solid-State NMR Spectroscop.* American Pharmaceutical Review, 2016.
36. Runt, F. and J.P. Runt, *Dielectric Spectroscopy of Polymeric Materials: Fundamentals and Applications*. 1997: American Chemical Society.
37. Tomić, S., et al., *Dynamics and Structure of Biopolyelectrolytes Characterized by Dielectric Spectroscopy*. Macromolecular Symposia, 2011. **305**(1): p. 43-54.
38. *Introduction to Energy Dispersive X-ray Spectrometry (EDS)*. Available from: http://cfamm.ucr.edu/documents/eds-intro.pdf.
39. Goodhew, P.J., J. Humphreys, and R. Beanland, *Electron Microscopy and Analysis, Third Edition*. 2000: Taylor & Francis.
40. Barnes, T.J., I.M. Kempson, and C.A. Prestidge, *Surface analysis for compositional, chemical and structural imaging in pharmaceutics with mass spectrometry: A ToF-SIMS perspective.* International Journal of Pharmaceutics, 2011. **417**(1–2): p. 61-69.
41. Baer, D.R., et al., *Application of surface chemical analysis tools for characterization of nanoparticles.* Analytical and Bioanalytical Chemistry, 2010. **396**(3): p. 983-1002.
42. Royall, P.G., et al., *The development of DMA for the detection of amorphous content in pharmaceutical powdered materials.* International Journal of Pharmaceutics, 2005. **301**(1–2): p. 181-191.
43. Kestur, U.S., et al., *Nonlinear optical imaging for sensitive detection of crystals in bulk amorphous powders.* J Pharm Sci, 2012. **101**(11): p. 4201-13.
44. Ding, Y. *Fundamental Theory of Transmission Electronic Microscopy*. Available from: http://www.nanoscience.gatech.edu/zlwang/research/tem.html.
45. Weymouth, A. and F. Giessibl. *Atomic force microscopy at the picometer length scale*. Available from: http://www.vacuum-uk.org/pdfs/vs5/SurfaceMods/Weymouth.pdf.
46. Farber, L., G. Tardos, and J.N. Michaels, *Use of X-ray tomography to study the porosity and morphology of granules.* Powder Technology, 2003. **132**(1): p. 57-63.
47. Saleki-Gerhardt, A., C. Ahlneck, and G. Zografi, *Assessment of disorder in crystalline solids.* International Journal of Pharmaceutics, 1994. **101**(3): p. 237-247.
48. Clas, S.D., et al., *Quantification of crystallinity in blends of lyophilized and crystalline MK-0591 using x-ray powder diffraction.* International Journal of Pharmaceutics, 1995. **121**(1): p. 73-79.

49. Bates, S., et al., *Analysis of amorphous and nanocrystalline solids from their X-ray diffraction patterns.* Pharm Res, 2006. **23**(10): p. 2333-49.
50. Rietveld, H.M., *A profile refinement method for nuclear and magnetic structures.* Journal of Applied Crystallography, 1969. **2**(2): p. 65-71.
51. Proffen, T. and S. Billinge, *PDFFIT, a program for full profile structural refinement of the atomic pair distribution function.* Journal of Applied Crystallography, 1999. **32**(3): p. 572-575.
52. Newman, A., et al., *Characterization of amorphous API:Polymer mixtures using X-ray powder diffraction.* J Pharm Sci, 2008. **97**(11): p. 4840-56.
53. Bernadó, P., et al., *Structural Characterization of Flexible Proteins Using Small-Angle X-ray Scattering.* Journal of the American Chemical Society, 2007. **129**(17): p. 5656-5664.
54. Nunes, C., A. Mahendrasingam, and R. Suryanarayanan, *Quantification of Crystallinity in Substantially Amorphous Materials by Synchrotron X-ray Powder Diffractometry.* Pharmaceutical Research, 2005. **22**(11): p. 1942-1953.
55. Padilla, A.M., et al., *The study of phase separation in amorphous freeze-dried systems. Part I: Raman mapping and computational analysis of XRPD data in model polymer systems.* J Pharm Sci, 2011. **100**(1): p. 206-22.
56. Rumondor, A.C. and L.S. Taylor, *Application of partial least-squares (PLS) modeling in quantifying drug crystallinity in amorphous solid dispersions.* Int J Pharm, 2010. **398**(1-2): p. 155-60.
57. Sinclair, W., et al., *Physical stability and recrystallization kinetics of amorphous ibipinabant drug product by fourier transform raman spectroscopy.* Journal of Pharmaceutical Sciences. **100**(11): p. 4687-4699.
58. Karavas, E., et al., *Combining SEM, TEM, and micro-Raman techniques to differentiate between the amorphous molecular level dispersions and nanodispersions of a poorly water-soluble drug within a polymer matrix.* International Journal of Pharmaceutics, 2007. **340**(1): p. 76-83.
59. Kanaujia, P., et al., *Investigating the effect of moisture protection on solid-state stability and dissolution of fenofibrate and ketoconazole solid dispersions using PXRD, HSDSC and Raman microscopy.* Drug Development and Industrial Pharmacy, 2011. **37**(9): p. 1026-1035.
60. Taylor, L.S. and G. Zografi, *The Quantitative Analysis of Crystallinity Using FT-Raman Spectroscopy.* Pharmaceutical Research, 1998. **15**(5): p. 755-761.
61. Taylor, L.S. and G. Zografi, *Spectroscopic characterization of interactions between PVP and indomethacin in amorphous molecular dispersions.* Pharm Res, 1997. **14**(12): p. 1691-8.
62. Khougaz, K. and S.-D. Clas, *Crystallization inhibition in solid dispersions of MK-0591 and poly(vinylpyrrolidone) polymers.* Journal of Pharmaceutical Sciences, 2000. **89**(10): p. 1325-1334.
63. Painter, P.C., Y. Park, and M.M. Coleman, *Hydrogen bonding in polymer blends. 2. Theory.* Macromolecules, 1988. **21**(1): p. 66-72.
64. Painter, P.C., J. Graf, and M.M. Coleman, *A lattice model describing hydrogen bonding in polymer mixtures.* The Journal of Chemical Physics, 1990. **92**(10): p. 6166-6174.

65. Painter, P.C., Y. Park, and M.M. Coleman, *Thermodynamics of hydrogen bonding in polymer blends. 1. The application of association models.* Macromolecules, 1989. **22**(2): p. 570-579.
66. Wanapun, D., et al., *Selective Detection and Quantitation of Organic Molecule Crystallization by Second Harmonic Generation Microscopy.* Analytical Chemistry, 2010. **82**(13): p. 5425-5432.
67. Wanapun, D., et al., *Single Particle Nonlinear Optical Imaging of Trace Crystallinity in an Organic Powder.* Analytical Chemistry, 2011. **83**(12): p. 4745-4751.
68. Toth, S.J., et al., *Selective imaging of active pharmaceutical ingredients in powdered blends with common excipients utilizing two-photon excited ultraviolet-fluorescence and ultraviolet-second order nonlinear optical imaging of chiral crystals.* Anal Chem, 2012. **84**(14): p. 5869-75.
69. Zeitler, J.A., et al., *Relaxation and Crystallization of Amorphous Carbamazepine Studied by Terahertz Pulsed Spectroscopy.* Journal of Pharmaceutical Sciences. **96**(10): p. 2703-2709.
70. Berendt, R.T., et al., *Solid-state NMR spectroscopy in pharmaceutical research and analysis.* TrAC Trends in Analytical Chemistry, 2006. **25**(10): p. 977-984.
71. Aso, Y., S. Yoshioka, and S. Kojima, *Relationship between the crystallization rates of amorphous nifedipine, phenobarbital, and flopropione, and their molecular mobility as measured by their enthalpy relaxation and (1)H NMR relaxation times.* J Pharm Sci, 2000. **89**(3): p. 408-16.
72. Aso, Y., S. Yoshioka, and S. Kojima, *Explanation of the crystallization rate of amorphous nifedipine and phenobarbital from their molecular mobility as measured by (13)C nuclear magnetic resonance relaxation time and the relaxation time obtained from the heating rate dependence of the glass transition temperature.* J Pharm Sci, 2001. **90**(6): p. 798-806.
73. Pham, T.N., et al., *Analysis of Amorphous Solid Dispersions Using 2D Solid-State NMR and 1H T1 Relaxation Measurements.* Molecular Pharmaceutics, 2010. **7**(5): p. 1667-1691.
74. Wenslow, R.M., *19F Solid-State NMR Spectroscopic Investigation of Crystalline and Amorphous Forms of a Selective Muscarinic M3 Receptor Antagonist, in Both Bulk and Pharmaceutical Dosage Form Samples.* Drug Development and Industrial Pharmacy, 2002. **28**(5): p. 555-561.
75. Carpenter, J., et al., *Measurement of T g in lyophilized protein and protein excipient mixtures by dynamic mechanical analysis.* Journal of Thermal Analysis and Calorimetry, 2008. **95**(3): p. 881.
76. Szczepanski, C.R., C.S. Pfeifer, and J.W. Stansbury, *A new approach to network heterogeneity: Polymerization Induced Phase Separation in photo-initiated, free-radical methacrylic systems.* Polymer, 2012. **53**(21): p. 4694-4701.
77. Park, J.S., J.W. Park, and E. Ruckenstein, *Thermal and dynamic mechanical analysis of PVA/MC blend hydrogels.* Polymer, 2001. **42**(9): p. 4271-4280.
78. Karabanova, L.V., et al., *Phase separation in the polyurethane/poly(2-hydroxyethyl methacrylate) semi-interpenetrating polymer networks synthesized by different ways.* Polymer Engineering & Science, 2008. **48**(3): p. 588-597.

79. Poirier-Brulez, F., et al., *Influence of sucrose and water content on molecular mobility in starch-based glasses as assessed through structure and secondary relaxation.* Biopolymers, 2006. **81**(2): p. 63-73.
80. Alie, J., et al., *Dielectric study of the molecular mobility and the isothermal crystallization kinetics of an amorphous pharmaceutical drug substance.* J Pharm Sci, 2004. **93**(1): p. 218-33.
81. Bhardwaj, S.P., et al., *Correlation between molecular mobility and physical stability of amorphous itraconazole.* Mol Pharm, 2013. **10**(2): p. 694-700.
82. Bhardwaj, S.P. and R. Suryanarayanan, *Subtraction of DC Conductivity and Annealing: Approaches To Identify Johari–Goldstein Relaxation in Amorphous Trehalose.* Molecular Pharmaceutics, 2011. **8**(4): p. 1416-1422.
83. Bhardwaj, S.P. and R. Suryanarayanan, *Molecular Mobility as an Effective Predictor of the Physical Stability of Amorphous Trehalose.* Molecular Pharmaceutics, 2012. **9**(11): p. 3209-3217.
84. Bhardwaj, S.P. and R. Suryanarayanan, *Use of Dielectric Spectroscopy To Monitor Molecular Mobility in Glassy and Supercooled Trehalose.* The Journal of Physical Chemistry B, 2012. **116**(38): p. 11728-11736.
85. Bhattacharya, S. and R. Suryanarayanan, *Local mobility in amorphous pharmaceuticals--characterization and implications on stability.* J Pharm Sci, 2009. **98**(9): p. 2935-53.
86. Bhugra, C., et al., *Prediction of the onset of crystallization of amorphous sucrose below the calorimetric glass transition temperature from correlations with mobility.* J Pharm Sci, 2007. **96**(5): p. 1258-69.
87. Bhugra, C., et al., *Prediction of onset of crystallization from experimental relaxation times. II. Comparison between predicted and experimental onset times.* J Pharm Sci, 2008. **97**(1): p. 455-72.
88. Dantuluri, A.K., et al., *Role of α-relaxation on crystallization of amorphous celecoxib above T g probed by dielectric spectroscopy.* Molecular pharmaceutics, 2011. **8**(3): p. 814-822.
89. Power, G., J.K. Vij, and G.P. Johari, *Dielectric relaxation and crystallization of nanophase separated 1-propanol-isoamylbromide mixture.* J Chem Phys, 2007. **127**(9): p. 094507.
90. Bernes, A., et al., *Thermally Stimulated Current Studies of Transitions in Amorphous Polymers*, in *Order in the Amorphous "State" of Polymers*, S.E. Keinath, R.L. Miller, and J.K. Rieke, Editors. 1987, Springer US: Boston, MA. p. 305-326.
91. Andronis, V., M. Yoshioka, and G. Zografi, *Effects of sorbed water on the crystallization of indomethacin from the amorphous state.* J Pharm Sci, 1997. **86**(3): p. 346-51.
92. Shamblin, S.L. and G. Zografi, *The Effects of Absorbed Water on the Properties of Amorphous Mixtures Containing Sucrose.* Pharmaceutical Research, 1999. **16**(7): p. 1119-1124.
93. Tong, P. and G. Zografi, *Effects of water vapor absorption on the physical and chemical stability of amorphous sodium indomethacin.* AAPS PharmSciTech, 2004. **5**(2): p. e26.

94. Dahlberg, C., A. Millqvist-Fureby, and M. Schuleit, *Surface composition and contact angle relationships for differently prepared solid dispersions.* European Journal of Pharmaceutics and Biopharmaceutics, 2008. **70**(2): p. 478-485.
95. Lauer, M.E., et al., *Rapid Assessment of Homogeneity and Stability of Amorphous Solid Dispersions by Atomic Force Microscopy—From Bench to Batch.* Pharmaceutical Research, 2013. **30**(8): p. 2010-2022.
96. Meeus, J., et al., *Surface characteristics of spray-dried microspheres consisting of PLGA and PVP: relating the influence of heat and humidity to the thermal characteristics of these polymers.* Mol Pharm, 2013. **10**(8): p. 3213-24.
97. Price, R. and P.M. Young, *Visualization of the crystallization of lactose from the amorphous state.* J Pharm Sci, 2004. **93**(1): p. 155-64.
98. Qi, S., et al., *Compositional analysis of low quantities of phase separation in hot-melt-extruded solid dispersions: a combined atomic force microscopy, photothermal fourier-transform infrared microspectroscopy, and localised thermal analysis approach.* Pharm Res, 2011. **28**(9): p. 2311-26.
99. Yang, Z., et al., *Microstructure of an Immiscible Polymer Blend and Its Stabilization Effect on Amorphous Solid Dispersions.* Molecular Pharmaceutics, 2013. **10**(7): p. 2767-2780.
100. Dazzi, A., et al., *AFM–IR: Combining Atomic Force Microscopy and Infrared Spectroscopy for Nanoscale Chemical Characterization.* Applied Spectroscopy, 2012. **66**(12): p. 1365-1384.
101. D. Ticehurst, M., et al., *Characterisation of the influence of micronisation on the crystallinity and physical stability of revatropate hydrobromide.* International Journal of Pharmaceutics, 2000. **193**(2): p. 247-259.
102. Sun, Y., et al., *Stability of Amorphous Pharmaceutical Solids: Crystal Growth Mechanisms and Effect of Polymer Additives.* The AAPS Journal, 2012. **14**(3): p. 380-388.
103. Oh, D.-M., R.L. Curl, and G.L. Amidon, *Estimating the Fraction Dose Absorbed from Suspensions of Poorly Soluble Compounds in Humans: A Mathematical Model.* Pharmaceutical Research, 1993. **10**(2): p. 264-270.
104. Serajuddin, A.T., *Solid dispersion of poorly water-soluble drugs: early promises, subsequent problems, and recent breakthroughs.* J Pharm Sci, 1999. **88**(10): p. 1058-66.
105. Paudel, A., et al., *Manufacturing of solid dispersions of poorly water soluble drugs by spray drying: Formulation and process considerations.* International Journal of Pharmaceutics, 2013. **453**(1): p. 253-284.
106. Lang, B., J.W. McGinity, and R.O. Williams, *Hot-melt extrusion - basic principles and pharmaceutical applications.* Drug Development & Industrial Pharmacy, 2014. **40**(9): p. 1133-1155.
107. Williams, H.D., et al., *Strategies to Address Low Drug Solubility in Discovery and Development.* Pharmacological Reviews, 2013. **65**(1): p. 315-499.
108. Mudie, D.M., G.L. Amidon, and G.E. Amidon, *Physiological parameters for oral delivery and in vitro testing.* Mol Pharm, 2010. **7**(5): p. 1388-405.
109. Jantratid, E., et al., *Dissolution Media Simulating Conditions in the Proximal Human Gastrointestinal Tract: An Update.* Pharmaceutical Research, 2008. **25**(7): p. 1663.

110. Sugano, K., *Biopharmaceutics Modeling and Simulations: Theory, Practice, Methods, and Applications*. 2012: John Wiley & Sons, Inc.
111. Custodio, J.M., C.-Y. Wu, and L.Z. Benet, *PREDICTING DRUG DISPOSITION, ABSORPTION / ELIMINATION / TRANSPORTER INTERPLAY AND THE ROLE OF FOOD ON DRUG ABSORPTION.* Advanced drug delivery reviews, 2008. **60**(6): p. 717-733.
112. Giacomini, K.M., et al., *Membrane transporters in drug development.* Nat Rev Drug Discov, 2010. **9**(3): p. 215-36.
113. Strickley, R.G., *Solubilizing excipients in oral and injectable formulations.* Pharm Res, 2004. **21**(2): p. 201-30.
114. Dannenfelser, R.M., et al., *Development of clinical dosage forms for a poorly water soluble drug I: Application of polyethylene glycol-polysorbate 80 solid dispersion carrier system.* J Pharm Sci, 2004. **93**(5): p. 1165-75.
115. Nielsen, F.S., K.B. Petersen, and A. Müllertz, *Bioavailability of probucol from lipid and surfactant based formulations in minipigs: Influence of droplet size and dietary state.* European Journal of Pharmaceutics and Biopharmaceutics, 2008. **69**(2): p. 553-562.
116. Guzmán, H.R., et al., *Combined use of crystalline salt forms and precipitation inhibitors to improve oral absorption of celecoxib from solid oral formulations.* Journal of Pharmaceutical Sciences, 2007. **96**(10): p. 2686-2702.
117. Taylor, L.S. and G.G. Zhang, *Physical chemistry of supersaturated solutions and implications for oral absorption.* Adv Drug Deliv Rev, 2016.
118. McLaughlin, C.K., et al., *Stable Colloidal Drug Aggregates Catch and Release Active Enzymes.* ACS Chem Biol, 2016. **11**(4): p. 992-1000.
119. Owen, S.C., et al., *Colloidal Drug Formulations Can Explain "Bell-Shaped" Concentration–Response Curves.* ACS Chemical Biology, 2014. **9**(3): p. 777-784.
120. Wang, J. and E. Matayoshi, *Solubility at the Molecular Level: Development of a Critical Aggregation Concentration (CAC) Assay for Estimating Compound Monomer Solubility.* Pharmaceutical Research, 2012. **29**(7): p. 1745-1754.
121. Hoffman, J.D., *Thermodynamic Driving Force in Nucleation and Growth Processes.* The Journal of Chemical Physics, 1958. **29**(5): p. 1192-1193.
122. Murdande, S.B., et al., *Solubility advantage of amorphous pharmaceuticals: I. A thermodynamic analysis.* J Pharm Sci, 2010. **99**(3): p. 1254-64.
123. Paus, R., et al., *Predicting the Solubility Advantage of Amorphous Pharmaceuticals: A Novel Thermodynamic Approach.* Molecular Pharmaceutics, 2015. **12**(8): p. 2823-2833.
124. Ilevbare, G.A. and L.S. Taylor, *Liquid–Liquid Phase Separation in Highly Supersaturated Aqueous Solutions of Poorly Water-Soluble Drugs: Implications for Solubility Enhancing Formulations.* Crystal Growth & Design, 2013. **13**(4): p. 1497-1509.
125. Dai, W.-G., et al., *Evaluation of drug precipitation of solubility-enhancing liquid formulations using milligram quantities of a new molecular entity (NME).* Journal of Pharmaceutical Sciences, 2007. **96**(11): p. 2957-2969.
126. Vandecruys, R., et al., *Use of a screening method to determine excipients which optimize the extent and stability of supersaturated drug solutions and application of this system to solid formulation design.* Int J Pharm, 2007. **342**(1-2): p. 168-75.

127. Ilevbare, G.A., et al., *Maintaining Supersaturation in Aqueous Drug Solutions: Impact of Different Polymers on Induction Times.* Crystal Growth & Design, 2012. **13**(2): p. 740-751.
128. Alonzo, D.E., et al., *Understanding the behavior of amorphous pharmaceutical systems during dissolution.* Pharm Res, 2010. **27**(4): p. 608-18.
129. Barrett, P. and B. Glennon, *Characterizing the Metastable Zone Width and Solubility Curve Using Lasentec FBRM and PVM.* Chemical Engineering Research and Design, 2002. **80**(7): p. 799-805.
130. Liu, X., et al., *Monitoring of Antisolvent Crystallization of Sodium Scutellarein by Combined FBRM–PVM–NIR.* Journal of Pharmaceutical Sciences, 2011. **100**(6): p. 2452-2459.
131. Van Eerdenbrugh, B., D.E. Alonzo, and L.S. Taylor, *Influence of particle size on the ultraviolet spectrum of particulate-containing solutions: implications for in-situ concentration monitoring using UV/Vis fiber-optic probes.* Pharm Res, 2011. **28**(7): p. 1643-52.
132. Bohren, C.F. and D.R. Huffman, *Absorption and scattering of light by small particles*. 1983: Wiley.
133. Alonzo, D.E., et al., *Dissolution and precipitation behavior of amorphous solid dispersions.* J Pharm Sci, 2011. **100**(8): p. 3316-31.
134. Luo, Y.-H., et al., *Monitoring the Crystallization Process of Methylprednisolone Hemisuccinate (MPHS) from Ethanol Solution by Combined ATR-FTIR-FBRM-PVM.* Separation Science and Technology, 2013. **48**(12): p. 1881-1890.
135. Su, W., et al., *The impact of operating parameters on the polymorphic transformation of D-mannitol characterized in situ with Raman spectroscopy, FBRM, and PVM.* Organic Process Research & Development, 2010. **14**(6): p. 1432-1437.
136. Bevernage, J., et al., *Evaluation of gastrointestinal drug supersaturation and precipitation: strategies and issues.* Int J Pharm, 2013. **453**(1): p. 25-35.
137. Hancock, B.C. and M. Parks, *What is the true solubility advantage for amorphous pharmaceuticals?* Pharm Res, 2000. **17**(4): p. 397-404.
138. Almeida e Sousa, L., et al., *Assessment of the Amorphous "Solubility" of a Group of Diverse Drugs Using New Experimental and Theoretical Approaches.* Molecular Pharmaceutics, 2015. **12**(2): p. 484-495.
139. Higuchi, T., *Rate of release of medicaments from ointment bases containing drugs in suspension.* Journal of Pharmaceutical Sciences, 1961. **50**(10): p. 874-875.
140. Siepmann, J. and N. Peppas, *Modeling of drug release from delivery systems based on hydroxypropyl methylcellulose (HPMC).* Advanced drug delivery reviews, 2012. **64**: p. 163-174.
141. Harmon, P., et al., *Mechanism of Dissolution-Induced Nanoparticle Formation from a Copovidone-Based Amorphous Solid Dispersion.* Mol Pharm, 2016. **13**(5): p. 1467-81.
142. Friesen, D.T., et al., *Hydroxypropyl methylcellulose acetate succinate-based spray-dried dispersions: an overview.* Molecular pharmaceutics, 2008. **5**(6): p. 1003-1019.
143. Karavas, E., et al., *Investigation of the release mechanism of a sparingly water-soluble drug from solid dispersions in hydrophilic carriers based on physical*

state of drug, particle size distribution and drug–polymer interactions. European Journal of Pharmaceutics and Biopharmaceutics, 2007. **66**(3): p. 334-347.
144. Kanaujia, P., et al., *Nanoparticle formation and growth during in vitro dissolution of ketoconazole solid dispersion.* J Pharm Sci, 2011. **100**(7): p. 2876-85.
145. Craig, D.Q.M., *The mechanisms of drug release from solid dispersions in water-soluble polymers.* International Journal of Pharmaceutics, 2002. **231**(2): p. 131-144.
146. Mukerjee, P. and K.J. Mysels, *Critical micelle concentrations of aqueous surfactant systems*. 1971, DTIC Document.
147. Carey, M.C. and D.M. Small, *Micelle formation by bile salts: Physical-chemical and thermodynamic considerations.* Archives of Internal Medicine, 1972. **130**(4): p. 506-527.
148. Nilsson, S., *Interactions between Water-Soluble Cellulose Derivatives and Surfactants. 1. The HPMC/SDS/Water System.* Macromolecules, 1995. **28**(23): p. 7837-7844.
149. Qi, S., et al., *Insights into the Role of Polymer-Surfactant Complexes in Drug Solubilisation/Stabilisation During Drug Release from Solid Dispersions.* Pharmaceutical Research, 2013. **30**(1): p. 290-302.
150. Ueda, K., et al., *Equilibrium State at Supersaturated Drug Concentration Achieved by Hydroxypropyl Methylcellulose Acetate Succinate: Molecular Characterization Using 1H NMR Technique.* Molecular Pharmaceutics, 2015. **12**(4): p. 1096-1104.
151. Long, M.A., E.W. Kaler, and S.P. Lee, *Structural characterization of the micelle-vesicle transition in lecithin-bile salt solutions.* Biophysical Journal, 1994. **67**(4): p. 1733-1742.
152. Hildebrand, A., et al., *Thermodynamics of Demicellization of Mixed Micelles Composed of Sodium Oleate and Bile Salts.* Langmuir, 2004. **20**(2): p. 320-328.
153. Madenci, D. and S.U. Egelhaaf, *Self-assembly in aqueous bile salt solutions.* Current Opinion in Colloid & Interface Science, 2010. **15**(1–2): p. 109-115.
154. Indulkar, A.S., et al., *Impact of Micellar Surfactant on Supersaturation and Insight into Solubilization Mechanisms in Supersaturated Solutions of Atazanavir.* Pharmaceutical Research, 2017: p. 1-20.
155. Carroll, B.J., *The kinetics of solubilization of nonpolar oils by nonionic surfactant solutions.* Journal of Colloid and Interface Science, 1981. **79**(1): p. 126-135.
156. Ariyaprakai, S. and S.R. Dungan, *Contribution of molecular pathways in the micellar solubilization of monodisperse emulsion droplets.* Langmuir, 2008. **24**(7): p. 3061-9.
157. Gamache, P.H., et al., *HPLC analysis of nonvolatile analytes using charged aerosol detection.* Lc Gc Europe, 2005. **18**(6): p. 345.
158. Konno, H., et al., *Effect of polymer type on the dissolution profile of amorphous solid dispersions containing felodipine.* Eur J Pharm Biopharm, 2008. **70**(2): p. 493-9.
159. Qian, F., et al., *Solution Behavior of PVP-VA and HPMC-AS-Based Amorphous Solid Dispersions and Their Bioavailability Implications.* Pharmaceutical Research, 2012. **29**(10): p. 2766-2776.

160. Mitra, A., et al., *Impact of polymer type on bioperformance and physical stability of hot melt extruded formulations of a poorly water soluble drug.* International Journal of Pharmaceutics, 2016. **505**(1–2): p. 107-114.
161. Ueda, K., et al., *The effect of HPMCAS functional groups on drug crystallization from the supersaturated state and dissolution improvement.* Int J Pharm, 2014. **464**(1-2): p. 205-13.
162. Ting, J.M., et al., *Deconstructing HPMCAS: Excipient Design to Tailor Polymer–Drug Interactions for Oral Drug Delivery.* ACS Biomaterials Science & Engineering, 2015. **1**(10): p. 978-990.
163. DiNunzio, J.C., et al., *Production of advanced solid dispersions for enhanced bioavailability of itraconazole using KinetiSol® Dispersing.* Drug Development & Industrial Pharmacy, 2010. **36**(9): p. 1064-1078.
164. Simonelli, A.P., S.C. Mehta, and W.I. Higuchi, *Dissolution Rates of High Energy Polyvinylpyrrolidone (PVP)-Sulfathiazole Coprecipitates.* Journal of Pharmaceutical Sciences, 1969. **58**(5): p. 538-549.
165. Corrigan, O.I., *Retardation of Polymeric Carrier Dissolution by Dispersed Drugs: Factors Influencing the Dissolution of Solid Dispersions Containing Polyethlene Glycols.* Drug Development and Industrial Pharmacy, 1986. **12**(11-13): p. 1777-1793.
166. Doherty, C. and P. York, *Mechanisms of dissolution of frusemide/PVP solid dispersions.* International Journal of Pharmaceutics, 1987. **34**(3): p. 197-205.
167. Sertsou, G., et al., *Solvent change co-precipitation with hydroxypropyl methylcellulose phthalate to improve dissolution characteristics of a poorly water-soluble drug.* J Pharm Pharmacol, 2002. **54**(8): p. 1041-7.
168. Sjökvist, E. and C. Nyström, *Physicochemical aspects of drug release. VI. Drug dissolution rate from solid particulate dispersions and the importance of carrier and drug particle properties.* International Journal of Pharmaceutics, 1988. **47**(1): p. 51-66.
169. Sugano, K., *Estimation of effective intestinal membrane permeability considering bile micelle solubilisation.* Int J Pharm, 2009. **368**(1-2): p. 116-22.
170. Avdeef, A., *Permeability*, in *Absorption and Drug Development*. 2003, John Wiley & Sons, Inc. p. 116-246.
171. Aungst, B.J., *Intestinal permeation enhancers.* J Pharm Sci, 2000. **89**(4): p. 429-42.
172. Anderberg, E.K., C. Nystrom, and P. Artursson, *Epithelial transport of drugs in cell culture. VII: Effects of pharmaceutical surfactant excipients and bile acids on transepithelial permeability in monolayers of human intestinal epithelial (Caco-2) cells.* J Pharm Sci, 1992. **81**(9): p. 879-87.
173. Jang, D.-J., T. Sim, and E. Oh, *Formulation and optimization of spray-dried amlodipine solid dispersion for enhanced oral absorption.* Drug Development & Industrial Pharmacy, 2013. **39**(7): p. 1133-1141.
174. Sugano, K., *Possible reduction of effective thickness of intestinal unstirred water layer by particle drifting effect.* Int J Pharm, 2010. **387**(1-2): p. 103-9.
175. Lenhardt, T., et al., *Evaluation of Nanosuspensions for Absorption Enhancement of Poorly Soluble Drugs: In Vitro Transport Studies Across Intestinal Epithelial Monolayers.* The AAPS Journal, 2008. **10**(3): p. 435-438.

176. Frank, K.J., et al., *What Is the Mechanism Behind Increased Permeation Rate of a Poorly Soluble Drug from Aqueous Dispersions of an Amorphous Solid Dispersion?* Journal of Pharmaceutical Sciences, 2014. **103**(6): p. 1779-1786.
177. Lian, X., et al., *Soluplus® based 9-nitrocamptothecin solid dispersion for peroral administration: Preparation, characterization, in vitro and in vivo evaluation.* International Journal of Pharmaceutics, 2014. **477**(1): p. 399-407.
178. Yildiz, H.M., et al., *Size selectivity of intestinal mucus to diffusing particulates is dependent on surface chemistry and exposure to lipids.* J Drug Target, 2015. **23**(7-8): p. 768-74.
179. Raina, S., et al., *Impact of Solubilizing Additives on Supersaturation and Membrane Transport of Drugs.* Pharmaceutical Research, 2015. **32**(10): p. 3350-3364.
180. Artursson, P., *Epithelial transport of drugs in cell culture. I: A model for studying the passive diffusion of drugs over intestinal absorptive (Caco-2) cells.* J Pharm Sci, 1990. **79**(6): p. 476-82.
181. Lennernäs, H., S. Nylander, and A.-L. Ungell, *Jejunal Permeability: A Comparison Between the Ussing Chamber Technique and the Single-Pass Perfusion in Humans.* Pharmaceutical Research, 1997. **14**(5): p. 667-671.
182. Setiawan, N. and P. Marsac, *What Is the True Driving Force for Drug Absorption in the Presence of Solubilizing Excipients?* , in *AAPS Annual Meeting*. 2016: Denver, CO.
183. Crum, M.F., et al., *A new in vitro lipid digestion - in vivo absorption model to evaluate the mechanisms of drug absorption from lipid-based formulations.* Pharm Res, 2016. **33**(4): p. 970-82.
184. Ginski, M.J. and J.E. Polli, *Prediction of dissolution–absorption relationships from a dissolution/Caco-2 system.* International Journal of Pharmaceutics, 1999. **177**(1): p. 117-125.
185. Kataoka, M., et al., *Application of Dissolution/Permeation System for Evaluation of Formulation Effect on Oral Absorption of Poorly Water-Soluble Drugs in Drug Development.* Pharmaceutical Research, 2012. **29**(6): p. 1485-1494.
186. Miller, J.M., et al., *A Win–Win Solution in Oral Delivery of Lipophilic Drugs: Supersaturation via Amorphous Solid Dispersions Increases Apparent Solubility without Sacrifice of Intestinal Membrane Permeability*. Molecular Pharmaceutics, 2012. **9**(7): p. 2009-2016.
187. Gao, Y., et al., *A pH-dilution method for estimation of biorelevant drug solubility along the gastrointestinal tract: application to physiologically based pharmacokinetic modeling.* Mol Pharm, 2010. **7**(5): p. 1516-26.
188. Zheng, W., et al., *Selection of oral bioavailability enhancing formulations during drug discovery*. Drug Dev Ind Pharm, 2012. **38**(2): p. 235-47.
189. Mitra, A., W. Zhu, and F. Kesisoglou, *Physiologically Based Absorption Modeling for Amorphous Solid Dispersion Formulations.* Molecular Pharmaceutics, 2016. **13**(9): p. 3206-3215.
190. Alin, J.S., N, M. Defrese, and P.J. Marsac, *Thermodynamics of Amorphous Solid Dispersions in the Presence of Water - A Necessity for Comparing Kinetics Across Diverse Amorphous Systems*. 2017: Polymer.

191. Bellantone, R.A., et al., *A method to predict the equilibrium solubility of drugs in solid polymers near room temperature using thermal analysis.* Journal of Pharmaceutical Sciences, 2012. **101**(12): p. 4549-4558.
192. Byrn, S., et al., *Pharmaceutical Solids: A Strategic Approach to Regulatory Considerations.* Pharmaceutical Research, 1995. **12**(7): p. 945-954.
193. Hancock, B., S. Shamblin, and G. Zografi, *Molecular Mobility of Amorphous Pharmaceutical Solids Below Their Glass Transition Temperatures.* Pharmaceutical Research, 1995. **12**(6): p. 799-806.
194. Marsac, P.J., et al., *Recrystallization of Nifedipine and Felodipine from Amorphous Molecular Level Solid Dispersions Containing Poly(vinylpyrrolidone) and Sorbed Water.* Pharmaceutical Research, 2008. **25**(3): p. 647-656.
195. Rumondor, A.C.F., et al., *Phase Behavior of Poly(vinylpyrrolidone) Containing Amorphous Solid Dispersions in the Presence of Moisture.* Molecular Pharmaceutics, 2009. **6**(5): p. 1492-1505.
196. Fakes, M.G., et al., *Enhancement of oral bioavailability of an HIV-attachment inhibitor by nanosizing and amorphous formulation approaches.* Int J Pharm, 2009. **370**(1-2): p. 167-74.
197. Zhou, D., et al., *Physical stability of amorphous pharmaceuticals: Importance of configurational thermodynamic quantities and molecular mobility.* J Pharm Sci, 2002. **91**(8): p. 1863-72.
198. Siniti, M., et al., *Etude du comportement thermique des hexitols: Partie 1. Vitrification et cristallisation de Fiditol, du mannitol, du sorbitol et du dulcitol.* Thermochimica Acta, 1993. **224**(Supplement C): p. 97-104.
199. Andronis, V. and G. Zografi, *Crystal nucleation and growth of indomethacin polymorphs from the amorphous state.* Journal of Non-Crystalline Solids, 2000. **271**(3): p. 236-248.
200. Janssens, S., et al., *Influence of preparation methods on solid state supersaturation of amorphous solid dispersions: a case study with itraconazole and eudragit e100.* Pharm Res, 2010. **27**(5): p. 775-85.
201. Hancock, B.C., S.L. Shamblin, and G. Zografi, *Molecular mobility of amorphous pharmaceutical solids below their glass transition temperatures.* Pharmaceutical Research, 1995. **12**(6): p. 799-806.
202. Van den Mooter, G., P. Augustijns, and R. Kinget, *Stability prediction of amorphous benzodiazepines by calculation of the mean relaxation time constant using the Williams–Watts decay function.* European Journal of Pharmaceutics and Biopharmaceutics, 1999. **48**(1): p. 43-48.
203. Marshall, A.S. and S.E.B. Petrie, *Rate-determining factors for enthalpy relaxation of glassy polymers. Molecular weight.* Journal of Applied Physics, 1975. **46**(10): p. 4223-30.
204. Hancock, B.C. and G. Zografi, *Characteristics and significance of the amorphous state in pharmaceutical systems.* Journal of Pharmaceutical Sciences, 1997. **86**(1): p. 1-12.
205. Baird, J.A., B. Van Eerdenbrugh, and L.S. Taylor, *A Classification System to Assess the Crystallization Tendency of Organic Molecules from Undercooled Melts.* Journal of Pharmaceutical Sciences, 2010. **99**(9): p. 3787-3806.

206. Miyazaki, T., S. Yoshioka, and Y. Aso, *Physical stability of amorphous acetanilide derivatives improved by polymer excipients.* Chemical & Pharmaceutical Bulletin, 2006. **54**(8): p. 1207-1210.
207. Miyazaki, T., et al., *Ability of polyvinylpyrrolidone and polyacrylic acid to inhibit the crystallization of amorphous acetaminophen.* Journal of Pharmaceutical Sciences, 2004. **93**(11): p. 2710-2717.
208. Crowley, K.J. and G. Zografi, *The Effect of Low Concentrations of Molecularly Dispersed Poly(Vinylpyrrolidone) on Indomethacin Crystallization from the Amorphous State.* Pharmaceutical Research, 2003. **20**(9): p. 1417-1422.
209. Janssens, S. and G. Van den Mooter, *Review: physical chemistry of solid dispersions.* Journal of Pharmacy and Pharmacology, 2009. **61**(12): p. 1571-1586.
210. Broman, E., C. Khoo, and L.S. Taylor, *A comparison of alternative polymer excipients and processing methods for making solid dispersions of a poorly water soluble drug.* International Journal of Pharmaceutics, 2001. **222**(1): p. 139-151.
211. Fujii, M., et al., *The Solid Dispersion of Benzodiazepins with Phosphatidylcholine. The Effect of Substituents of Benzodiazepins on the Formation of Solid Dispersions.* CHEMICAL & PHARMACEUTICAL BULLETIN, 1991. **39**(11): p. 3013-3017.
212. Khougaz, K. and S.D. Clas, *Crystallization Inhibition in Solid Dispersions of MK-0591 and Poly(vinylpyrrolidone) Polymers.* Journal of Pharmaceutical Sciences, 2000. **89**(10): p. 1325-1334.
213. Law, D., et al., *Physicochemical considerations in the preparation of amorphous ritonavir–poly(ethylene glycol) 8000 solid dispersions.* Journal of Pharmaceutical Sciences, 2001. **90**(8): p. 1015-1025.
214. Law, D., et al., *Ritonavir–PEG 8000 amorphous solid dispersions: In vitro and in vivo evaluations.* Journal of Pharmaceutical Sciences, 2004. **93**(3): p. 563-570.
215. Sethia, S. and E. Squillante, *Solid dispersion of carbamazepine in PVP K30 by conventional solvent evaporation and supercritical methods.* International Journal of Pharmaceutics, 2004. **272**(1–2): p. 1-10.
216. Suzuki, H. and H. Sunada, *Influence of Water-Soluble Polymers on the Dissolution of Nifedipine Solid Dispersions with Combined Carriers.* CHEMICAL & PHARMACEUTICAL BULLETIN, 1998. **46**(3): p. 482-487.
217. Tantishaiyakul, V., N. Kaewnopparat, and S. Ingkatawornwong, *Properties of solid dispersions of piroxicam in polyvinylpyrrolidone K-30.* International Journal of Pharmaceutics, 1996. **143**(1): p. 59-66.
218. Taylor, L.S. and G. Zografi, *Spectroscopic Characterization of Interactions Between PVP and Indomethacin in Amorphous Molecular Dispersions.* Pharmaceutical Research, 1997. **14**(12): p. 1691-1698.
219. Van den Mooter, G., et al., *Physical stabilisation of amorphous ketoconazole in solid dispersions with polyvinylpyrrolidone K25.* European Journal of Pharmaceutical Sciences, 2001. **12**(3): p. 261-269.
220. Weuts, I., et al., *Phase behaviour analysis of solid dispersions of loperamide and two structurally related compounds with the polymers PVP-K30 and PVP-VA64.* European Journal of Pharmaceutical Sciences, 2004. **22**(5): p. 375-385.

221. Marsac, P.J., S.L. Shamblin, and L.S. Taylor, *Theoretical and Practical Approaches for Prediction of Drug-Polymer Miscibility and Solubility.* Pharmaceutical Research, 2006. **23**(10): p. 2417-2426.
222. Flory, P.J., *Principles of Polymer Chemistry*. 1953, Ithaca, New York: Cornell University Press 495 pp and 548 pp.
223. Thakral, S. and N.K. Thakral, *Prediction of drug–polymer miscibility through the use of solubility parameter based flory–huggins interaction parameter and the experimental validation: PEG as model polymer.* Journal of Pharmaceutical Sciences, 2013. **102**(7): p. 2254-2263.
224. Brunacci, A., et al., *The thermodynamics of mixing polystyrene and poly(α-methylstyrene) from a calorimetric viewpoint.* Polymer, 1994. **35**(13): p. 2893-6.
225. Righetti, M.C., et al., *Thermodynamics of mixing of poly(vinyl chloride) and poly(ethylene-co-vinyl acetate).* Polymer, 2002. **43**(18): p. 5035-5042.
226. Weeks, N.E., F.E. Karasz, and W.J. MacKnight, *Enthalpy of mixing of poly(2,6-dimethylphenylene oxide) and polystyrene.* Journal of Applied Physics, 1977. **48**(10): p. 4068-71.
227. Alin, J., et al., *Solution Calorimetry for Determination of Room Temperature Miscibility and Solubility of a Drug in a Polymer Matrix*. 2017, University of Kentucky, College of Pharmacy.
228. Hancock, B.C. and M. Parks, *What is the true solubility advantage for amorphous pharmaceuticals?* Pharmaceutical Research, 2000. **17**(4): p. 397-404.
229. Parks, G.S., L.J. Snyder, and F.R. Cattoir, *Studies of glass. XI. Some thermodynamic relations of glassy and alpha-crystalline glucose.* J. Chem. Phys., 1934. **2**: p. 595-8.
230. Surov, A.O., et al., *Crystallization and Polymorphism of Felodipine.* Crystal Growth & Design, 2012. **12**(8): p. 4022-4030.
231. Flory, P.J., *Principles of Polymer Chemistry*. 1953, Ithaca, New York: Cornell University Press
232. Alin, J., et al., *Thermodynamics of Amorphous Solid Dispersions in the Presence of Water – A Necessity for Comparing Kinetics Across Diverse Amorphous Systems*. 2017, University of Kentucky, College of Pharmacy.
233. Takagi, T., et al., *A Provisional Biopharmaceutical Classification of the Top 200 Oral Drug Products in the United States, Great Britain, Spain, and Japan.* Molecular Pharmaceutics, 2006. **3**(6): p. 631-643.
234. Reintjes, T. *Solubility Enhancement with BASF Pharma Polymers*. 2011.
235. Matteucci, M.E., et al., *Highly supersaturated solutions from dissolution of amorphous itraconazole microparticles at pH 6.8.* Mol Pharm, 2009. **6**(2): p. 375-85.
236. de Campo, L., et al., *Five-component food-grade microemulsions: structural characterization by SANS.* Journal of Colloid and Interface Science, 2004. **274**(1): p. 251-267.
237. Feng, S., *STUDIES ON DRUG SOLUBILIZATION MECHANISM IN SIMPLE MICELLE SYSTEMS*, in *Pharmaceutical Sciences*. 2009, University of Kentucky: Lexington, KY. p. 241.

238. Raina, S.A., et al., *Enhancements and limits in drug membrane transport using supersaturated solutions of poorly water soluble drugs.* J Pharm Sci, 2014. **103**(9): p. 2736-48.
239. Kuldipkumar, A., G.S. Kwon, and G.G.Z. Zhang, *Determining the Growth Mechanism of Tolazamide by Induction Time Measurement.* Crystal Growth & Design, 2006. **7**(2): p. 234-242.
240. Patel, D.D., et al., *Maintenance of supersaturation I: indomethacin crystal growth kinetic modeling using an online second-derivative ultraviolet spectroscopic method.* J Pharm Sci, 2011. **100**(7): p. 2623-41.
241. Canselier, J.P., et al., *Surfactant effects in crystallization: nucleation and crystal habit of γ-aminobutyric acid*, in *Trends in Colloid and Interface Science VIII*, R.H. Ottewill and A.R. Rennie, Editors. 1994, Steinkopff. p. 174-178.
242. Chen, J., et al., *Bile Salts as Crystallization Inhibitors of Supersaturated Solutions of Poorly Water-Soluble Compounds.* Crystal Growth & Design, 2015. **15**(6): p. 2593-2597.
243. Mosquera-Giraldo, L.I., N.S. Trasi, and L.S. Taylor, *Impact of surfactants on the crystal growth of amorphous celecoxib.* Int J Pharm, 2014. **461**(1-2): p. 251-7.
244. Rodríguez-Hornedo, N. and D. Murphy, *Surfactant-facilitated crystallization of dihydrate carbamazepine during dissolution of anhydrous polymorph.* Journal of Pharmaceutical Sciences, 2004. **93**(2): p. 449-460.
245. Chauhan, H., et al., *Correlation of Inhibitory Effects of Polymers on Indomethacin Precipitation in Solution and Amorphous Solid Crystallization Based on Molecular Interaction.* Pharmaceutical Research, 2014. **31**(2): p. 500-515.
246. Ozaki, S., et al., *Inhibition of crystal nucleation and growth by water-soluble polymers and its impact on the supersaturation profiles of amorphous drugs.* J Pharm Sci, 2013. **102**(7): p. 2273-81.
247. Setiawan, N., Campbell, H. R., Nethercott, M. J., Su, Y., Marsac, P. J., *What is the True Driving Force for Absorption of Poorly Water-Soluble Drugs in the Presence of Solubilizing Additives?* 2017.
248. Fagerberg, J.H., et al., *Dissolution Rate and Apparent Solubility of Poorly Soluble Drugs in Biorelevant Dissolution Media.* Molecular Pharmaceutics, 2010. **7**(5): p. 1419-1430.
249. Andrew, E.R., A. Bradbury, and R.G. Eades, *Removal of dipolar broadening of nuclear magnetic resonance spectra of solids by specimen rotation.* Nature, 1959. **183**(4678): p. 1802-1803.
250. Barich, D.H., et al., *3-Methylglutaric acid as a ^{13}C solid-state NMR standard.* Solid State Nuclear Magnetic Resonance, 2006. **30**(3–4): p. 125-129.
251. Pines, A., M.G. Gibby, and J.S. Waugh, *Proton-enhanced NMR of dilute spins in solids.* The Journal of Chemical Physics, 1973. **59**(2): p. 569-590.
252. Dixon, W.T., et al., *Total suppression of sidebands in CPMAS C-13 NMR.* Journal of Magnetic Resonance, 1982. **49**(2): p. 341-345.
253. Fung, B.M., A.K. Khitrin, and K. Ermolaev, *An improved broadband decoupling sequence for liquid crystals and solids.* Journal of Magnetic Resonance, 2000. **142**(1): p. 97-101.
254. Mullin, J.W., *5 - Nucleation*, in *Crystallization (Fourth Edition)*. 2001, Butterworth-Heinemann: Oxford. p. 181-215.

255. Rosen, M.J., *Reduction of Surface and Interfacial Tension by Surfactants*, in *Surfactants and Interfacial Phenomena*. 2004, John Wiley & Sons, Inc. p. 208-242.
256. Rosen, M.J., *Adsorption of Surface-Active Agents at Interfaces: The Electrical Double Layer*, in *Surfactants and Interfacial Phenomena*. 2004, John Wiley & Sons, Inc. p. 34-104.
257. Variankaval, N.E., K.I. Jacob, and S.M. Dinh, *Characterization of crystal forms of β-estradiol – thermal analysis, Raman microscopy, X-ray analysis and solid-state NMR.* Journal of Crystal Growth, 2000. **217**(3): p. 320-331.
258. Rosen, M.J., *Solubilization by Solutions of Surfactants: Micellar Catalysis*, in *Surfactants and Interfacial Phenomena*. 2004, John Wiley & Sons, Inc. p. 178-207.
259. Fendler, J.H. and E.J. Fendler, *Chapter 4 - Principles of Micellar Catalysis in Aqueous Solutions*, in *Catalysis in Micellar and Macromoleular Systems*. 1975, Academic Press. p. 86-103.
260. Terebetski, J.L. and B. Michniak-Kohn, *Combining ibuprofen sodium with cellulosic polymers: A deep dive into mechanisms of prolonged supersaturation.* Int J Pharm, 2014. **475**(1-2): p. 536-546.
261. Raghavan, S.L., et al., *Crystallization of hydrocortisone acetate: influence of polymers.* Int J Pharm, 2001. **212**(2): p. 213-21.
262. Nickell, J.R., et al., *1,4-Diphenalkylpiperidines: A new scaffold for the design of potent inhibitors of the vesicular monoamine transporter-2.* Bioorg Med Chem Lett, 2016. **26**(13): p. 2997-3000.
263. Murdande, S.B., et al., *Solubility Advantage of Amorphous Pharmaceuticals: II. Application of Quantitative Thermodynamic Relationships for Prediction of Solubility Enhancement in Structurally Diverse Insoluble Pharmaceuticals.* Pharmaceutical Research, 2010. **27**(12): p. 2704-2714.
264. Paudel, A., J. Van Humbeeck, and G. Van den Mooter, *Theoretical and Experimental Investigation on the Solid Solubility and Miscibility of Naproxen in Poly(vinylpyrrolidone).* Molecular Pharmaceutics, 2010. **7**(4): p. 1133-1148.
265. Bansal, S.S., A.M. Kaushal, and A.K. Bansal, *Enthalpy relaxation studies of two structurally related amorphous drugs and their binary dispersions.* Drug development and industrial pharmacy, 2010. **36**(11): p. 1271-80.

VITA

NICO SETIAWAN

Birthplace: Surabaya, Indonesia

EDUCATION

2012 – 2017	Ph.D. Candidate in Pharmaceutical Sciences, University of Kentucky, Lexington, KY
2008 – 2012	B.S. in Chemical Engineering, University of Kentucky, Lexington, KY

PROFESSIONAL EXPERIENCES

2017 – present	Senior Scientist, SSCI., West Lafayette, IN
2013 – 2017	Research Assistant – University of Kentucky, College of Pharmacy, Lexington, KY
2015	Industrial Internship – Merck & Co., Rahway, NJ
2012 – 2013	Teaching Assistant – University of Kentucky, College of Pharmacy, Lexington, KY
2010 – 2011	Industrial Co-op – CAER, Lexington, KY

HONORS AND AWARDS

- Dennis Casey Pharmaceutical Chemistry and Engineering Travel Award (2015)
- Formulation Design and Development (FDD) Section of American Association of Pharmaceutical Scientists (AAPS) Travel Award (2014)
- Third place, Outstanding Elevator Talk, Symposium on Drug Discovery and Development, University of Kentucky (2014)
- Peter G. Glavinos, Jr., Ph.D. Graduate Student Travel Award (2014)

PUBLICATIONS

S. Poozesh, **N. Setiawan**, F. Arce, P. Sundararajan, J.D. Rocca, A. Rumondor, S. Zhang, D. Wei, R. Wenslow, H. Xi, Y. Su, J. Stellabot, J. Moser, P.J. Marsac (2017). "Understanding the Process-Product-Performance Interplay of Spray Dried Drug-Polymer Systems Through Complete Structural and Chemical Characterization of Single Spray Dried Particles." Pow Tech 320:685-695.

J. Alin, **N. Setiawan**, J. DiNunzio, H. Lau, L. Lupton, H. Xi, N. Hesse, L.S. Taylor, P.J. Marsac (2018). "A novel approach for measuring room temperature enthalpy of mixing and associated solubility estimation of a drug in a polymer matrix." Polymer 135:50-60.

S. Poozesh, **N. Setiawan**, N. K. Akafuah, K. Saito, P.J. Marsac (2018). "Assessment of Predictive Models for Characterizing the Atomization Process in a Spray Dryer's Bi-fluid Nozzle." Chemical Engineering Science 180:42-51.

J. Alin, **N. Setiawan**, M. Defrese, P.J. Marsac (2018). "Crystalline Solubility and Amorphous Phase Stability of Drugs in Poly(vinyl pyrrolidone) (PVP) Dispersions Containing Water – a Solution Calorimetry Based Approach." Polymer (Submitted)

N. Setiawan, S. Poozesh, F. Arce, J. Alin, A. Mitra, P.J. Marsac (2018). "Pharmaceutical Amorphous Solid Dispersion: Detection Tools of Solid State Failure Modes and Bioperformance Assessment" Mol Pharm (In Preparation)

N. Setiawan, H.R. Campbell, M.J. Nethercott, Y. Su, P.J. Marsac (2018). "What is the True Driving Force for Absorption of Poorly Water-Soluble Drugs in the Presence of Solubilizing Additives?" Pharm Res (In Preparation)

N. Setiawan, P.J. Marsac, P.M. Bummer (2018). "Elucidating the Impact of Drug-Excipient Intermolecular Interactions on Estradiol Crystallization Kinetics at Equivalent Thermodynamic Activity" (In Preparation)

N. Setiawan, H. Xi, P.J. Marsac (2018). "The Amorphous Energy Landscape." (In Preparation)

X. Lu, **N. Setiawan**, H. R. Campbell, M.J. Nethercott, Y. Su, P.J. Marsac (2018). "Mechanistic Investigation of Drug Supersaturation in the Presence of Solubilizing Additives by NMR Spectroscopy." (In Preparation)

N. Setiawan, E. Denehy, P. Crooks, L. Dwoskin, P.J. Marsac, M. Leggas (2018). "Pharmaceutics Approaches to Maximize Oral Bioavailability of Methamphetamine Abuse Deterrent, JPC-077" Intl J Pharm (In Preparation)